SOFT X-RAY PROJECTION LITHOGRAPHY

Sponsored by
Optical Society of America

TECHNICAL DIGEST

MAY 10–12, 1993
MONTEREY, CALIFORNIA

DISCLAIMER NOTICE

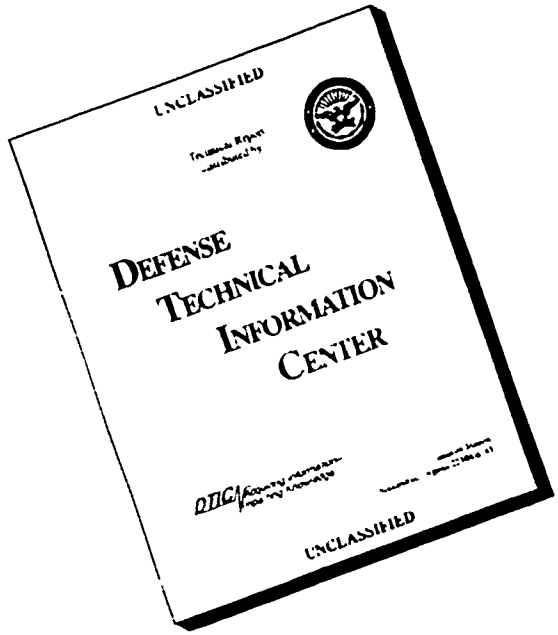

THIS REPORT IS INCOMPLETE BUT IS THE BEST AVAILABLE COPY FURNISHED TO THE CENTER. THERE ARE MULTIPLE MISSING PAGES. ALL ATTEMPTS TO DATE TO OBTAIN THE MISSING PAGES HAVE BEEN UNSUCCESSFUL.

REPORT DOCUMENTATION PAGE

Form Approved
OMB No. 0704-0188

1. AGENCY USE ONLY (Leave blank)	2. REPORT DATE	3. REPORT TYPE AND DATES COVERED
		Final Report 15 Feb 93 - 14 Jan 94

4. TITLE AND SUBTITLE

Soft X-ray projection lithography
Organization of the 1993 Photonics Science Topical Meetings

5. FUNDING NUMBERS

E49620-93-1-0181

6. AUTHOR(S)

Dr Jarus W Quinn

7. PERFORMING ORGANIZATION NAME(S) AND ADDRESS(ES)

Optical Society of America
2010 Massachusetts Avenue NW
Washington DC 20036

8. PERFORMING ORGANIZATION REPORT NUMBER

AFOSR-TR 93 0641

9. SPONSORING/MONITORING AGENCY NAME(S) AND ADDRESS(ES)

AFOSR/NE
110 Duncan Avenue Suite B115
Bolling AFB DC 20332-0001

10. SPONSORING/MONITORING AGENCY REPORT NUMBER

2301/DS

11. SUPPLEMENTARY NOTES

12a. DISTRIBUTION/AVAILABILITY STATEMENT

UNLIMITED

12b. DISTRIBUTION CODE

13. ABSTRACT *(Maximum 200 words)*

The following symposium was held

Advanced Solid State Lasers
Compact Blue-Green Lasers
Integrated Photonics Research
Nonlinear Guide-Wave Optics
Optical Amplifiers & Their Applications
Optical Design for Photonics
Photonics in Switching
Quantum Optoelectronics
Shortwavelength: Physics With Intense Laser Pulses
Soft X-Ray Protection Lithography
Ultrafast Electronics & Optoelectronics
Optical Computing
Spatial Light Modulators

14. SUBJECT TERMS			15. NUMBER OF PAGES
			16. PRICE CODE
17. SECURITY CLASSIFICATION OF REPORT	18. SECURITY CLASSIFICATION OF THIS PAGE	19. SECURITY CLASSIFICATION OF ABSTRACT	20. LIMITATION OF ABSTRACT
UNCLASS	UNCLASS	UNCLASS	UL

PAGES _____

ARE

MISSING

IN

ORIGINAL

DOCUMENT

Soft X-Ray Projection Lithography

Summaries of papers presented at the
Soft X-Ray Projection Lithography Topical Meeting

May 10–12, 1993
Monterey, California

TECHNICAL DIGEST
CONFERENCE EDITION

Sponsored by
Optical Society of America

Partially Supported by
Air Force Office of Scientific Research
Defense Advance Research Projects Agency
Department of Energy

Optical Society of America
2010 Massachusetts Avenue, NW
Washington, DC 20036–1023

Articles in this publication may be cited in other publications. In order to facilitate access to the original publication source, the following form for the citation is suggested:

> Name of Author(s), "Title of Paper," in Soft X-Ray Projection Lithography Technical Digest, 1993 (Optical Society of America, Washington, D.C., 1993), pp. xx–xx.

ISBN Number
Conference Edition 1-55752-303-7

Library of Congress Catalog Card Number
Conference Edition 92-62914

Printed in U.S.A.

CONTENTS

TECHNICAL PROGRAM COMMITTEE

Andrew M. Hawryluk, *Chair*
Lawrence Livermore National Laboratory

Richard H. Stulen, *Chair*
Sandia National Laboratories

David T. Attwood
Lawrence Berkeley Laboratory

Jeffrey Boker
University of California, Berkeley

John H. Bruning
GCA/Tropel

Natale M. Ceglio
Lawrence Livermore National Laboratory

John Frank
SEMATECH

Donald C. Hofer
IBM Almaden Research Center

Hiroo Kinoshita
NTT LSI Laboratories, Japan

Marc Levenson
IBM Almaden Research Center

David A. Markle
Ultratechstepper

William T. Silfvast
University of Central Florida (CREOL)

David L. Windt
AT&T Bell Laboratories

Frits Zernike
SVG Lithography Systems, Inc

MONDAY, MAY 10, 1993

BONSAI II & III

8:30 am–8:45 am
OPENING REMARKS
R H Stulen, *Sandia National Laboratories, Chair*
Andrew M. Hawryluk, *Lawrence Livermore National Laboratory, Chair*

8:45 am–12:00 m
MA, MODELING
Richard R Freeman, *AT&T Bell Laboratories, Presider*

8:45 am (Keynote)
MA1 Future lithographic requirements, John R Carruthers, *Intel Corp* The future manufacture of ICs beyond 2000 will require pattern transfer systems of considerable complexity and cost The implications of these requirements on continuing the scaling treadmill approach for ULSI development are discussed **(p. 2)**

9:15 am (Invited)
MA2 Simulation of soft-x-ray images from a 1:1 ringfield optic, O R Wood, II, R. M D'Souza, M Himel, J. E Bjorkholm, K Early, L A Fetter, R R Freeman, L H Szeto, D E Tennant, D W Taylor, A A MacDowell, L Eichner, W K Waskiewicz, D. L White, D. L. Windt, *AT&T Bell Laboratories,* D M Williamson, F Zernike, *SVG Lithography Systems, Inc ,* T E Jewell, *Optical Design Consulting.* D Lee, A R Neureuther, D M. Newmark, *UC-Berkeley* We have analyzed the experimentally observed effects of annular illumination and surface figure errors on the soft x-ray images produced with a 1 1 ringfield optic by including wavefront error data on the reflecting surfaces in a diffraction-based optical image simulation. **(p. 3)**

9:45 am
MA3 Two aspheric mirror system design development for SXPL, T. E Jewell, *Optical Design Consultant* A generalized procedure for an optical design of a two aspheric mirror system free of spherical aberration, coma, astigmatism, and field curvature at any given magnification is described **(p. 7)**

10:05 am
MA4 Physical optics modeling of SXPL imaging experiments, Weng W Chow, William C Sweatt, *Sandia National Laboratories,* George N Lawrence, *Applied Optics Research,* Tanya E Jewell, *Consultant.* We report our progress on the physical optics modeling of Sandia/AT&T SXPL experiments The code is benchmarked and the 10x Schwarzchild system is being studied **(p. 9)**

10:25 am–10:50 am COFFEE BREAK (Bonsai Foyer)

10:50 am (Invited)
MA5 Application of lithography simulation to projection x-ray, A R Neureuther, *UC-Berkeley.* Simulation tools from optical lithography are helping address x-ray projection technology issues such as effects of residual lens aberrations, resist characterization, and scattering in multilayer masks **(p. 12)**

MONDAY, MAY 10, 1993—*Continued*

11:20 am
MA6 Solutions to critical problems in SXPL, Andrew M Hawryluk, Gary Sommargren, Richard Levesque, *Lawrence Livermore National Laboratory* We have devised a mask repair procedure which should recover the local x-ray reflectivity from defects in the multilayer coating Simulations of this process are presented **(p. 13)**

11:40 am
MA7 Study of defects in multilayer reflective coatings for SXPL mask, Khanh B Nguyen, Tai D Nguyen, David Attwood, *Lawrence Berkeley Laboratory,* Alfred K Wong, Andrew R Neureuther, *UC-Berkeley* The effects of absorber imperfections, incidence angle and defects in the multilayer reflective coatings on the performance of reflection masks for SXPL are studied by cross-sectional TEM and by TEMPEST, a massively parallel time domain finite difference program **(p. 14)**

12:00 m–1:30 pm LUNCH BREAK (on your own)

BONSAI II & III

1:30 pm–3:50 pm
MB, CONDENSER
Natale Ceglio, *Lawrence Livermore National Laboratory, Presider*

1:30 pm (Keynote)
MB1 Limits of ultraviolet lithography, R. Fabian Pease, *Stanford Univ* Any new technology must offer significant improvement over an entrenched technology to become adopted We describe where ultraviolet lithography might evolve in ten years, the earliest possible time for soft x ray lithography to be ready for manufacture **(p. 20)**

2:00 pm
MB2 Condenser optics for SXPL, Steve Vernon, *Vernon Applied Physics,* Gary Sommargren, Lynn Seppala, David Gaines, *Lawrence Livermore National Laboratory* Condenser optics has been designed, fabricated, and coated for use in a front-end test bed facility at LLNL Details of condenser design and coating processes are discussed. **(p. 21)**

2:20 pm
MB3 X-ray characterization of a three-element condenser system for soft x-ray projection lithography, D P Gaines, *Brigham Young Univ ,* G L Sommargren, *Lawrence Livermore National Laboratory,* S P Vernon, *Vernon Applied Physics* A three-stage evaluation procedure has been designed to characterize the performance of the condenser system. First, the figure and radii of curvature of the uncoated optics were measured using conventional visible-wavelength techniques Second, a point by point x-ray characterization of the individual (coated) optics was performed Finally, these data were used in an optics ray-trace code to predict condenser system performance. **(p. 22)**

2:40 pm–3:10 pm REFRESHMENT BREAK (Bonsai Foyer)

3:10 pm
MB4 High-efficiency condenser for laser plasma sources and ringfield masks, D. L. White, *AT&T Bell Laboratories.* A SXPL for ringfield cameras is described. It has two reflections and can collect over 50% of the energy radiated from a laser plasma source. **(p. 23)**

3:30 pm
MB5 High-efficiency condenser design for illuminating a ring field, William C. Sweatt, *Sandia National Laboratories.* This condenser couples a laser-plasma source into the 60° ring field of a camera designed for projection lithography. Quasi-Köhler illumination is achieved over the whole ring field. **(p. 27)**

BONSAI II & III

3:50 pm–4:50 pm
MC, MULTILAYER 1
Glenn Kubiak, *Sandia National Laboratories, Presider*

3:50 pm
MC1 Surface finish requirements for SXPL optics, D. L. Windt, W. K. Waskiewicz, J. Griffith, J. E. Bjorkholm *AT&T Bell Laboratories.* We describe the surface finish requirements and metrology techniques necessary to develop high-reflectance, normal-incidence x-ray mirrors for projection lithography at 14 nm. **(p. 32)**

4:10 pm
MC2 Substrate recovery of Mo-Si multilayer coated optics, D. G. Stearns, S. L. Baker, *Lawrence Livermore National Laboratory.* Mo-Si multilayer coatings have been removed from optical substrates using reactive ion etching in a SF_6 plasma, and effects of the etching process on the surface finish and substrate figure have been investigated. **(p. 35)**

4:30 pm
MC3 Masked deposition techniques for controlling multilayer period variation on shortwavelength reflective lenses, J. B. Kortright, E. M. Gullikson, P. E. Denham, *Lawrence Berkeley Laboratory.* Deposition and measurement techniques are described for production of multilayer reflective coatings with specifically tailored thickness variation on curved optics. A Schwarzschild objective coated to operate at 68 Å is discussed as an example. **(p. 36)**

BONSAI II & III

8:30 am–11:30 am
TuA, IMAGING EXPERIMENTS
David A. Markle, *Ultratechstepper, Presider*

8:30 am (Keynote)
TuA1 Migration path to nanometer lithography—from the viewpoint of VLSIs, Eiji Takeda, *Hitachi Ltd., Japan.* This paper discusses which technologies are most promising as a nanometer (<0.1 μm) lithography system—optical, e-beam, proximity x-ray, and projection x-ray lithographies, from the viewpoint of gigascale integrations. **(p. 40)**

9:00 am (Invited)
TuA2 Soft x-ray projection lithography in Japan, Hiroo Kinoshita, *NTT LSI Laboratories, Japan.* The present state of SXPL in Japan will be reviewed, including major recent results achieved at NTT. **(p. 44)**

9:30 am (Invited)
TuA3 Development and characterization of a 10x Schwarzschild system for SXPL, D. A. Tichenor, G. D. Kubiak, M. E. Malinowski, R. H. Stulen, S. J. Haney, K. W. Berger, R. P. Nissen, R.L. Schmitt, G. A. Wilkerson, L. A. Brown, P. A. Spence, P. S. Jin, W. C. Sweatt, W. W. Chow, *Sandia National Laboratories;* J. E. Bjorkholm, R. R. Freeman, M. D. Himel, A. A. MacDowell, D. M. Tennant, O. R. Wood, II, W. K. Waskiewicz, D. L. White, D. L. Windt, *AT&T Bell Laboratories;* T. E. Jewell, *Optical Engineering Consultant.* A 10x Schwarzschild system for SXPL imaging using a plasma source is described. The objective is designed for a 0.4-mm FOV using 0.1-μm design rules. **(p. 45)**

10:00 am–10:30 am COFFEE BREAK (Bonsai Foyer)

10:30 am
TuA4 Soft x-ray projection imaging using 32:1 Schwarzschild optics, Hiroshi Nagata, Masayuki Ohtani, Katsuhiko Murakami, Tetsuya Oshino, *Nikon Corp., Japan;* Yukihiko Maejima, Toshihiko Tanaka, Tadeo Watanabe, Yoshio Yamashita, Nobufumi Atoda, *SORTEC Corp., Japan.* We examine 32:1 reduction lithography suing a Mo-Si multilayer coated Schwarzschild objective with a SR light source. Line-and-space patterns down to 0.1 μm were fabricated. **(p. 49)**

10:50 am
TuA5 New surface imaging resist technology for SXPL, A. A. MacDowell, O. R. Wood, II, *AT&T Bell Laboratories;* J. M. Calvert, T. S. Koloski, *U.S. Naval Research Laboratory.* An x-ray sensitive self-assembled monolayer organosilane film was patterned using a 20:1 reduction Schwarzschild optic illuminated at 14 nm. The resulting latent image was then selectively metallized via electroless deposition of nickel to form a plasma etch mask for pattern transfer. **(p. 52)**

11:10 am
TuA6 High-resolution imaging of laser-produced plasmas at 130 Å using normal incidence multilayer mirror microscope, J. F Seely, G. E. Holland, J. V Giasson, *U.S. Naval Research Laboratory* Laser-irradiated targets were imaged at 130 Å and with resolution of 5 μm using a Cassegrain-type microscope consisting of two Mo-Si multilayer mirrors. **(p. 56)**

11:30 am–1:00 pm LUNCH BREAK (on your own)

BONSAI II & III

1:00 pm–3:10 pm
TuB, OPTICAL METROLOGY
Frits Zernike, Jr., *SVG Lithography Systems, Inc , Presider*

1:00 pm (Keynote)
TuB1 Cost of ownership for SXPL, William H Arnold, Kathleen Early, *Advanced Micro Devices.* This paper explores the projected cost of ownership for a SXPL process The results of the calculations are stated in terms of dollars per wafer level exposed. These are then compared with current cost estimates for optical lithography processes in order to frame the problem in a realistic way. **(p. 62)**

1:30 pm (Invited)
TuB2 To be announced, John H. Bruning, *GCA/Tropel* **(p. 63)**

2:00 pm (Invited)
TuB3 Optic fabrication and metrology for SXPL, Marc D Himel, *AT&T Bell Laboratories* I review the techniques being investigated to fabricate and characterize high accuracy aspheric mirrors and systems for SXPL **(p. 64)**

2:30 pm
TuB4 Surface metrology of soft x-ray optics, T Vorburger, T McWaid, J. Fu, C J. Evans, W T Estler, R E Parks, *NIST-Gaithersburg* We are developing approaches for the calibrated measurement of surface topography of x-ray mirrors over a spatial wavelength range of 1–150 mm Results for both figure and finish measurement are presented. **(p. 66)**

2:50 pm
TuB5 Nanometer-precision Fizeau interferometer for testing SXPL optics, Chunsheng Huang, John H Bruning, *General Signal* An ultraprecise interferometer suing a HeNe laser is described The interferometer is characterized and demonstrates 1-nm reproducibility over a clear aperture of 61 mm **(p. 69)**

3:10 pm–3:40 pm REFRESHMENT BREAK (Bonsai Foyer)

TUESDAY, MAY 11, 1993—*Continued*

3:40 pm–4:30 pm
TuC, X-RAY METROLOGY
David T Attwood, *Lawrence Berkeley Laboratory, Presider*

3:40 pm (Invited)
TuC1 Point diffraction interferometry at soft x-ray wavelengths, Gary E Sommargren, *Lawrence Livermore National Laboratory;* Ralph Hostetler, *Allied Signal Technical Services* We describe the design and lithographic fabrication of an array of point diffraction interferometers on a Si_3N_4 membrane that has been overcoated with a spatially graded absorbing film to provide fringe contrast control Experimental results are presented. **(p. 74)**

4:10 pm
TuC2 Beamline design for at wavelength interferometry, K Jackson, R Beguiristain, M Koike, D. Attwood, *Lawrence Berkeley Laboratory,* G. Sommargren, *Lawrence Livermore National Laboratory.* As part of the national program in projection x-ray lithography the Center for X-ray Optics (CXRO/LBL) proposes to construct a beamline for "at wavelength" interferometry **(p. 75)**

DeANZA III

4:30 pm–6:00 pm
TuD, POSTER SESSION/CONFERENCE RECEPTION

TuD1 New reflectometry facility at the National Institute of Standards and Technology, C Tarrio, R N. Watts, T. B Lucatorto, *NIST,* M Haass, T A Calcott, J Jia, *Univ. Tennessee* We describe the characteristics and performance of our newly commissioned soft x-ray monochromator and the hybrid optical reflectometry beam line to be used during 1993 **(p. 80)**

TuD2 Subaperture testing for SXPL aspherical optical surfaces, Chunsheng Huang, *General Signal.* A method for testing SXPL aspheres without a null lens is developed. Capability of testing an asphere with 1-nm precision is demonstrated **(p. 81)**

TuD3 Specifying the surface finish of x-ray mirrors, E L Church, *US ARDEC,* P Z. Takacs, *Brookhaven National Laboratory* Our measurement of synchrotron x-ray mirrors indicate that the power spectral densities of their finish errors have inverse power-law or fractal forms, rather than being flat at low frequencies as is usually assumed. We review these data and discuss how this apparent divergent behavior leads to finite but unconventional effects in imaging **(p. 85)**

TuD4 FEL sources for SXPL on the Duke 1 GeV storage ring, Lewis E Johnson, John M. J. Madey, *Duke Univ.* Construction of a 1 GeV electron storage ring at the Duke Free Electron Laser Laboratory (Duke University, Durham, NC) is currently in the second of three phases Commissioning of the ring and the first source (NIST undulator) is scheduled to being in the fourth quarter of 1993. We describe the FEL laboratory and its soft x-ray and UV-VUV sources. **(p. 89)**

TuD5 Soft X-ray conversion efficiencies from laser-produced plasmas for SXPL sources, R C Spitzer, R L Kauffman, T Orzechowski, D W Phillion, C Cerjan, *Lawrence Livermore National Laboratory* Laser-produced plasmas have been investigated as a source for x-ray projection lithography The dependence of conversion efficiency on target material, intensity, spot diameter, wavelength and pulse width has been studied using absolutely calibrated detectors. **(p. 91)**

TuD6 Thermal distortion effects on optical substrates that reduce coherence properties of undulator beamlines, Raul Beguiristain, *Lawrence Berkeley Laboratory.* Calculation of the surface deformation that will degrade partial coherence and brightness properties of the beam will be presented for different types of optical substrates submitted to high thermal load in undulator beamlines. **(p. 93)**

TuD7 Monochromator optics for coherent illumination of an undulator beamline, Masato Koike, *Lawrence Berkeley Laboratory* Soft x-ray beamline optics consisting of a variable spaced spherical grating monochromator, with a Kirkpatrick-Baez prefocus system, is investigated for provision of spatially and temporally coherent illumination of an "at wavelength" XUV interferometer Throughput and stabilities in the presence of source instabilities are also discussed **(p. 95)**

TuD8 Printing a 500-Å period grating using x-ray interference, Max Wei, *Lawrence Berkeley Laboratory,* Erik Anderson, *UC-Berkeley* A method for printing a 500 Å period grating using x-ray interference is described Preliminary results are presented and a grating gate transistor proposed **(p. 98)**

TuD9 Manufacture and characterization of holographic diffraction gratings for soft x-rays, Alexander Irtel von Brenndorff, *Geo.g-August Univ. Gottingen, Germany* Holographic diffraction gratings for soft x rays have been fabricated and tested Variation of the manufacture process and examination with a STM yields a minimum surface roughness **(p. 102)**

TuD10 Modeling SXPL, Bernice M Lum, *Lawrence Berkeley Laboratory,* Andrew R Neureuther, *UC-Berkeley,* Glenn D. Kubiak, *Sandia National Laboratories* Quantitative models for simulating resist dissolution at soft x-ray wavelengths in SAMPLE are being established through analysis of existing data and measurements of promising new deep-UV resist materials **(p. 106)**

TuD11 Image simulation for soft-x-ray projection printing, Derek C Lee, *Lawrence Berkeley Laboratory;* Andrew R Neureuther, *UC-Berkeley* The effect of measured imperfections in lens elements on projection x-ray imaging can be simulated in SPLAT based on detailed optical systems wavefront maps output from CodeV **(p. 107)**

TuD12 Computational analysis of debris formation in SXPL laser-plasma sources, Timothy G. Trucano, Dennis E Grady, Richard E. Olson, Archie Farnsworth, *Sandia National Laboratories* We present a computational methodology for predicting the formation of target debris in laser generated XUV sources applicable to SXPL **(p. 109)**

TUESDAY, MAY 11, 1993—*Continued*

TuD13 Velocity characterization of target debris from a laser-produced plasma utilizing a "time-of-flight" technique, H A Bender, A M Eligon, A Hanzo, W T Silfvast, *Univ Central Florida* Measurements of the velocity and particle size distributions as well as calculations of ejected mass for particulate emission from a laser produced plasma have been made on solid Sn and Au targets for conditions associated with SXPL Results indicate that small particles, $< 1-2$ μm in diameter, with speeds in excess of 9000 cm/s, are the dominant constituents of the debris **(p. 113)**

TuD14 Constraints on pulse power and duration for soft x-ray lithography systems, J A Liddle, *AT&T Bell Laboratories* The practicable ranges of pulse power and duration of a pulsed source system are constrained by thermal effects We describe an appropriate model and present its results **(p. 116)**

TuD15 Computational simulations of a SXPL laser plasma source, R E Olson, W. C Sweatt, P D Rockett, *Sandia National Laboratories* An understanding of 14 nm source brightness has been gained via experimentally benchmarked computer simulations of laser plasma source experiments **(p. 118)**

TuD16 Cryogenic targets for laser plasma x-ray lithography sources, Martin Richardson, Kai Gabel, Feng Jin, William T Silfvast, *Univ Central Florida* We propose the use of mass-limited cryogenic targets for SXPL, permitting a continuous supply of targets without the problems of particulate debris **(p. 121)**

TuD17 Calibration and metrology of x-ray optics at the center for x-ray optics, E M Gullikson, J H Underwood, *Lawrence Berkeley Laboratory.* Efforts in the area of calibrations and standards particularly for x-ray lithography, are summarized A bending magnet beamline dedicated to standards will be constructed at the advanced light source **(p. 124)**

WEDNESDAY, MAY 12, 1993

BONSAI II & III

8:30 am–12:00 m
WA, SOURCES 1
Donald C Hofer, *IBM Almaden Research Center, Presider*

8:30 am (Invited)
WA1 Enhanced performance of KrF laser-induced x-ray sources and multilayer mirrors for SXPL, F Bijkerk, E Louis, L Shmaenok, H -J Voorma, M. J van der Wiel, *FOM-Institute for Plasma Physics Rijnhutzen, The Netherlands,* R Schlatmann, J. Verhoeven, *FOM-Institute AMOLF, The Netherlands,* E. W J. M. van der Drift, J Romijn, B A. C Rousseeuw, *Delft Institute for Microelectronics and Submicron Technology, The Netherlands,* F Vaß, R. Dėsor, B. Nikolaus, *Lambda Physik GmbH, Germany.* We report results of a joint SXPL program on KrF laser plasma sources and Mo-Si multilayer mirrors a source conversion efficiency of 0.7% at 13 5 nm (2% BW), and elimination of accumulative layer roughness of the mirrors **(p. 128)**

9:00 am (Invited)
WA2 Laser plasma source characterization for SXPL, William Silfvast, M C Richardson, H. Bender, A M Eligon, A Hanzo E Miesak, F Jin, *Univ. Central Florida.* A review of the status of laser plasma soft x-ray sources is reviewed and includes discussions of radiation properties as well as particulate emission and interdiction techniques **(p. 131)**

9:30 am
WA3 Laser plasma source targets for SXPL: production and mitigation of debris, Glenn D. Kubiak, Kurt W. Berger, Steven J. Haney, *Sandia National Laboratories* Studies of the debris production from various laser plasma source target materials and geometries, as well as methods to suppress its deposition onto nearby optical elements, are presented The effects of target ejecta on the performance and morphology of multilayer-coated optics, both before and after chemical removal of debris deposits, are discussed. **(p. 132)**

9:50 am
WA4 Investigation of discharge-laser-driven plasmas as sources for SXPL, Paul D. Rockett, John A Hunter, Richard E Olson, William C Sweatt, Glenn D. Kubiak, Kurt W Berger, Randal L Schmitt, *Sandia National Laboratories,* Harry Shields, Michael Powers, *Jamar Technology Co Inc ,* David L. Windt, *AT&T Bell Laboratories* The optical characteristics of several discharge-laser-plasma x-ray sources were studied in order to optimize their use in SXPL **(p. 134)**

10:10 am–10:40 am COFFEE BREAK

WEDNESDAY, MAY 12, 1993—*Continued*

10:40 am
WA5 Spectral characterization of plasma soft x-ray sources for lithographic applications, Charles Cerjan, *Lawrence Livermore National Laboratory* Synthetic spectra are presented that characterize the evolution of plasma conditions achieved during irradiation of Sn targets as a function of laser intensity and wavelength. **(p. 138)**

11:00 am
WA6 Solid-state laser driver for projection x-ray lithography, Lloyd A. Hackel, C. Brent Dane, Mark R. Hermann, Luis E Zapata, *Lawrence Livermore National Laboratory* The design of a diode pumped solid state laser for use as an x-ray driver is described Progress to date and experimental results are presented. **(p. 139)**

11:20 am
WA7 Soft x-ray generation by a tabletop highly repetitive glass laser, H Aritome, K Haramura, *Osaka Univ., Japan,* H Sekiguchi, H. Hara, T. Mochizuki, *HOYA Corp , Japan.* Soft x-ray generation from a recently developed, tabletop, highly repetitive, high energy moving glass slab laser is demonstrated, and the absolute intensity is measured **(p. 140)**

11:40 am
WA8 Compact synchrotron and condenser for SXPL, D L. White, A. A MacDowell, O. R. Wood II, *AT&T Bell Laboratories;* J B Murphy, *Brookhaven National Laboratory.* A preliminary design is given for an integrated synchrotron soft-x-ray source and condenser system that could be used in the commercial production of semiconductor chips **(p. 141)**

12:00 m–1:30 pm LUNCH BREAK (on your own)

BONSAI II & III

1:30 pm–2:30 pm
WB, MULTILAYER 2
David L Windt, *AT&T Bell Laboratories, Presider*

1:30 pm
WB1 Residual stresses in Mo-Si multilayers and their response to thermal annealing, J Koike, M. E. Kassner, F J. Weber, *Oregon State Univ.,* D. G Stearns, R S. Rosen, *Lawrence Livermore National Laboratory,* S. P Vernon, *Vernon Applied Physics* The thermal stability of sputter-deposition Mo-Si multilayers was investigated by annealing studies at relatively low temperatures for various times Two distinct stages of thermally-activated Mo-Si interlayer growth were found a relatively rapid initial "surge" of approximately one monolayer, followed by a (slower) secondary "steady-state" growth that is diffusion controlled. The interdiffusion coefficients for the interlayer formed during deposition of Mo on Si are substantially higher than those of the interlayer formed during deposition of Si on Mo It was also observed that significant residual tensile elastic strains develop within the Mo layer (normal to the multilayer) as a result of annealing. Explanations for these observed behaviors are presented **(p. 146)**

1:50 pm
WB2 Effects of microstructure and interfacial roughness on normal incidence reflectivity of Ru/C and Ru/B_4C multilayers at 7 nm wavelength, Tai D. Nguyen, Ronald Gronsky, Jeffrey B. Kortright, *Lawrence Berkeley Laboratory.* Effects of interfacial roughness on the normal incidence reflectivity of Ru/C and RuB_4C multilayers at 7 nm. wavelength upon annealing are presented. The relationship of the roughness to the microstructure in the multilayers is discussed. **(p. 147)**

2:10 pm
WB3 Tarnishing and restoration of Mo-Si multilayer x-ray mirrors, J. H. Underwood, E. M. Gullikson, Khanh Nguyen, *Lawrence Berkeley Laboratory.* Mo-Si multilayer mirrors were found to decline in reflectivity with time, primarily due to oxidation of the uppermost molybdenum layer. Various methods of prevention and restoration are discussed. **(p. 151)**

2:30 pm–3:00 pm REFRESHMENT BREAK
(Bonsai Foyer)

BONSAI II & III

3:00 pm–3:40 pm
WC, ALTERNATE STRATEGIES
John Frank, *SEMATECH, Presider*

3:00 pm
WC1 SXPL using two arrays of phase zone plates, Scott D. Hector, Henry I. Smith, *Massachusetts Institute of Technology.* A system for unity magnification, scanning, SXPL is described that consists of two planar arrays of phase zone plates ($\sim 10^4/cm^2$) **(p. 156)**

3:20 pm
WC2 Zone plate arrays in projection x-ray lithography, M. Feldman, *Louisiana State Univ.* Arrays of zone plates are used for projection x-ray lithography in both 1:1 and reduction imaging systems, with high resolution and high x-ray beam utilization **(p. 160)**

3:40 pm–4:00 pm
CLOSING REMARKS

Modeling

MA 8:45am–12:00m
Bonsai II & III

Richard R. Freeman, *Presider*
AT&T Bell Laboratories

Future Lithographic Requirements

John R. Carruthers
Intel Corporation
Santa Clara, CA 95052

The future manufacture of IC's beyond 2000 will require pattern transfer systems of considerable complexity and cost. Critical dimensions below 150 nm must be controlled in three dimensions without interference from proximity effects and with an overlay/alignment capabili.y that approaches 50 nm (3 sigma) from layer to layer over larger field sizes of 25 to 30 mm on a side. The metrology to develop and control these systems also needs to be developed with precision approaching atomic dimensions. The implications of these requirements on continuing the scaling treadmill approach for ULSI development are discussed.

Simulation of Soft-X-Ray Images from a 1:1 Ring-Field Optic

O. R. Wood, II, R. M. D'Souza, M. Himel, J. E. Bjorkholm,
K. Early, L. A. Fetter, R. R. Freeman, L. H. Szeto,
D. E. Tennant, D. W. Taylor
AT&T Bell Laboratories, Crawfords Corner Road, Holmdel, NJ 07733
(908) 949-6339

T. E. Jewell
Optical Design Consulting, Boulder, CO 80304

D. Lee, A. R. Neureuther, D. M. Newmark
EECS Department, University of California, Berkeley, CA 94720

A. A. MacDowell
AT&T Bell Laboratories, 510E Brookhaven Lab., Upton, NY 11973

L. Eichner, W. K. Waskiewicz, D. L. White, D. L. Windt
AT&T Bell Laboratories, 600 Mountain Ave., Murray Hill, NJ 07974

D. M. Williamson, F. Zernike
SVG Lithography Systems, Inc., Wilton, CT 06897

Using a recently extended version of the two-dimensional aerial image simulator, SPLAT[1], we show that annular illumination of a soft-x-ray 1:1 ring-field camera at 13 nm increases image contrast for features with spatial frequencies immediately above the coherent cutoff and that surface figure errors are responsible for the asymmetric, spatially-shifted images that have been observed experimentally.

The experimental arrangement recently used[2] to produce soft-x-ray images with a Mo/Si multilayer coated 1:1 ring-field optic is shown in Fig. 1. The 13 nm wavelength radiation (the third harmonic from the undulator on the U13 beam line of the VUV storage ring at the National Synchrotron Light Source) is incident upon a two-mirror rotator that produces a cone of illumination whose apex is located at a mask. The imaging optic, a modified 1:1 Offner ring-field camera[3] (from a Perkin-Elmer Model 300 Micralign Projection Printer), produces a unity magnification image of the mask on a resist coated wafer. During a resist exposure the rotator completes more than one revolution and, hence, the resist image is a composite of a number of images each produced with a different source position. Thus, use of the rotator is expected to result in partially coherent illumination of the imaging optic with the degree of partial coherence determined by the cone angle (the degree of partial coherence is set to 0.42 in the present work).

According to the Rayleigh Criterion, at a numerical aperture (NA) of 0.0835 the ring-field optic should be able to produce diffraction limited images of 0.1 μm features when illuminated at

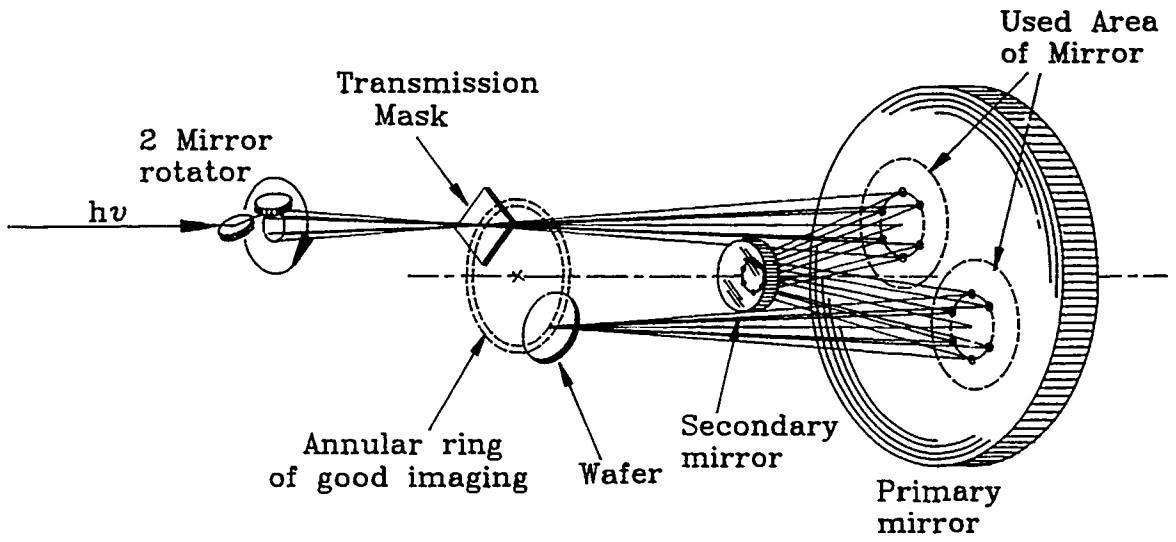

Figure 1. Experimental arrangement for soft-x-ray imaging with a Mo/Si multilayer coated 1:1 ring-field optic illuminated with undulator radiation.

13 nm.[4] Experimentally, the imaging limit was found to be 0.15 μm for coherent illumination (rotator stopped) and 0.2 μm for partially coherent illumination (rotator continuously moving).[2] In addition, most resist images exhibited some evidence of spatial shifts during the exposure. These observations led us to suspect either that the undulator radiation-rotator combination is not providing a good approximation to partially coherent illumination or that surface figure errors are limiting the imaging performance.[2]

To separate the effects of annular illumination from those caused by surface figure errors, we used the SPLAT image simulation program to calculate aerial images of equal line and space gratings of varying periods for a diffraction limited 0.0835 NA system annularly illuminated at 13 nm. The two-mirror rotator, shown in Fig. 1, produces an annulus of illumination in the pupil of the imaging system (located at the secondary mirror) with an outer radius filling 42% of the pupil radius and an inner radius filling 41.96%. The annulus is thin because the ring-field optic focuses distant objects, such as the undulator source, which is 14 m away, on the pupil. The SPLAT simulations show that image contrast with annular illumination is approximately 10% lower than with disk illumination for spatial frequencies below the coherent cutoff frequency and is slightly higher for frequencies immediately above the coherent cutoff frequency. The SPLAT simulations also show that a diffraction limited 0.0835 NA ring-field system, annularly illuminated at 13 nm, should image 0.1 μm features with a contrast exceeding 90%. Since, 0.2 μm features were the smallest that could be cleanly printed using this type of illumination, we now conclude that the imagery is not being dominated by the effects of annular illumination.

To calculate the effect of surface figure errors on the performance of our ring-field optic we modified the SPLAT image simulation program so that it would accept wave aberration data. A phase map of our primary ring-field mirror was obtained from phase measuring interferometry (PMI) at 633 nm. Measurement of our secondary was dominated by interferometer effects and was not included in the simulation. These data were attached to the spherical surfaces of the ring-field system using Code V.[5] The system was then evaluated, again using Code V, to give wave aberration data at the exit pupil of the system which were then used as inputs for the SPLAT simulations. In Fig. 2 we show

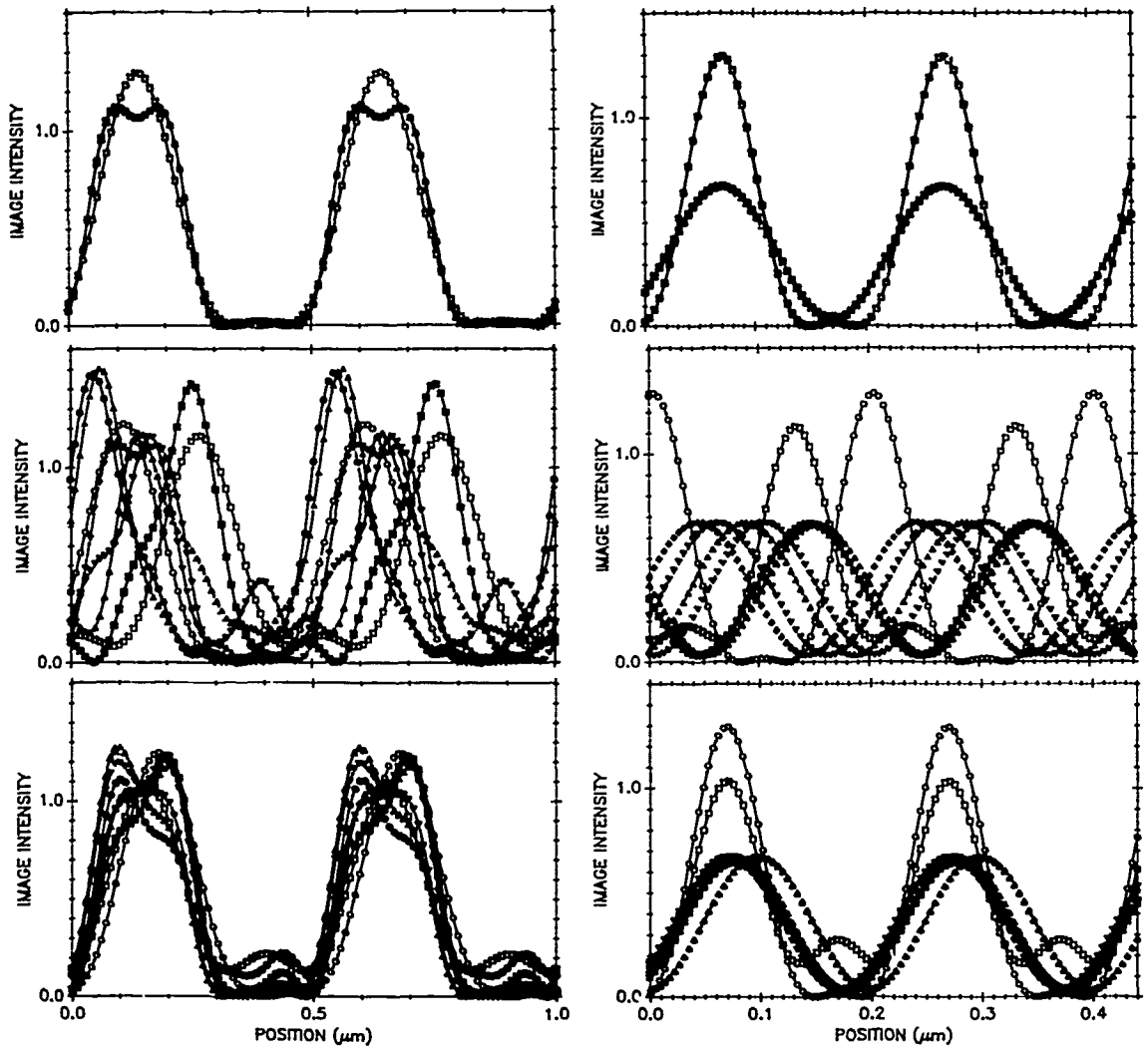

Figure 2. Calculated image intensity of 0.5 μm period grating (left-hand-side) and 0.2 μm period grating (right-hand-side) for a 0.0835 NA ring-field optic with perfect (top plots), highly aberrated (middle plots) and slightly aberrated (bottom plots) mirrors at 13 nm wavelength.

SPLAT simulations of the aerial images of 0.5 μm (left-hand-side plots) and 0.2 μm (right-hand-side plots) period grating objects produced by a 0.0835 NA ring-field optic with perfect (top

plots), highly aberrated (middle plots) and slightly aberrated (bottom plots) mirrors when illuminated with 13 nm radiation from the stationary undulator source at 8 equally spaced rotator positions. Each stationary rotator position represents a separate coherent source. The summation of the 8 separate images closely approximates partially coherent illumination. In the diffraction-limited case (top plots), the image intensity is higher at 12 and 6 o'clock than at other rotator positions where one or more diffraction orders are blocked by the aperture stop. In the highly aberrated mirror case (middle plots) the aerial images are seen to be shifted by varying amounts relative to their position on the mask. Based on these simulations, a 0.5 μm period grating is expected to produce a recognizable resist image whereas a 0.2 μm period grating is not. This is what was observed experimentally.[2] The simulations show that the highly aberrated mirrors result in aerial images that are asymmetrical and have finite amplitudes at spatial positions where the amplitude should be zero. The simulations also show that some rotator positions result in aerial images with higher contrast and higher fidelity than others. This was also observed experimentally.[2] The principal effect of the surface figure errors, however, is to limit the resolution of the system to that feature size which is comparable to the magnitude of the image shifts. In the slightly aberrated mirror case (bottom plots) the aerial images are reasonable close to those produced by perfect mirrors. These slightly aberrated mirrors have recently been multilayer coated and experiments to test their imaging performance are currently in progress.

In conclusion, SPLAT (Version 4.2) has been found to be a reliable aerial image simulator for annular illumination and surface figure errors in soft-x-ray projection lithography.

1. D. M. Newmark, "Computer aided design tools for phase-shift masks and spatial filtering," MS Thesis, Memorandum No. UCB/ERL M91/117, December 1991: K. H. Toh and A. R. Neureuther, Proc. SPIE **722** (1987).
2. A. A. MacDowell, et al.,in Soft-X-Ray Projection Lithography Technical Digest, 1992 (Optical Society of America, Washington, C.D., 1992), Vol. 8, pp. 75-78.
3. A. Offner, Opt. Eng. **14**, 130 (1975.
4. O. R. Wood, II, W. T. Silfvast and T. E. Jewell, J. Vac. Sci. Technol. B **7**, 1613 (1989).
5. Code V, Version 7.20, Optical Research Associates, 550 N. Rosemead Boulevard, Pasadena, California 91107.

Two Aspheric Mirror System Design Development for Soft-X-Ray Projection Lithography

T. E. Jewell
Optical Design Consultant
Boulder, CO 80304

Two-mirror reduction system design for soft-x-ray projection lithography application has been described[1,2]. 5X reduction two-aspheric-mirror design reported earlier[2] has small back clearance distance, which makes it difficult to build. In order to find an optimum design solution, which can provide the maximum back clearance distance at the minimum system length, the system magnification should be included in the design process as one of the variable parameters.

Several analytical expressions which describe system design parameters (mirror radius, the distance between mirrors, back clearance, and the system total length) as a function of system angular magnification (reduction ratio) have been developed. They describe the design solution for the system of a given magnification where third order spherical aberration and field curvature are corrected. The maximum back clearance relative to the system's total length is achieved at the reduction ratio of 7.5X. To correct coma and astigmatism in the ring field configuration, simple aspheric (conic) surfaces are used.

This design can be made telecentric at the image side, if the aperture stop is placed in the focal plane of the secondary mirror, although this makes the aperture non-accessible. To correct this problem, an off-axis aperture is placed on the primary mirror, which preserves an image space telecentricity at the center of the image field, but introduces small non-telecentricity error which increases linearly toward the edges of the field.

Distortion in this design is not corrected, since there are not enough degrees of freedom in the two-mirror configuration. The wavefront aberrations in this design form can be corrected to produce high resolution over the ring width of several millimeters, but uncorrected distortion limits this design. The difference in reduction ratio across the ring width in radial direction (local distortion) can be reduced at the expense of the ring width, and even brought down to a required level, for example, down to below 10 nm over the ring width of 0.4 mm [1].

One may think that when distortion is corrected locally, as the difference in reduction ratio across the ring width, it is possible to use this design in a scanning configuration, where both the mask and the wafer are scanned during exposure. Unfortunately, this is not the case. Conceptually, the act of scanning creates a non-rotationally symmetric condition for the system in use. In a scanning system,

distortion should be corrected not only locally, but it is also important to have no difference between the local and paraxial magnification. It is this difference in magnification that causes the shift of image point when the mask and wafer are scanned, resulting in the image smear. In this design, there is significant difference between the paraxial and the ring magnification that can not be controlled sufficiently.

Although, this ring-field, two-aspheric-mirror design can not be used in a scanning system, it can be used as an experimental prototype non-scanned system to demonstrate capabilities of important technologies: fabrication, testing and alignment of simple aspheric surfaces to required level of accuracy. This design can be used in the system serving as an intermediate step toward a practical three or four-mirror ring-field scanning system, where mirrors have more complicated aspheric surfaces.

1. K. Kurihara, H. Kinoshita, N. Takeuchi, T. Mizota, T. Haga, Y. Torii, "Two-mirror Telecentric Optics for Soft-x-ray Reduction Lithography." J. Vac. Sci. Technol. B9-6 (1991).

2. T. E. Jewell, K. P. Thompson and J. M. Rodgers, "Reflective Optical Designs for Soft-X-Ray Projection Lithography," Proc. SPIE, Vol. 1527, p. 163-173 (1991).

Physical Optics Modelling of Soft X-ray Projection Lithography (SXPL) Imaging Experiments

Weng W. Chow and William C. Sweatt
Sandia National Laboratories
Albuquerque, NM 87185
(505) 845-8566

George N. Lawrence
Applied Optics Research
4455 N. Osage Road
Tucson, AZ 85718

Tanya E. Jewell
Consultant
1105 N. Cedarbrook Road
Boulder, CO 80304

We report our progress on the modelling of the soft X-ray projection lithography imaging experiments that are being performed at Sandia National Laboratories and at AT&T Bell Laboratories. The system is shown in Fig. 1. It uses an elliptical mirror (condenser) to image a laser generated x-ray plasma source onto the entrance pupil of a Schwarzchild camera. The camera then images the mask ont the semiconductor wafer.

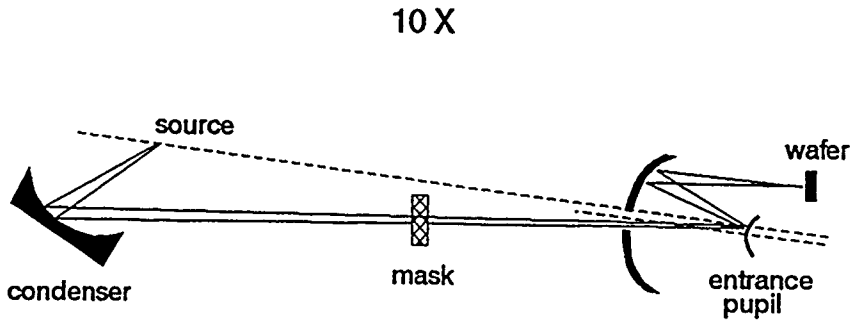

Fig. 1: 10X soft X-ray projection lithography experiment.

Our paper discusses the simulation of the partially coherent 14nm soft X-ray source. We model the X-ray source as a collection of point sources. The degree of coherence of the source is determined by the total area these point sources occupy at the entrance pupil of the camera. Considerable work as gone into verifying the accuracy of our model.

The above described X-ray source model was incorporated into a commercially available physical optics code, GLAD, from Applied Optics Research. In this paper, we present results of the images of a two-dimension mask pattern obtained from the code. In particular, we investigated the resolution of the system, the effects of coherence on

the image and the effects of aberrations in both the camera and the condenser. Figure 2 shows an example of the effects of astigmatism at the condenser.

This work is supported by the U.S. Department of Energy under Contract DE-AC04-76DP00789.

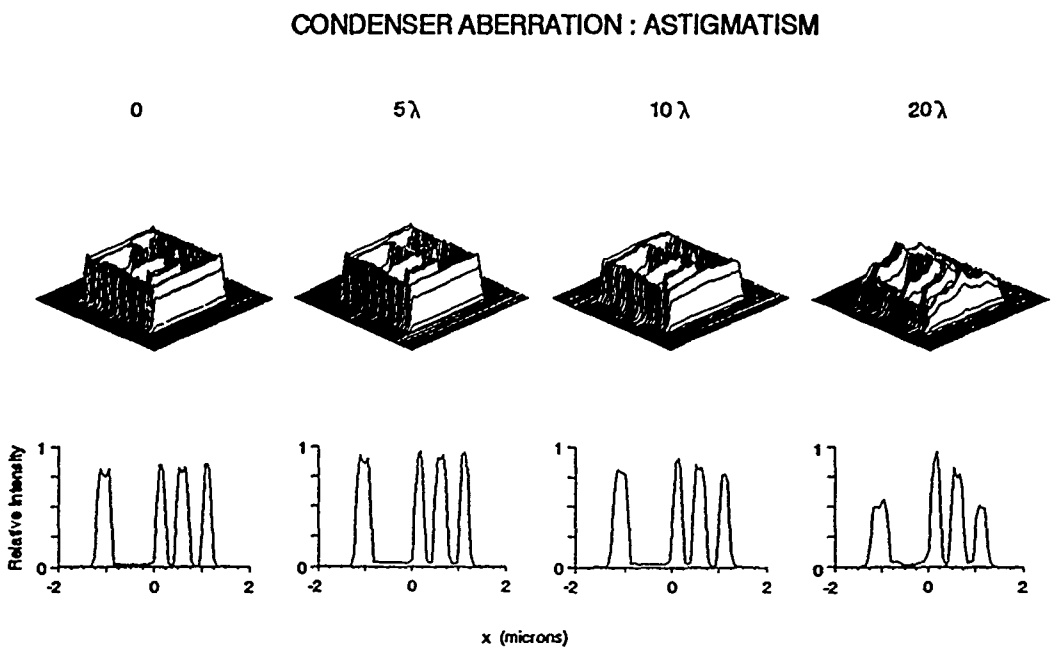

Fig. 2: Effects of astigmatism at the condenser on the mask image. The numbers above the figures indicates the number of wave (at 14nm) of astigmatism. The second row shows the isometric views of the mask image and the third row shows the intensity profile of a slice taken in the middle to the mask. Source incoherence is assumed to be 0.6.

Application of Lithography Simulation to Projection X-Ray

A.R.Neureuther
Department of Electrical Engineering & Computer Sciences and
The Electronics Research Laboratory
University of California, Berkeley 94720
(510) 642-4590

Simulators and materials modeling approaches from optical projection printing provide an advantageous starting point in addressing technology issues in the emerging field of projection x-ray lithography. A brief overview will be given of relevant imaging, resist characterization, resist exposure, resist dissolution, pattern transfer, and electromagnetic scattering programs available from Berkeley. The overview will also highlight important observations drawn from simulation and modeling which are helping optical projection printing at todays 0.35 um feature sizes. Key issues in projection x-ray lithography imaging, materials, and masks where these Technology CAD tools are making an impact will then be discussed.

The simulators and optical applications which will be discussed include, aerial image formation with modified illumination and phase-shift masks in SPLAT, phase-shift mask edge topography scattering effects in TEMPEST, resist dissolution characterization with PARMEX, and 3-D patterning and pattern transfer with SAMPLE-3D.

Pushing projection x-ray optical systems toward the ideal goal of diffraction limited optics is a key issue where aerial image simulation with SPLAT has been helpful. At x-ray wavelengths (13 nm) the level of residual aberrations with which the system designer may be forced to make tradeoffs during design is expected to be much higher that at optical wavelengths. To support the exploration of aberration effects SPLAT has been extended in collaboration with O. Wood of AT&T to accept wave front data synthesized from the optical elements and apply it to images of 2-D patterns [1].

The high absorption at projection x-ray wavelengths creates problems both in patterning wafers and in measuring resist dissolution characteristics. The optical projection printing simulators such as SAMPLE-3D can be used without change provided the quantitative values for optical constants and resist dissolution data can be determined. Since the exposure is confined to the near surface region the direct measurement of resist dissolution rates is difficult and indirect inference from alternative measurements may be necessary [2].

The multi-layer mask is another area where simulation may speed the technology development. Given the multiple reflection within the multi-layer structure the signal reflected from small openings in coated masks might be expected to walk sideways under the coating and enhance feature size dependent effects. The presence of a defect during the multi-layer coating process could produce widely different imaging effects depending upon the step coverage of the deposition process. The application of the TEMPEST electromagnetic simulation program to characterize these phenomena will be discussed [3].

[1-3] The SPLAT extensions, resist models, and TEMPEST applications are subjects of individual papers in this conference by D. Lee, B. Lum and K. Nguyen.

† Research supported by the Semiconductor Research Corporation via SEMATECH and by DARPA BG91-285.

Solutions To Critical Problems In Soft X-ray Projection Lithography

Andrew M. Hawryluk, Gary Sommargren and Richard Levesque
Lawrence Livermore National Laboraotory
Livermore, California 94551

Present soft x-ray projection lithography systems rely on laser produced plasmas for the production of x-rays and on multilayer coated reflective masks. Target debris from the laser produced plasma can coat condenser optics and reduce system performance. The difficulty in target debris mitigation results from the large range of velocities and masses ejected from the laser produced plasma. Proposed solutions have included the use of electrostatic deflectors, a partial pressure of helium and mechanical shutters. We have completed designs on a target debris mitigation system which should efficiently transmit soft x-rays ($\lambda \sim$ 13 nm) and prevent the ejected particles from reaching the condenser optics.

Repair of reflection masks is a critical issue in SXPL. Work on the repair of opaque and clear defects in the patterned layer (i.e., the metallization layer on top of the multilayer coating) has been reported. However, defects in the multilayer coating are likely to degrade the local x-ray reflectivity and print as an opaque defect. We have devised a mask repair procedure which should recover the local x-ray reflectivity from defects in the multilayer coating. Simulations of this process will be presented.

Study of Defects in Multilayer Reflective Coatings for Soft X-ray Projection Lithography Mask

Khanh B. Nguyen
Department of Electrical Engineering and Computer Science,
University of California, Berkeley
Center for X-ray Optics, Lawrence Berkeley Laboratory
MS 2-400, 1 Cyclotron Road, Berkeley, CA 94720
(510) 486-4051

Tai D. Nguyen
Department of Material Science and Mineral Engineering
Applied Science and Technology Graduate Group,
Center for X-ray Optics, Lawrence Berkeley Laboratory
University of California, Berkeley, CA 94720

Alfred K. Wong
Department of Electrical Engineering and Computer Science,
University of California, Berkeley, CA 94720

Andrew R. Neureuther
Department of Electrical Engineering and Computer Science,
University of California, Berkeley, CA 94720

David T. Attwood
Center for X-ray Optics, Lawrence Berkeley Laboratory
University of California, Berkeley, CA 94720

In a soft x-ray/EUV projection lithography system, multilayer reflective coatings consisting of 30-50 bilayers of alternating high-Z/low-Z materials would be used on all reflecting surfaces - collection optics, masks, and imaging optics. A reflection mask would likely be a multilayer coating with a top layer of patterned absorber [1, 2]. Since the mask is to be faithfully reproduced on the wafer, any mask defects and imperfections would also be reproduced.

In this paper, defects in the multilayer coatings on a reflective mask is studied, both in the way defect geometry propagates with subsequent layers in the stack and in their effects on the areal image. The effect on the reflected image of the incidence angle, non-vertical absorber profile, and absorber thickness are also investigated.

Defects in the multilayer coatings must be kept extremely low in order to satisfy the performance requirement of an EUV projection printer. These defects could arise from various sources including imperfections in the deposition process, cleanroom contaminants, and imperfect substrates. While a local defect on an optic results in a distributed degradation of system performance, a local defect on a mask is reproduced as a feature on the wafer. As the result, while some defect might be tolerable on optics, none can be tolerated on a mask.

With incidence wavelength of 140 Å, a surface height variation of only 40 Å would be sufficient to create a zero crossing in the reflected amplitude, resulting in a significant drop-off in the reflected image intensity, even for defect sizes below the resolution of the optical system. This implies very stringent defect control on the mask substrates before multilayer coating deposition and careful inspection afterwards. In addition, the manner in which the multilayer coating deposition process covers the defect might have a greater impact on the areal image than the initial defect geometry. Directional deposition may lead to abrupt vertical offset in the multilayer stack, damaging the multilayer structures and reducing reflectivity. More conformal and planarizing deposition may lead to greater lateral defect propagation through the multilayer stack, increasing its apparent size, and thus making it more likely to print.

In addition to defects in the multilayer coatings, absorber layer topography also affect the reflected image. Since reflective masks are distributed reflectors of roughly 20 to 30 wavelengths thick, significant diffraction occurs in the presence of the absorber layer. This could have an effect on the allowed range of incidence angle onto the mask and on the optimal absorber layer thickness. Other mask imperfections such as non-vertical absorber sidewall also affect the reflected image.

The experimental studies in this paper consist of first creating programmed defects on substrates by printing small features of different widths and heights. The multilayer coatings are then deposited on top of these patterns by planar magnetron sputtering. Deposition parameters including target-to-substrate distance, substrate rotation rate, and sputtering gas pressure are varied to examine their effects on the coating profile in the presence of defects. The multilayer cross-section are examined by TEM.

The effect of these defect, together with absorber imperfections, are investigated with TEMPEST [3, 4], a massively parallel time-domain finite-difference program. This version of TEMPEST includes both TE and TM polarizations and allows off-axis incidence. Plots of fields within the structures show the interaction between the incident radiation and local features such as edges and bumps. Areal image synthesis from the diffracted fields is used to quantify the effect of multilayer defects and absorber imperfections.

Acknowledgment

The work on x-ray lithography is supported by the Defense Advanced Research Projects Agency, U. S. Department of Defense.

References

[1] A. M. Hawryluk, L. G. Seppala, J. Vac. Sci. Technol. B 6, pg. 2162 (1988).
[2] D. Tennant et al., J. Vac. Sci. Technol. B, Vol. 9, pg. 3176 (1991).
[3] R. Guerrieri et al., IEEE Trans. on Computer-Aided Design, Vol. 10, pg. 1091 (1991).
[4] A. K. Wong, Master's Thesis, University of California, Berkeley (1992).

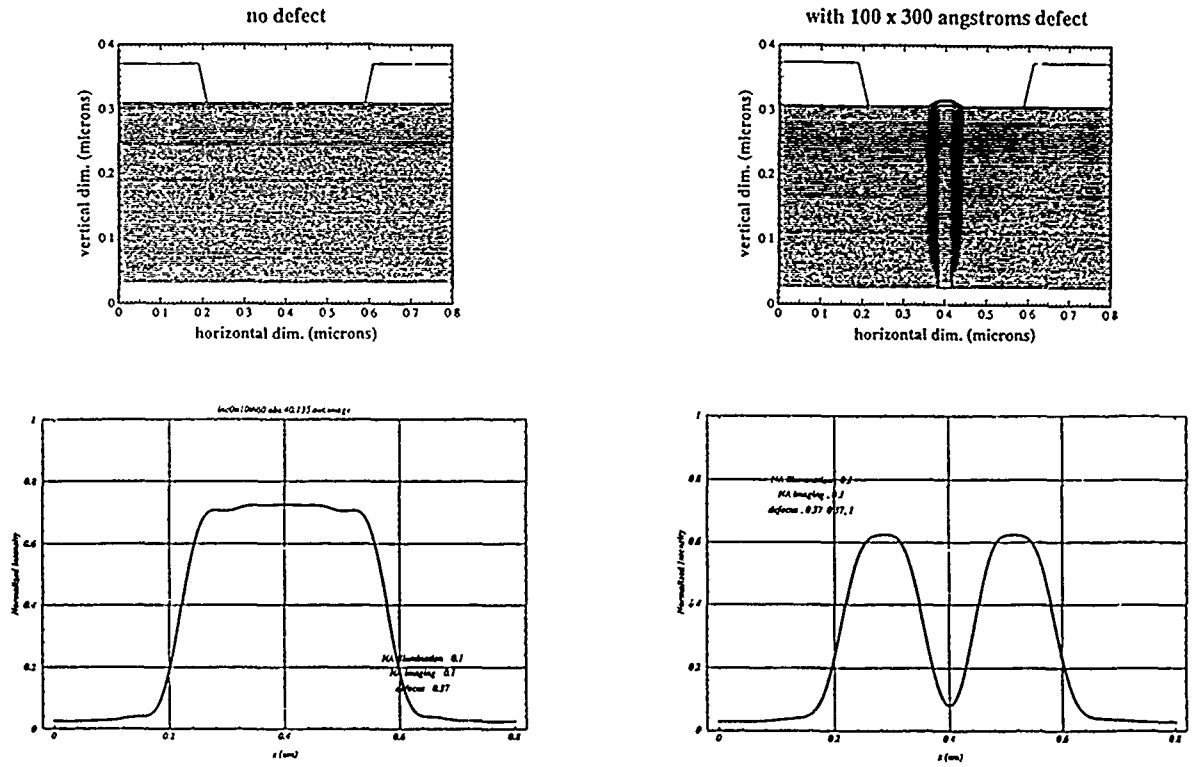

Figure 1. The effect of 100 x 300 Å substrate defect on the reflected image, simulated for 1-to-1 imaging of a 0.4 mm line. The absorber is 60 nm of Ge, and the Mo/Si multilayer consists of 40 bilayers.

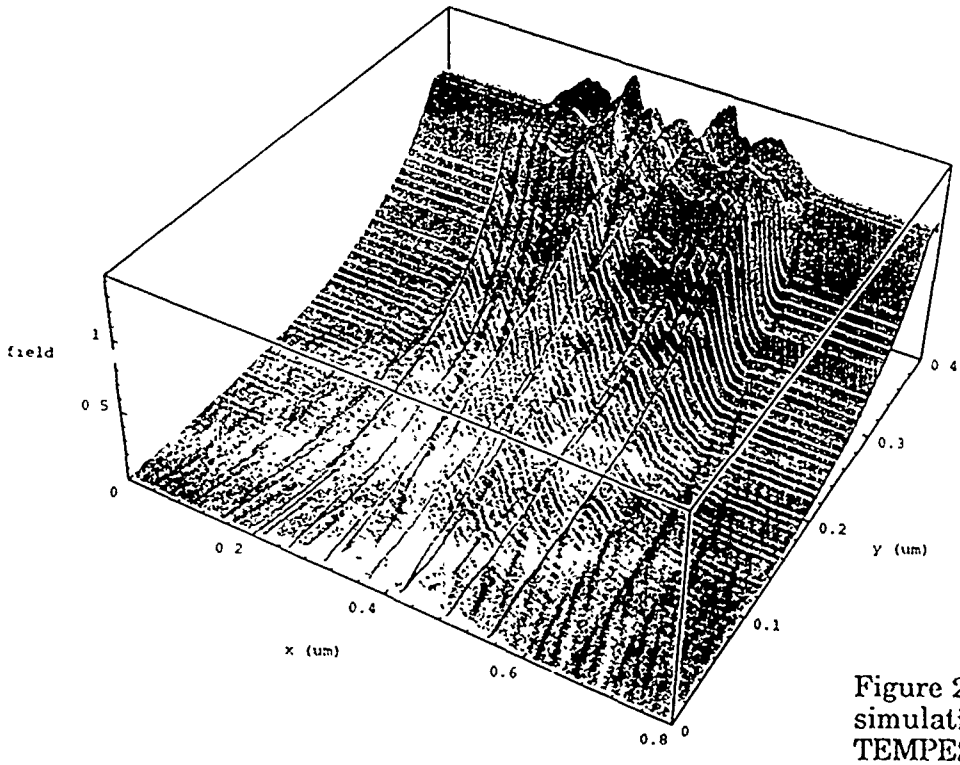

Figure 2. Amplitudes of field in the simulation domain as calculated by TEMPEST

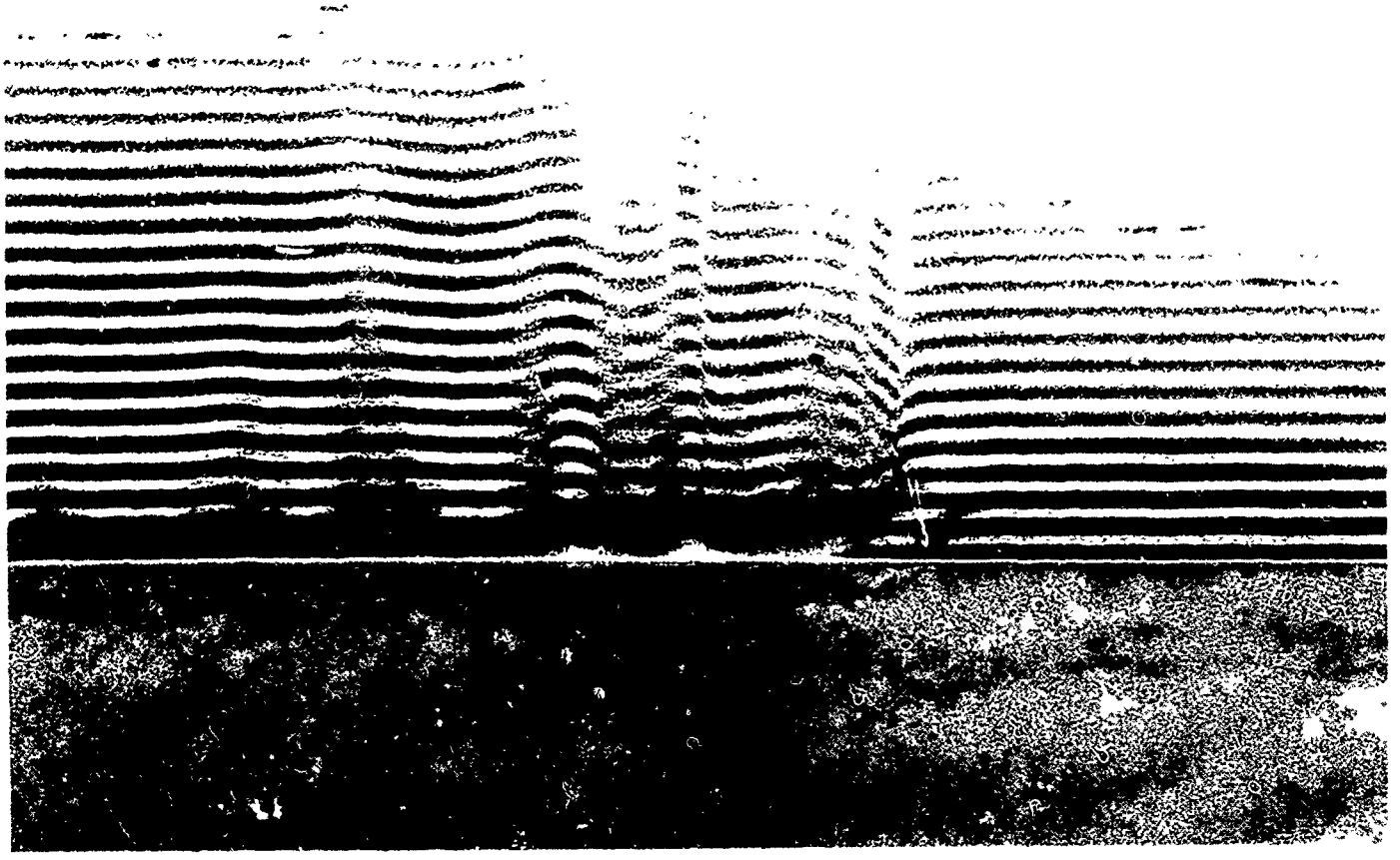

Figure 3. Cross section of 40 bilayer Mo/Si with a 40 Å step defect, as imaged by transmission electron microscopy (TEM).

Condenser

MB 1:30pm–3:50pm
Bonsai II & III

Natale M. Ceglio, *Presider*
Lawrence Livermore National Laboratory

Limits of Ultra Violet Lithography

R. Fabian Pease
Stanford University
Stanford, CA 94305

Any new technology must offer significant improvement over an entrenched technology to become adopted. Here we describe where ultra-violet lithography might evolve to in ten years time the earliest possible time for soft x-ray lithography to be ready for manufacture.

Already there have been examples of optical projection systems operating at 248 nm with a numerical aperture (NA) of 0.7. Credible designs exist for 193nm at an NA of 0.7 with substantial field of view. This suggests a minimum feature size of 0.18μm without "tricks" such as phase-shifting masks and rather less when employing such tricks; 0.125μm has already been demonstrated with phase shifting masks at 248nm. So on grounds of resolution ultraviolet lithography can evolve to minimum features of 0.15μm. Wavelengths shorter than 193nm, e.g. 157nm using an F2 laser, are possible but the practical problems of bright sources and lack of refracting materials make this and expensive step. Depth of focus becomes an issue at high numerical apertures and strategies, such as pupil filtering may be useful with certain patterns. Overlay is a problem for any lithographic technology; it may well be that simultaneous exposure of a complete chip area will be impractical at design rules below 0.2μm and some form of dynamic alignment will be needed. Such a strategy may also help the depth of focus problem.

Condenser Optics for Soft X-ray Projection Lithography

Steve Vernon†, Gary Sommargren,
Lynn Seppala and David Gaines
Lawrence Livermore National Laboratory
Livermore, CA 94550

†Vernon Applied Physics
Torrance, CA

Condenser optics has been designed, fabricated and coated for use in a "front-end" test bed facility at LLNL. Details of condenser design and coating processes will be discussed.

X-ray characterization of a three-element condenser system for soft x-ray projection lithography

D.P. Gaines[a], G.L. Sommargren[b], S.P. Vernon[c]

(a) Brigham Young University, Provo, Utah
(b) Lawrence Livermore National Laboratory, Livermore, California
(c) Vernon Applied Physics, Torrance, California

A three-element condenser system has been designed and fabricated for use in a soft x-ray projection lithography facility at Lawrence Livermore National Laboratory. The design uses Kohler illumination to transport x-rays generated by a laser-produced plasma onto an x-ray reflection mask. The condenser optics are coated with molybdenum silicon multilayers to provide peak reflectance at an operating wavelength of approximately 13.0 nm.

A three-stage evaluation procedure has been designed to characterize the performance of the condenser system. First, the figure and radii of curvature of the uncoated optics were measured using conventional visible-wavelength techniques. Second, a point by point x-ray characterization of the individual (coated) optics was performed. Finally, this data was used in an optics ray-trace code to predict condenser system performance.

A High Efficiency Condenser for Laser Plasma Sources and Ringfield Masks

D. L. White

AT&T Bell Labs, 600 Mountain Ave., Murray Hill, NJ 07974

Condensers and Constraints

A laser produced plasma x-ray source has a 150 to 350 microns in diameter, while the mask for a ringfield camera is an arc 1 to 5 mm wide and 50 to 150 mm long. This is a gross mismatch - the strip is too small in the scanning direction and too large in the transverse direction. Using the LaGrange invariant, we have:

$$I = D_{source} \sin(\theta_{source}/2) \approx \sigma NA_{mask} \cdot W_{mask} \quad (1)$$

where D_{source} is the diameter of the source, θ_{source} the total collection angle of radiation from the source, σ the 'filling factor' and NA_{mask}. Using normal parameters, e.g. $\sigma NA_{mask} = 0.01$ to 0.02 we see that in the scanning direction, $W_{mask} = W_{scan} = 1\text{-}5$ mm, the collection angle, θ_{source}, is in the 5 to 30° range, resulting in low collection efficiency. In the other direction $W_{mask} = W_{trans} = 50\text{-}150$ mm, requires impossibly high collection angles. However it is not impossible to match the source to the mask. This is seen from the fact that the etendue (Etendue = $\Omega \cdot$Area) the two dimensional analog of the LaGrange Invariant, of the mask and source are comparable.

Here a highly efficiency condenser is described in which the long dimension is divided up into several smaller sections, each section illuminated by a separate branch of the condenser. A multifaceted mirror array is used to stitch the parallel branches together smoothly.

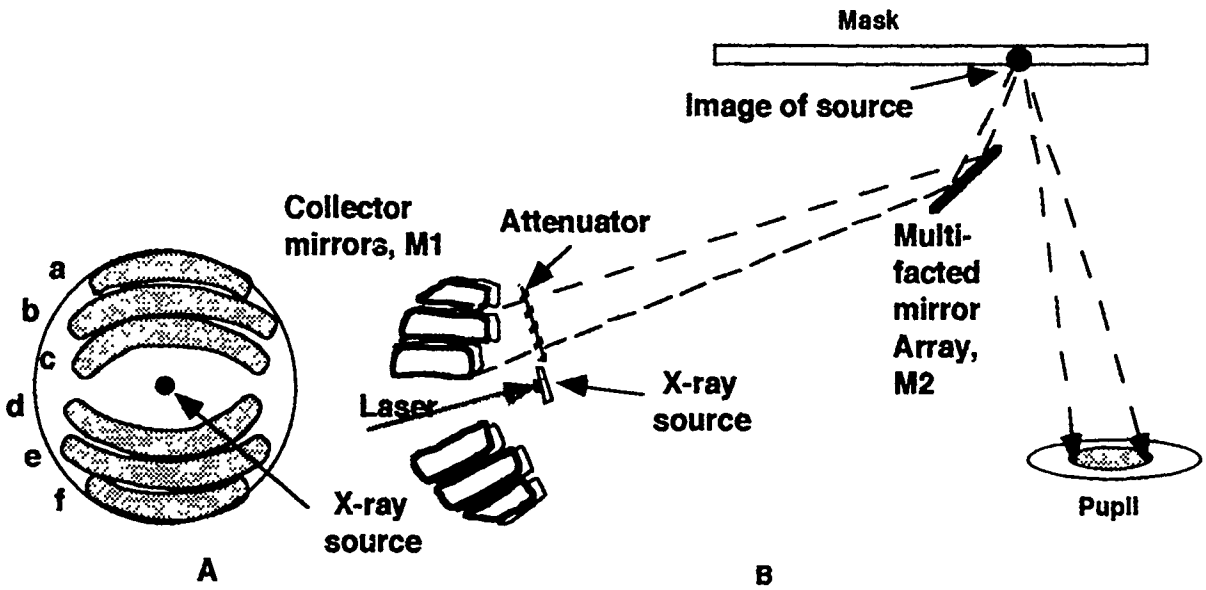

Fig. 1a A frontal view of mirror array M1. Fig. 1b the optics in the scanning direction.

Optics, Scanning Direction. The optics for the small (scanning) dimension consists of an ellipsoidal collection mirror, M1, with the source as one focus, that projects an image of the source either on or near the mask. This is a simple optical system that provides critical illumination, i e. the source is focused on the mask. The mirror M1 is really several mirrors, each collecting radiation for a condenser branch similar to the one shown in Fig. 1b.

The collection angle, θ_{source}, is calculated from Eqn. 1.

When viewed from the scanning direction, the mirror M2 is simply a turning mirror that directs the radiation onto the mask and into the camera pupil. Since the position of the collection mirror for each branch varies (see Fig. 1), the tilt and position of the facets on M2 must be adjusted accordingly to properly illuminate the system.

Optics, Transverse direction The optics for the transverse direction of the mask has several parallel branches., shown in Fig. 2.

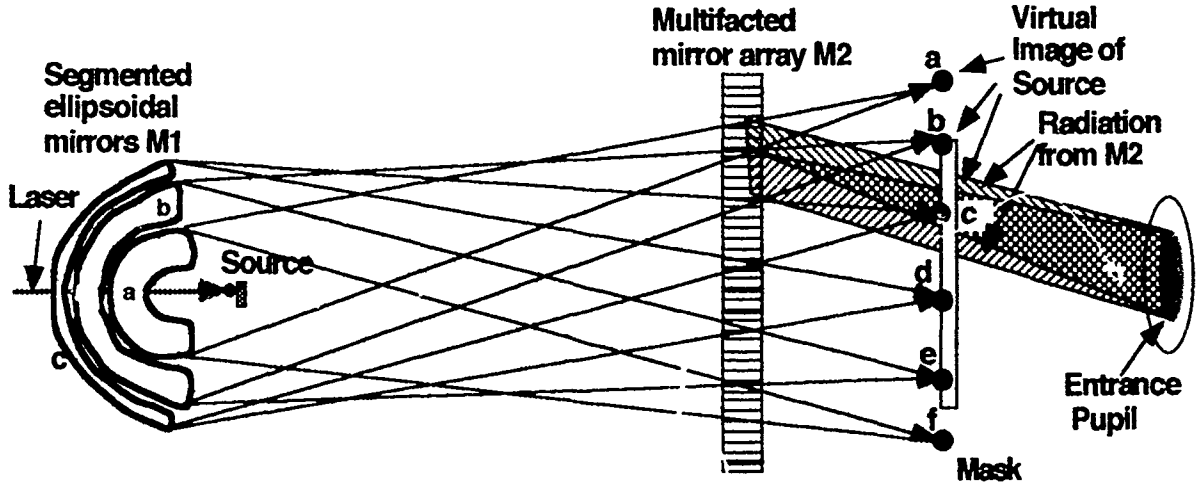

Fig. 2. The optics for the transverse direction.

Here six mirrors illuminate the multifaceted mirror, M2. Each facet of M2 directs radiation off the mask and into the pupil.

In Fig. 1a a frontal view of the collection mirror assembly, M1, the vertical height of the mirrors corresponds to the collection angle, θ_{source}, is small, while the horizontal dimension is the transverse collection angle, θ_{tran} , which can be much larger. This produces a thin fan of radiation converging on the image of the source which is near the mask. Each facet in M2 directs radiation onto the mask at an angle such that the reflection will be directed toward the entrance pupil of the camera. The facets are positioned such that the each point on the mask sees radiation from several facets, producing a divergence of $\pm\sigma \cdot NA_{mask}$. The optical system is essentially critical illumination in the scanning (small) direction and closer to Köhler illumination in the transverse direction.

Depending primarily on the source and the mask size, the collection angle, θ_{source}, may vary from 5° to over 35°. The smaller collection angles will require more mirrors. Each condenser-camera system requires it own custom design of mirrors in M1 and M2. But the strategy is always to divide the long mask into a number of sections, with a collection mirror for each. The collection mirrors are generally stacked on top of each other to collect more energy in the vertical (scanning) direction. e.g. if $\theta_{source} = 15°$ we could stack 6 mirrors in the *scanning* direction and collect 90° of the radiation emitted and use this power to illuminate different sections in the *transverse* direction,(Fig. 2).

The Mirrors M1 and M2. The illumination need not be uniform in the scanning direction - during scanning non-uniformitys are averaged out. However, to produce good commercial product, the intensity integrated in the scanning direction must be uniform in the transverse direction to about ±1% This means that the individual beams should have uniform intensity when they strike M2 and the interface between two adjacent beams must be stitched together seamlessly. Small intensity variations can be ironed out by adjusting the width of the aperture over the mask and the size the facets in M2, but the real burden on uniformity should be placed on the mirrors of M1.

Intensity variations in the transverse directions will be minimized if all points on each mirror in M1 are an equal distance from the source. Hence the curvature of the long mirrors seen in Fig. 1a However this is not always possible. Furthermore reflectivity of the mirrors and flux from the source varies with angle. Thus a graded attenuator will be needed to make the beam intensity more uniform. An attenuator can be made by placing a fine mesh screen of wires just behind the mirrors of M1.

At the mirror M2 beams from different mirrors meet and overlap slightly. The individual facets of M2 are oriented to reflect radiation from only one mirror, not both. Radiation from the undesired mirror will be at an angle that will not pass through the system.

Each facet might be thought of as a linearized pin hole camera - if the image of the source is focused on the mask in Fig. 1b, the facet will also produce an image of the source on the mask. However the facets may be only a quarter to a half mm in size, so the images from each facet overlaps, producing a uniform strip of radiation on the mask. If the source is imaged to a point in front of the mask, there will be even more overlap and greater uniformity.

Fig. 3 shows the radiation pattern in the entrance pupil of a typical system. This is the radiation pattern for a single point on the mask. Each vertical strip is caused by one facet on M2. On the left the etendue of the source and the mask are matched, which fills the center of the pupil. On the right side the source entendue is about half of that of the mask. This produces gaps in the radiation from the different facets in the pupil. However the imaging properties will be almost identical.

It is also possible to put in a scatter plate in each of the optical paths. By providing a controlled but small amount of additional scatter, the coherent beam for a small source would be made more diffuse, and the narrow stripes in Fig. 3b would be broadened to look more like that of Flg 3a.

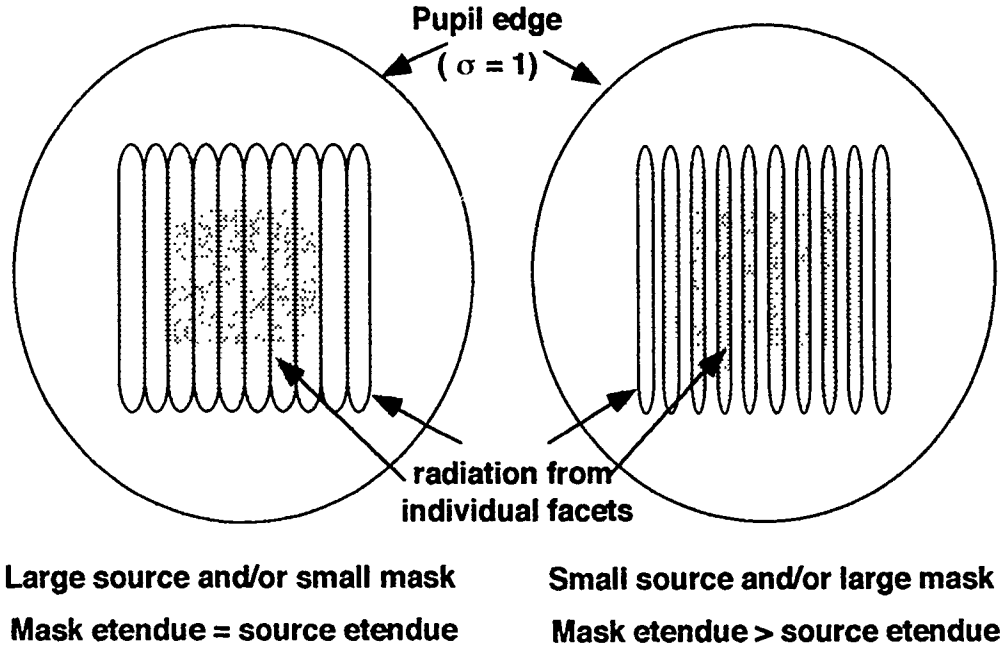

Fig. 3. Illumination in the entrance pupil for systems with matched and unmatched etendue.

Summary of condenser properties. The high efficiency condenser described matches a laser produced plasma x-ray source to the high aspect ratio mask of a ring field camera used in a scanning mode. The collection efficiency is limited either by 1) the etendue of the system, which would be the theoretical maximum, or 2) by practical considerations because it is difficult to properly collect much more than 70% of the emitted radiation. This system is efficient even with unfavorable parameters - a large plasma source and a small mask width. The power delivered to the mask however would be somewhat lower because attenuators might be needed to make the radiation uniform. The optics consists of a collection mirror used at normal incidence and a multifaceted array of plane mirrors used at grazing incidence, so the reflection losses would be low. The entire ring field is illuminated simultaneously, so a source with a repetition rate of a hundred pulses per second would be fine for a scanning system.

If the transmission is 40% and 50% of the emitted radiation is collected, and if a 200 watt laser produces 4 watts of useful x-ray, 0.8 watts of x-rays would be delivered to the mask. If the camera transmits 10% of the incident power to the target, we would have 80 mw of x-rays on the resist. This is enough to expose several cm^2 of product per sec., a commercially viable throughput.

High Efficiency Condenser Design for Illuminating a Ring Field

William C. Sweatt
Space Initiatives Department
Sandia National Laboratories
Albuquerque, NM 87185-5800
(505) 845-8566

This condenser couples a small, incoherent source into the 60° ring-field of a camera designed for projection lithography. Quasi-Köhler illumination uniformly illuminates the whole field and a degree of partial coherence is achieved ($\sigma \approx 0.8$). This design was conceived with a soft-X-ray laser-plasma source in mind; hence, it is all reflective. However, it would also be suitable for any other lithographic system employing a small, bright source.

This illuminator is being designed to mate to a lithographic camera being built for Sandia and AT&T[1]. The camera images a 60°, 125-mm long by 5-mm wide ring field onto the wafer with a 5x reduction. The entrance pupil is 3.6 m. behind the reflective object mask, and the numerical aperture of the camera is $n.a. = 0.08$.

The laser plasma source is now being optimized, so we only have estimates of its size. In recent experiments, Rockett, et al[2] have measured the dimensions of laser-generated plasmas. The volume that radiates the 14-nm soft X-rays is roughly 200 μm in both diameter and height. We have suggested that smaller, brighter sources would be better, and they are trying to accomodate us. They hope to reduce the size to the 100-μm to 125-μm range[3]-- so for the time being, we design for a median size of 150 μm.

The illuminator is composed of five parallel beam lines, each beginning with an off-axis segment of an aspheric mirror. The parent aspheric mirror images the source into a ring image. Each of the 60° mirror sections images the source into a 60° segment of the ring image. The parent mirror and the four of the five segments are shown in Figure 1.

The five beams need to be rotated and translated so that the 60° ring focus segments illuminate the camera's 60° ring field. Furthermore, all five beams must be aimed through the camera's virtual entrance pupil. These requirements are met in two steps. First, the beams are individually rotated and translated using a set of three grazing-incidence flat mirrors. Three mirrors allow enough degrees of freedom to rotate and overlap the ring focus segments, and to point all of the beams through a real entrance pupil. The second step is to image this real entrance pupil into the camera's virtual entrance pupil using a spherical mirror. Figure 2 is a schematic of the complete system showing one of the five condenser beams.

The system efficiency depends on the size of the source and the reflectivity of the mirrors. The collection efficiency depends on the Entendu of the whole optical system, the concept of "Entendu" being derived from the theorem of conservation of energy. It teaches us that, for an unvignetted pencil of light, the product of image height and numerical aperture is the same at all image planes in the system. This leads us to an equivalence between source parameters (diameter and collection angle) and camera parameters (ring field width and numerical aperture). If we illuminated the ring field with only one beam, we could use all of the numerical aperture for it. However, we want to squeeze five non-overlapping beams into the entrance pupil, so we can only use about 38% of it for each one. Thus, our camera parameters and the 150-μm source size limit the beams sizes to 60° in azimuth by ~22° in elevation. This results in a collection efficiency of about 40%.

Delivering these soft X-rays to the object mask is the other half of the problem; this depends entirely on the reflectivity of the mirrors. The theoretically perfect reflectivities[4] at 14 nm are 54%, 90%, 85%, 90%, and 68%, where the first number is the average reflectivity of the aspheric collector, the next three are for the grazing incidence flats, and the last is for the reimaging sphere. The product of these ideal reflectivities is 25%, which means that 10% of the soft X-ray photons from the source could theoretically be delivered to the mask. With real reflectivities we can probably achieve ~6%.

REFERENCES:

[1] Private communication with Dan Tichenor, Sandia National Laboratories, California on Apr. 1, 1992
[2] Rockett, et al, SXPL Topical Meeting, May 10-12, 1993
[3] Private communication with Paul Rockett, Sandia National Laboratories, New Mexico on Dec. 7, 1992
[4] Private communication with Glenn Kubiak, Sandia National Laboratories, California on Oct 31, 1992

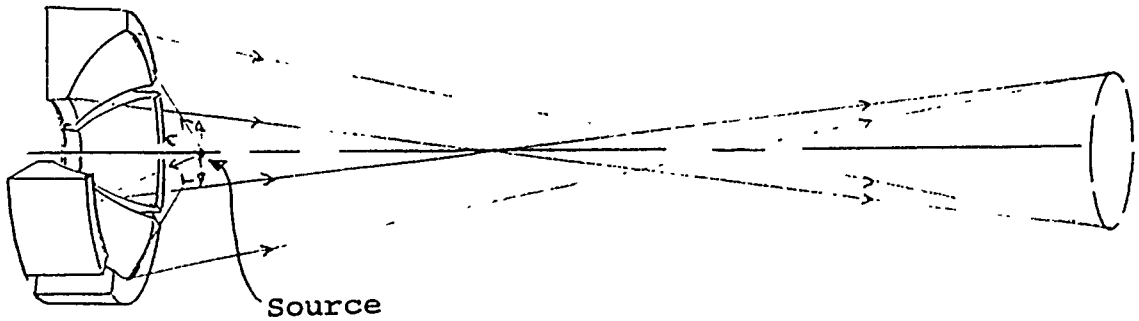

Fig. 1 At the left are the source and collector mirrors with one removed to give a cut-away view. At the right are the five 60° ring focus segments.

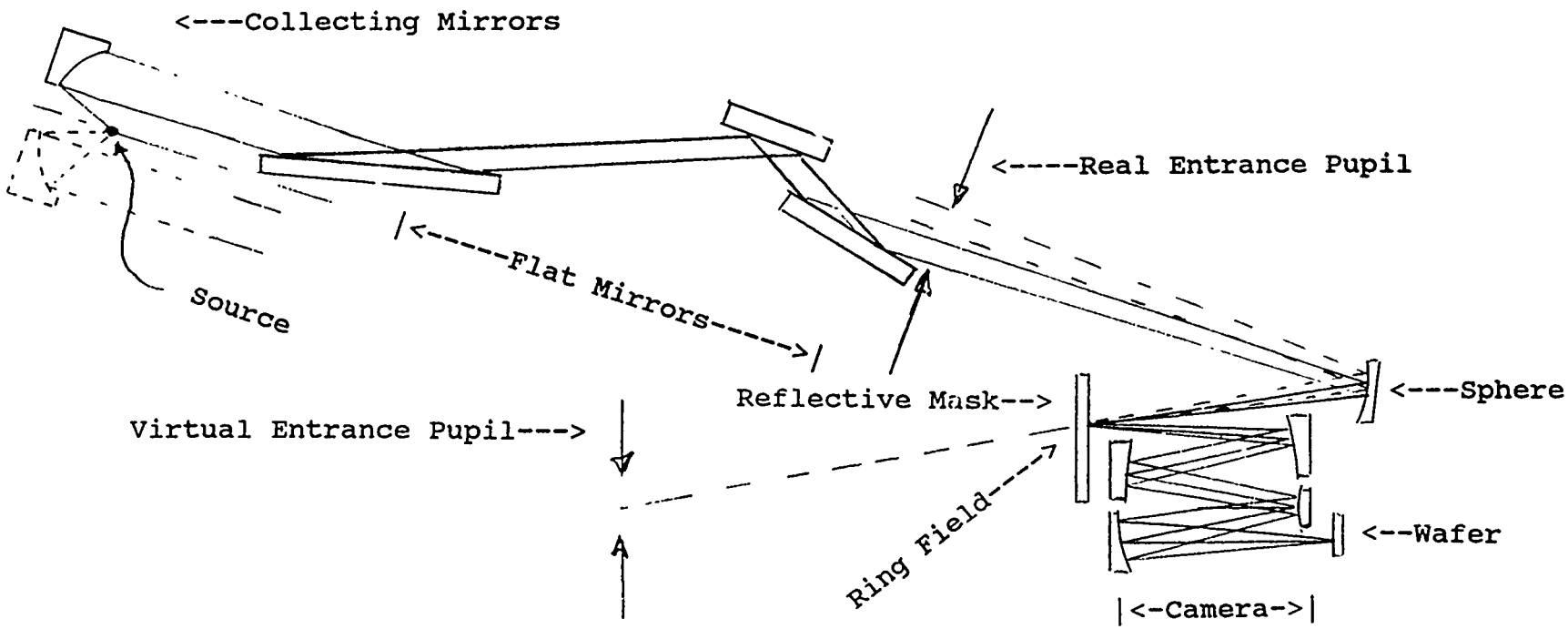

Fig. 2 This is the complete SXPL system with one of five condenser beams shown. A second beam is sketched in the entrance pupil.

Multilayer 1

MC 3:50pm–4:50pm
Bonsai II & III

Glenn D. Kubiak, *Presider*
Sandia National Laboratories

Surface Finish Requirements for SXPL Optics

D. L. Windt, W. K. Waskiewicz, J. Griffith and J. E. Bjorkholm

AT&T Bell Laboratories
Room 1D-456, 600 Mountain Ave, Murray Hill, NJ 07974
(908) 582-2367

In order for soft X-ray projection lithography to become a viable candidate for the mass production of integrated circuits having 0.1-μm design rules, it will be necessary to satisfy an array of technical performance requirements. Among these requirements is system throughput (i.e. wafers/hour.) For SXPL exposure tools operating at 14 nm using multilayer X-ray mirrors, the system throughput depends sensitively on the peak reflectance of the multilayers. The peak reflectance, in turn, can be deleteriously affected by the surface finish of the mirror substrates. That is, the roughness of the substrate can propagate through the multilayer during growth, resulting in reduced reflectance. Therefore, it is imperative to use X-ray mirror substrates with low surface roughness.

Techniques are now being developed to fabricate the large-diameter mirrors required for a practical SXPL exposure tool. As part of this development process, it is first necessary to accurately quantify the surface finish requirements of the mirror substrates, and to then identify the surface finish metrology tools that can be used by the manufacturer during the substrate fabrication process. To this end, we have examined correlations between direct surface finish measurement techniques and normal-incidence, soft X-ray reflectance measurements of highly-polished X-ray mirrors.

Our results indicate that to maintain high reflectance, the rms surface roughness of normal-incidence X-ray mirrors for use near 14 nm must be less than ~1 Å over the range of spatial frequencies extending approximately from 1-100 μm^{-1}(i.e. spatial wavelengths from 10 nm - 1 μm.) This range of spatial frequencies is accessible only through scanning probe metrology. Since the surface finish Fourier spectrum of such highly polished mirrors is described approximately by an inverse-power law (unlike a conventional surface)[1], bandwidth-limited rms roughness values measured using instruments sensitive only to lower spatial frequencies (i.e. optical or stylus profilers) are generally uncorrelated to the soft X-ray reflectance, and can lead to erroneous conclusions regarding the expected performance of substrates for X-ray mirrors.

These relationships are illustrated in Figures 1 and 2, which show the normal incidence reflectance curves and the one-dimensional power-spectral-density (PSD) functions, respectively, for three exemplary mirrors, and in Table 1, which lists the bandwidth-limited rms surface roughness values for these three mirrors. All three samples were coated during the same deposition run with 40 bilayers of Mo/Si, so any differences in the reflectance curves are presumed to be due to differences in the surface finish of the substrates. As indicated in Table 1, samples A and B have the highest peak reflectance — 62.5 ± 1.0% and 60.8 ± 1.0%, respectively— while sample C yields only 56.0 ± 0.9% reflectance, a value which is significantly lower than the other two, suggesting that this sample has greater surface roughness. Indeed, the rms roughness values for sample C obtained using the atomic force microscope (AFM), indicated in Table 1, are approximately 2.5× those obtained for samples A and B. Examination of Fig. 2 further reveals that the PSD functions

for samples A and B are very similar over the range of spatial frequencies spanned by the AFM data, whereas the PSD function for sample C shows significantly more power in the range from 0.5 to 10 μm^{-1}. In contrast, there is no correlation between the surface finish data measured at lower spatial frequencies (i.e. those spanned by the Wyko TOPO instrument) and the soft X-ray reflectance. For example, the low-frequency rms roughness of sample A is nearly 10 Å even though this sample has the highest reflectance.

We have also investigated both coated and uncoated X-ray mirror substrates and have found that the presence of the coating generally has little or no effect on the measured surface finish. This suggests that the surface finish metrology techniques investigated here, in particular atomic force microscopy, can be used on an uncoated mirror substrate in order to accurately predict the soft X-ray reflectance of the substrate once it is coated with a multilayer reflector. This result also suggests that the high-frequency cutoff for correlated roughness propagation (as discussed recently by Stearns[2]) in Mo/Si multilayers is at least as great (approximately) as the highest frequency investigated using an atomic force microscope, namely $(5\ nm)^{-1}$.

References

1. E. L. Church, "Fractal surface finish", Appl. Opt., 27, 1518 (1988)
2. D. G. Stearns, "A stochastic model for thin film growth and erosion", Submitted to Appl. Phys. Letters

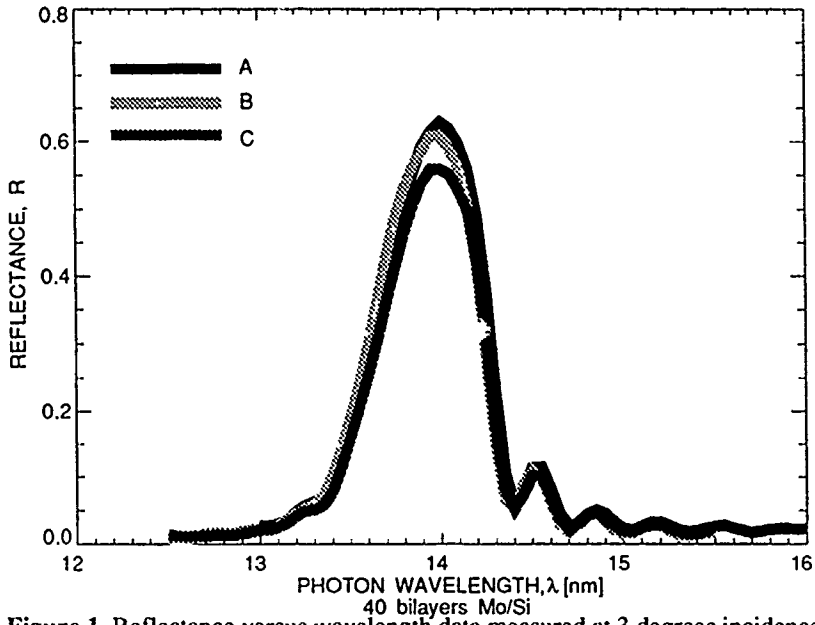

Figure 1. Reflectance versus wavelength data measured at 3 degrees incidence.

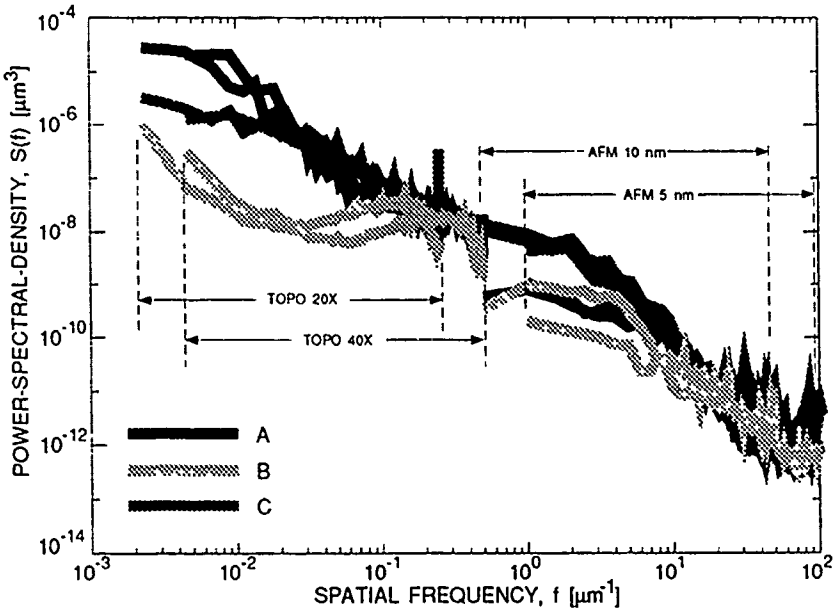

Figure 2. Power-spectral-density functions measured using an AFM and an optical profilometer (Wyko TOPO-3D).

Sample	AFM RMS Roughness		TOPO RMS Roughness		SXR Reflectance
	5 nm to 1 μm	*10 nm to 2 μm*	*1 μm to 219 μm*	*2 μm to 438 μm*	
A	0.78 Å	0.75 Å	9.00 Å	9.71 Å	62.5±1.0%
B	0.73 Å	0.72 Å	1.37 Å	1.99 Å	60.8±1.0%
C	2.05 Å	1.76 Å	3.66 Å	7.46 Å	56.0±0.9%

Table 1. RMS surface roughnesses and peak soft X-ray reflectances.

Substrate Recovery of Mo-Si Multilayer Coated Optics

D. G. Stearns and S. L. Baker

University of California, Lawrence Livermore National Laboratory, P. O. Box 808

Livermore CA 94550

Multilayer coated optics in a soft x-ray projection lithography system are subject to environmental effects that can degrade their performance such as corrosion, contamination and excessive radiation exposure. When the damage is limited to the multilayer coatings it is cost effective to recycle the optics by removing the damaged coatings and recoating the substrates. The main challenge is to develop a substrate recovery process that completely removes the coating without compromising the figure and surface finish requirements of the original substrate. Typical requirements for the precision imaging optics are a surface finish of less than 1 Å root-mean-square (RMS) and peak-to-valley figure error of less than 10 Å.

We have investigated the removal of Mo-Si mulitlayer coatings from fused silica and zerodur substrates using reactive ion etching (RIE) in a SF_6 plasma. Film erosion in the RIE process takes place due to a combination of chemical reaction and low energy (10 - 100 eV) ion bombardment. The choice of SF_6 gas provides the necessary selectivity: the SF_6 plasma efficiently etches Mo and Si but not SiO_2. The etching is observed to be significantly nonuniform. The etch rate in the center of the coating is reduced due to loading effects. In addition, we observe an anomaly in the etch rate and the erosion characteristics of the $MoSi_2$ interlayers.

We present results for a series of multilayer coated (Λ = 70 Å, N = 40) optical flats (1 inch diameter) etched for times ranging from 0.5 t_e to 10 t_e where t_e is the endpoint time required to completely remove the coating. The recovered substrates have been analyzed to assess the effects of the etching process on the figure and finish of the substrate surface. The surface finish has been evaluated by measuring the normal incidence reflectivity of the substrate recoated with Mo-Si multilayers. Alteration of the substrate figure has been investigated using heterodyne optical interferometry which has a surface height resolution of ~ 30 Å.

Masked Deposition Techniques for Controlling Multilayer Period Variation on Short Wavelength Reflective Lenses

J.B. Kortright, E.M. Gullikson and P.E. Denham
Center for X-ray Optics
Lawrence Berkeley Laboratory
University of California
Berkeley, CA 94720

Multilayer-coated focussing systems for XUV imaging, by their very nature, generally require laterally graded multilayer period or thickness across the clear aperture of mirrors to optimize performance. This requirement stems from the variation of incidence angles given by the optical design, and the inherint finite bandwidth of x-ray multilayers [1,2]. The ideal period (d) variation at each mirror is prescribed for small-field imaging systems by the variation in incidence angle θ across the clear aperture through the Bragg condition for constructive multilayer interference, $\lambda = 2d\cos\theta$. For large field systems the field angle can make an additional contribution to angular variations which can lead to vignetting under extreme cases [3]. The actual d variation should conform to the prescribed ideal d variation to a tolerance set by the multilayer bandwidth. Otherwise, degraded performance may result from unwanted phase and intensity variations across the clear aperture. The phase errors may contribute to limiting imaging performance if wavefront errors resulting from mirror figure and system alignment errors are reduced to much less than λ. The intensity errors result in nonuniform intensity across the wavefront, and will limit the effective aperture if d variation problems are severe. These effects can and should be investigated with appropriate calculations for specific optical systems of interest [4,5].

The bandwidth of soft x-ray multilayers scales with wavelength, and hence so does the need to precisely control the multilayer period variation. Mo/Si multilayers for use at $\lambda > 125$ Å have bandwidths of 4-5 percent or larger, leading to relatively generous tolerances for the control of d. Ru/B_4C multilayers have high reflectance at $\lambda > 66$ Å [6] and bandwidths of 1 percent or less. For a 20 times demagnifying Schwarzschild objective, the ideal d variation across the clear aperture of the primary mirror is several percent. Thus the broad Mo/Si bandwidth allows the 20X Schwarzschild to be coated with relative ease [1,2], but the narrow Ru/B_4C bandwidth requires development of new techniques to control and verify the d variation on this and similar optics. The narrow bandwidths not only necessitate improved control of d variation across each individual curved surface, but also increase the demands on matching the coatings of different mirrors in a compound imaging system.

Experimental techniques to control and verify the d variation of Ru/B_4C multilayers on a 20X demagnifying Schwarzschild have been developed. Two issues are key in these developments, the ability to precisely control d variation during deposition over steeply curved surfaces, and the ability to precisely measure the multilayer reflectance peaks with adequate spatial resolution over these curved surfaces. We obtain control over deposition profile by introducing masks between the source and substrate to alter the deposition profile in a specifically desired manner. Spatially resolved measurement of d variation across these curved surfaces is best accomplished using at-wavelength, near normal-incidence reflectance measurements, which were made using a laser-plasma based reflectometer [7]. An iterative approach of deposition profile modification and spatially resolved reflectometry converges on an acceptable solution to the coating problem [8], and demonstrates unprecedented control multilayer coatings on curved surfaces. These techniques are generally applicable to condenser and imaging optics of interest for soft x-ray projection lithography.

Acknowledgments

The optics of interest in this work were provided by O.R. Wood of AT&T Bell Laboratories and are of interest in a larger project investigating soft x-ray projection lithography at short wavelengths. We acknowledge useful discussions with J.H. Underwood. This work was supported by the Director, Office of Energy Research, Office of Basic Energy Sciences, Materials Sciences Division, of the U.S. Department of Energy under contract No. AC03-76SF00098.

References

1. J.B. Kortright and J.H. Underwood, "Design considerations for multilayer coated Schwarzschild objectives for the XUV," Proc. Int. Soc. Opt. Eng., **1343**, 95-103 (1990).
2. J.B. Kortright and R.N. Watts, "Multilayer uniformity and performance of soft x-ray imaging optics," in OSA Proceedings on Soft X-ray Projection Lithography, Vol. 12, J. Bokor, ed. (Optical Society of America, Washington, D.C., 1991) p. 92.
3. D.W. Berreman, "Multilayer reflecting x-ray optical systems: chromatic vignetting by narror reflection bands,: Appl. Opt., **30**, 1741-1745, (1991).
4. B. Lai, F. Cerrina and J.H. Underwood, "Image formation in multilayer optics: the Schwarzschild objective,: Proc. Int. Soc. Opt. Eng., 563, 174-179 (1985).
5. T.E. Jewell, "Effects of amplitude and phase dispersion on images in multilayer-coated soft x-ray projection systems, in OSA Proceedings on Soft X-ray Projection Lithography, Vol. 12, J. Bokor, ed. (Optical Society of America, Washington, D.C., 1991) p. 113.
6. D.G. Stearns, R.S. Rosen and S.P. Vernon, "Normal-incidence x-ray mirror for 7 nm," Optics Letters, **16**, 1283-1285, (1991).
7. E.M. Gullikson J. H. Underwood, P.C. Batson and V. Nikitin, "A soft x-ray/EUV reflectometer based on a laser produced plasma source," J. X-ray Science and Technology, in press.
8. J.B. Kortright. E.M. Gullikson, and P.E. Denham, "Masked deposition techniques for achieving multilayer period variations required for short wavelength (68 Å) soft x-ray imaging optics," Appl. Opt., in press.

Imaging Experiments

TuA 8:30am–11:30am
Bonsai II & III

David A. Markle, *Presider*
Ultratechstepper

A MIGRATION PATH TO NANO-METER LITHOGRAPHY
-- From the viewpoint of VLSIs --

Eiji Takeda

Central Research Laboratory, Hitachi Ltd.
Kokubunji, Tokyo 185, Japan

1. Introduction

The "VLSI revolution" that is opening a new epoch in the electronics industry has made such remarkable progress that now 10^8 - 10^9 transistors can be fabricated on a single chip. VLSI microfabrication technologies are being pushed to new extremes by the DRAM community, thereby expediting research on 256 Mbit DRAMs using the 0.2 μm design rule. Giga-bit DRAMs and sophisticated ULSI processors using 0.1 μm Si-MOSFETs could possibly appear in the latter half of the 1990s. Recently, a very high speed ring oscillator has achieved 10 psec/gate for 77 K operation[1]. In the field of advanced bipolar transistors, a 64 GHz cut-off frequency has been reported[2]. These speeds are comparable to those of conventional quantum devices such as HEMTs (High electron mobility transistors)[3], JJs (Josephson junction devices)[4], and STrs (Superconducting transistors)[5] as shown in Fig. 1. In addition, device operation of 7-10 nm Si-MOSFETs (corresponding to 1-16 Tera-bit memories) [6] and single electron transistors (SET) [7] have been confirmed, which implies an increased importance for nano-meter fabrication technology. Si devices have a promising future, which will pave the way to the 21st century.

From the manufacturing standpoint, process and device technologies in the deep-submicron region (0.1-0.3 μm) are, however, approaching practical limits and thus coincident achievement of high performance, high packing density, and high reliability will become increasingly difficult. Furthermore, due to the large initial investment required by the fabrication process complexity, it has recently become a matter of significant debate in the semiconductor industry whether such a large investment will ultimately be profitable. Thus, there is an urgent need to reduce the fabrication process cost by developing new approaches, such as single wafer processing [8] and tool clustering, and increasing process and factory control automation.

Among the fine-line patterning technologies, the lithography system is so important that its selection for each VLSI generation is a key factor for business success. Lithography systems, consisting of exposure tools, masks, resist materials and etching processes, require a large initial investment and have a large impact on factory operating cost. Thus, it is not too much to say that the lithography has dominated fabrication technology. Given its importance, new concepts in lithography might also pave the way to future, low-cost submicron processes.

This paper will discuss which technologies are most promising as a nano-meter (less than 0.1 μm) lithography system -- optical, e-beam, proximity x-ray, and projection x-ray lithographies, from the viewpoint of giga-scale integrations.

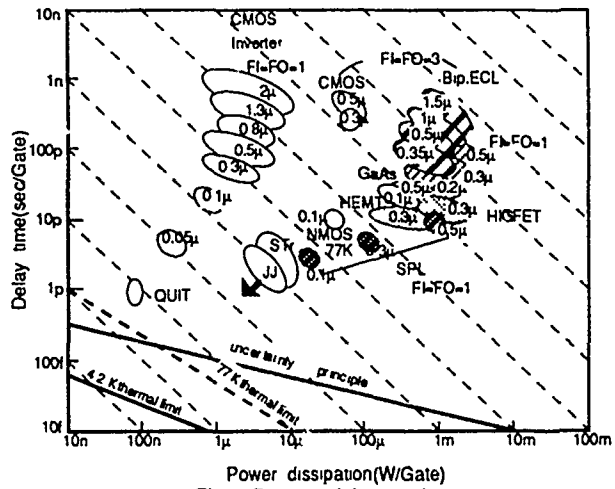

Fig.1. Power - delay products

2. Optical Lithography

So far, optical lithography has always pushed its limit not only by using shorter wave length (λ)(from g-line and i-line to excimer lasers: KrF and ArF, etc), recently, but by controlling the wave-phases, e.g. phase shift methods [9] and spatial filtering methods [10]. Such super

resolution techniques are still preventing e-beam and x-ray lithographies from entering production lines. Due to such great advances, it can be said that the resolution limit (R) of optical lithography will be extended down to ~ 0.15 μm, (corresponding to 1 Gbit DRAMs) according to a relation of $R = \kappa \lambda/NA$, where NA is the numerical aperture and $\kappa = 0.5 - 0.25$ (using super resolution techniques). Depth of focus (DOF) is also very important for the lithography, because the sum of VLSI topography, wafer variation, and focus-plane positioning control often exceeds 1 μm. At the moment, to overcome planarization problem, new technologies such as chemical mechanical polishing (CMP)[11] have been proposed, resulting in an improvement of resolution.

Furthermore, a step and scan method[12] recently developed by SVG, etc seems to make it easier to use an ArF excimer laser or similar exposure sources, compared with the conventional step and repeat methods. In addition, this system has an advantage that its optics is similar to that of projection x-ray lithography, which implies that the step and scan technology can be easily transferred to the projection x-ray lithography systems in nano-meter regions. Thus, the superiority of optical lithography will continue for a while. In this case, it is important to develop phase-shift masks and to implement modified illumination in a total system with mass-production reliability in mind. However, it will be impossible for optical lithography (even ArF and F_2 excimer lasers) to invade regions less than 0.1 μm. Therefore, other lithography systems will inevitably be introduced for use in the nano-meter regions.

3. Electron-Beam Lithography

Electron-beam lithography is now being used mainly for reticle making, direct writing of wire fabrication for ASICs (application specific ICs) and feasibility checking of small-sized devices, i.e. not mass-production. The items required are different in response to each purpose: for reticle making, a high positioning/overlay accuracy in the large area is needed, for direct writing of VLSIs a high throughput is required, and feasibility checking of scaled MOS devices and mesoscopic (quantum) devices requires ultra-fine patterning. There is still a severe trade-off between throughput and accuracy/fine-line patterning. This fact strongly calls for a new breakthrough satisfying high throughput and high accuracy simultaneously. Recently, such new concepts as a cell projection [13] and a multi-column [14] have been proposed, but are not sufficient, as shown in Fig. 2. New breakthroughs aiming at the mass production are strongly required.

On the other hand, in regard to reticles for optical and projection x-ray lithographies, the chip size becomes increasingly large with down-scaling of device dimensions, and as a matter of course, a larger reticle size will be demanded, leading to a further increase in exposure field in the stepper optics. This requires a decrease of demagnification, e.g. from 1:5 to 1:4, resulting in a more severe positioning/overlay accuracy.

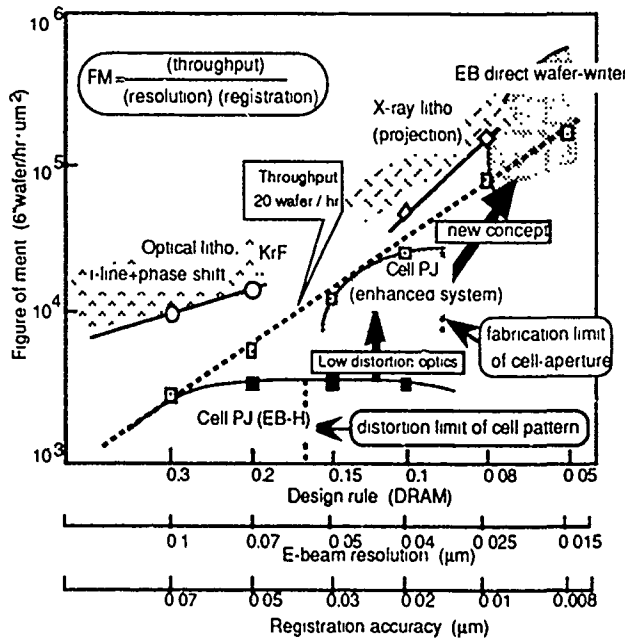

Fig 2 Figure of merits for each lithpgraphy system

4. Proximity X-Ray Lithography

Although it is commonly said that proximity x-ray lithography can be the most promising technique in the replication of patterns as small as 100 nm or less, there will exist a new physical phenomenon different from diffraction, which will determine the resolution limitation, as shown below. As a guiding principle for the resolution limit of proximity x-ray lithography, Fresnel's

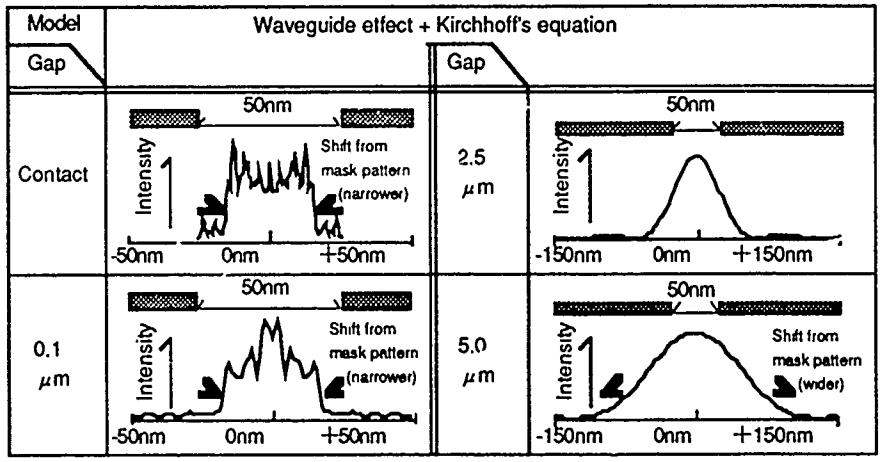

Fig. 3. Waveguide effect.

approximation has so far been most widely used [15]. In this approximation, x-ray mask patterns are considered as a slit with infinitely small thickness, which only obstructs x-rays.

However, for sub-100 nm pattern replication, the x-rays should be regarded as waves propagating in the waveguide [16-17] formed by the mask patterns, whose aspect ratio reaches 5 to 10, in the same way as that of micro-waves. As a result, many waves reflected from mask patterns interact each other, possibly resulting in the degradation of resolution. A new simulator based on Maxwell's equation, which is applied to a mask pattern of perfect conductors with finite thickness has been developed.

Fig. 3 shows simulation results of x-ray intensity profiles propagated through a mask pattern with a width of 50 nm and a thickness of 500 nm (aspect ratio 10). The x-ray wavelength is 1 nm. Because the incident waves interfere with phase-shifted waves reflected from the side-walls of the mask pattern, the width of the x-ray intensity profiles just below the mask (contact) and on the wafer very close to the mask (gap 0.1 μm) become narrower than the mask pattern. This tendency, of course, disappears as the mask pattern becomes thinner or wider. On the other hand, the width of intensity profiles for larger mask-wafer gaps (gap 2.5μm, 5μm) becomes wider than the mask pattern, because the diffraction effect is dominant in this range.

New findings on waveguide effect are as follows: 1) A narrower mask-wafer gap does not always lead to an enhancement in resolution. 2) the range of pattern replication decreases as the mask pattern sizes become smaller, e.g., 2.5 μm at 100 nm, 0.5 μm at 50 nm, and 0.1 μm at 30 nm. 3) The different optimal gap for various pattern sizes reduces the gap latitude when multiple patterns are replicated on an Si-wafer simultaneously. Thus, the waveguide effect will have a strong impact on the resolution limit in proximity x-ray lithography.

Going further, Fig. 4 shows the dependence of the optimum mask-wafer gap and gap latitude on mask pattern width From this figure, the resolution limit of proximity x-ray lithography can be evaluated by assuming two criteria: 1) a minimum mask-wafer gap (= 5 μm), and 2) a minimum gap latitude (= 1.0 μm corresponding to a single layer resist thickness). Thus, the resolution limit of proximity x-ray lithography under the practical production condition will be at most 70 nm. Of course, this value strongly depends on resist contrast and absorber thickness, and a fact that the absorber is not a perfect conductor also must be considered.

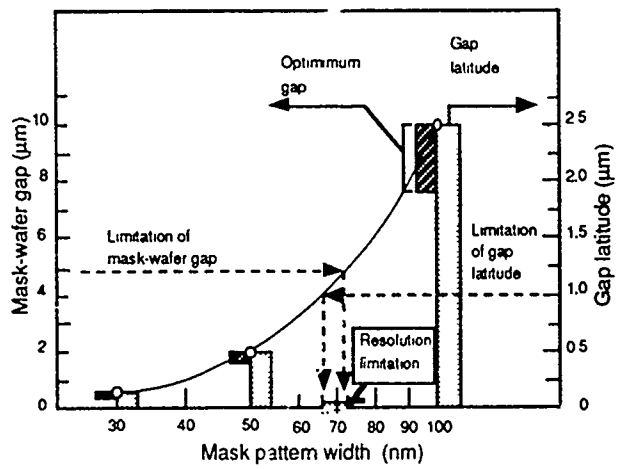

Fig 4 Resolution limit for proximity x-ray lithography

Besides such a wave interference effect, the proximity x-ray lithography has two more problems which degrade the resolution : 1) the secondary electron effect [18] in the resists and 2) the severe positioning accuracy required for the masks. Secondary electrons excited by x-rays

possibly degrade the resolution by a mechanism similar to the proximity effect of e-beam lithography. Also, the positioning accuracy must be as small as 10 nm even in the 0.1 μm design rule.

5. Projection X-ray Lithography

Projection x-ray lithography is known to have severe constraints, such as a 1 nm figure accuracy of aspherical mirrors with multi-layers(e.g. Mo/Si) in the 0.1 μm design rule and a reflectivity greater than 60 %, as shown in Table 1. However, in principle, the projection x-ray lithography system has the possibility that its resolution limit can be extended to about 30 nm. Of course, in the same way as optical lithography, the phase-shift method can be used. A final constraint on the resolution is a deteriorated reflectivity determined by a degraded figure accuracy of mirrors as shown in Fig. 5. To achieve such an accuracy, sophisticated metrology will be important.

Resolution (nm)	100	80	50	30
Throughput (wafers/hr)	20	20	20	20
Wavelength (nm)	13	10	7	5
Figure Accuracy (nm)	1.0	0.8	0.5	0.4
Reflectivity (%)	60	50	40	35

Table 1 Major reqiurements on an x-ray projection lithography system.

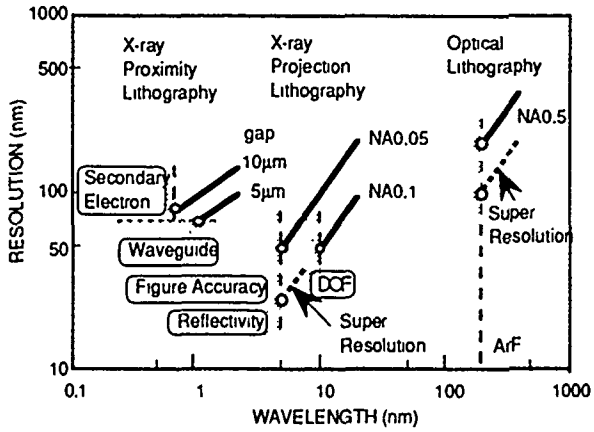

Fig.5 Theoretical resolution vs wavelength.

6. Conclusion

Nanometer lithography systems were discussed in the light of state-of-the art VLSIs. As a result, the best lithography system in the regions less that 0.2 μm is not yet clear. However, the optical lithography will enter regions as small as 0.15 μm. If this prediction is true, after that, projection x-ray and/or e-beam lithography would be very promising, if some breakthroughs occur. Also, in the near future, we will confront the limit of pattern miniaturization, which is brought about by the "fluctuation" of edge features in patterned resists[19]. This phenomenon is due more to resist polymer structure than to conventional beam scattering effects. The pattern size fluctuation will be a fatal effect in the same way as the impurity fluctuation in device reliability. More attention should be paid to resist materials in order to conquer the nanometer regime.

Reference

1] G.A. Sai-Halasz, Extended abstract of the 20th SSD&M, p. 5, 1988.
2] T. Shiba et al., IEDM, p. 225-228, 1989.
3] M. Abe et al., IEEE GaAs IC Symp. p. 127, 1990.
4] S. Kotani et al., ISSCC, pp. 150-151, 1988.
5] T. Nishino et al., IEEE Electron Device Letters, vol. 10, No. 2, pp. 61-63, 1989.
6] A.M. Hartstein et al., J. Appl. Phys. vol. 68,1990.
7] U. Meirav et al., Phys. Rev. Leet. vol. 65, p. 771, 1990.
8] R.R. Doering, 1992 Symp. on VLSI Technology, pp. 2-5.
9] M.D. Levenson et al., IEEE Trans. ED-29, p. 1828, 1982.
10] H. Fukuda et al., MicroProcess Conf., pp. 48-49, 1992.
11] C.W. Kaanta et al., VMIC Conf. pp. 144-152, 1991.
12] J.D. Buckley et al., SPIE vol. 1088 Optical/Laser Microlithography II, pp. 424-433, 1989.
13] Y. Sakitani et al., Proceedings of EIPB'92, 1992.
14] T.H. Chang et al., Proceeding of EIPB'92, 1992.
15] H. Betz et al., J.Vac.Sci.Technol., B4, p. 248, 1986.
16] T. Ogawa et al., MicroProcess Conf., pp. 210-211, 1992.
17] M.L. Schattenburg et al., J. Vac. Sci. Technol., B9, p. 3232, 1991.
18] T. Ogawa et al., Jpn J. Appl. Phys. vol. 28, pp. 2070-2073, 1989.
19] E.W. Scheckler et al., MicroProcess Conf., pp. 218-219, 1992.

Soft X-Ray Projection Lithography in Japan

Hiroo KINOSHITA

NTT LSI Laboratories
3-1 Morinosato Wakamiya, Atsugi-shi
Kanagawa, 243-01 Japan
Tel +81 462 40 2607
Fax +81 462 40 4317

Soft X-Ray Projection Lithography has attracted special interest recently. In Japan, reduction optics with multilayer mirrors has been developed and first demonstrated in 1986 by NTT[1].

Some other significant results include demonstrations of a demagnified pattern using a reflection mask at glancing angle by Matsumura et al.[2], at Hiroshima University, and reduction patterns using crystal by Sanyo Electric company[3]. The Canon group proposed three mirror demagnified optics in1987[4]. At present, the Hitachi and Nikon groups are conducting intense research to confirm the feasibility of soft X-ray projection system.

The Hitachi group has developed a Schwarzchild-type opticsand tried to replicate a fine pattern using KEK beam line, while the Nikon group has developed an X-ray microscope using Schwartzchild-type optics[5]. Demagnified fine patterns have been obtained using SORTEC beam line. All of these results will be presented at this conference.

According to recent findings, optical lithography is eminently capable of replicating patterns of less than 0.2 μm by utilizing annular illumination and phase shifting technologies. In addition, X-ray proximity lithography is useful in the same range. However, X-ray mask fabrication and inspection are very difficult with patterns less than 0.2 μm. Whichever system we choose, we still need major breakthroughs before either of them becomes practical even for a trial fabrication line.

Multigigabit DRAMs will require feature size on the order of 0.1 μm around the year 2005. Soft-x-ray projection lithography is only way we know at present to fabricate such ultrafine patterns with a high throughput.

Recently, we succeeded in replicating fine patterns less than 0.2 μm exposed on an exposure area larger than 20 mm x 0.4 mm. In addition, a high sensitivity resist of less than 2 mJ/cm^2 and a contrast of over 4.1 were obtained at a wavelength of 130 Å. However, much more still remains to be done before these techniques can be introduced to a test-fabrication line. For a wavelength of 130 Å, the figure error and roughness of the aspherical mirrors must be reduced. Furthermore, a more precise alignment technology and a step-and-scan wafer stage synchronized with the mask stage and that operates in a vacuum have to be devised.

In this paper, the present state of soft-x-ray projection lithography in Japan will be reviewed, including major recent results achieved at NTT.

Reference

1)H.Kinoshita,T.Kaneko,H.Takei,N.Takeuchi,and S.Ishihara, In Conf. of Appl. Phys., (28p-zf-15,Jpn.Soc.Appl.Phys.1986)
2)H.Matsumura et al., Jpn,J,Appl,Phys., 26-3(1987)487
3)S.Suzuki et al., Photon Factory Report 1988 No.6 267(1989)
4)M.Suzuki et al., European Patent App. 87306037.0 Date of filing;08.07.87
5)K.Murakami et al., 1992 Technical digest series vol. 8, 79

Development and Characterization of a 10x Schwarzschild System for Soft-X-Ray Projection Lithography

D. A. Tichenor, G. D. Kubiak, M. E. Malinowski, R. H. Stulen,
S. J. Haney, K. W. Berger, R. P. Nissen, R. L. Schmitt,
G. A. Wilkerson, L. A. Brown, P. A. Spence, P. S. Jin

Sandia National Laboratories
P.O. Box 969
Livermore, California 94551-0969

W. C. Sweatt, W. W. Chow

Sandia National Laboratories
P.O. Box 5800
Albuquerque, New Mexico 87185-5800

J. E. Bjorkholm, R. R. Freeman, M. D. Himel,
A. A. MacDowell, D. M. Tennant, O. R. Wood, II,

AT&T Bell Laboratories
101 Crawfords Corner Road, P.O. Box 3030
Holmdel, New Jersey 07733-3030

W. K. Waskiewicz, D. L. White, D. L. Windt

AT&T Bell Laboratories
600 Mountain Avenue
Murray Hill, New Jersey 07974-2070

T. E. Jewell

Optical Engineering Consultant
1105 N. Cedar Brook Road
Boulder, Colorado 80304

Multilayer-coated Schwarzschild imaging objectives have been used to demonstrate high-resolution soft-x-ray imaging.[1-2] In our previous work[3] a 20x reduction Schwarzschild imaging objective served a useful tool for studying the mounting and alignment of soft-x-ray optical elements and the quality and alignment of the condensing optics. However, the field of view, 25 μm by 50 μm, is much too small for a practical lithography tool. We have optimized and fabricated a new Schwarzschild system to achieve a 0.4 mm diameter field of view using 0.1 μm design rules. The increased field of view, although not large enough for a practical lithography tool, approximates the ring width in practical ring-field designs. This objective also covers enough area on the wafer to perform device fabrication experiments. This paper describes the development and characterization of the imaging system and the supporting illumination system.

The new Schwarzschild design is a 10x reduction system having an effective focal length of 26 mm. A decentered numerical aperture of 0.08 is defined by a stop located on the

convex primary, resulting in a depth of field at 13 nm wavelength of ± 1 μm. The objective is quasi-telecentric in image space. True telecentricity is not achieved, because the decentered aperture results in chief rays that are incident on the image plane at an angle of 12.1 degrees. However, the chief rays are parallel to each other, so that the magnification remains constant as the focal position varies within the depth of field. The latter property of telecentricity is required to control magnification in performing lithographic overlays. The angles of incidence of rays on the primary vary with radial location, requiring tapered multilayers to maintain a constant center wavelength throughout the soft-x-ray aperture.

The 10x Schwarzschild housing was designed using an approach that proved to be successful in the 20x design.[4] Figure 1 shows the housing and a set of mirror substrates. To maintain design performance the primary and secondary must be aligned to tolerances of ± 9 μm in separation and ± 2.5 μm in decentration. When correctly aligned third and fifth order spherical aberrations are balanced to reduce rms wavefront error in the subaperture.

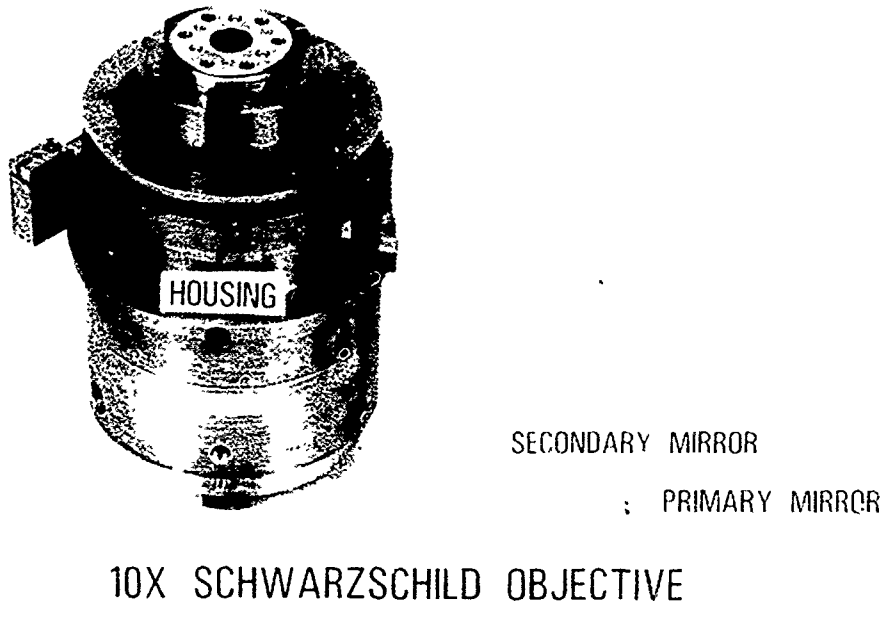

Figure 1. Photograph of 10x Schwarzschild imaging objective.

A key element in the fabrication strategy is to produce multiple sets of mirror substrates, measure the figure error, select matched pairs and clock them for best performance. In this system the elements are clocked for minimum rms wavefront error in the subaperture used for soft-x-ray imaging. Aberrations in the remainder of the full aperture do not affect x-ray imaging performance, and, therefore, do not constrain the clocking results.

Multiple primary and secondary substrates were fabricated and measured using a Zygo Mark IV XP interferometer. Figure errors were observed in the primaries ranging from 0.0011 to 0.0067 waves rms and in the secondaries ranging from 0.0069 to 0.0097 waves rms at HeNe wavelength. These magnitudes are very small at visible wavelengths but sufficient to cause significant degradation in the image resolution at soft-x-ray wavelengths. Both symmetric (zonal) errors and asymmetric errors were observed in the substrates. The spatial frequencies of the figure errors were generally lower than those of the 20x system, making it easier to identify matching pairs and find a well corrected subaperture. Three pairs were matched and clocked to achieve calculated wavefront errors approaching the design value. In the best result the rms wavefront error varied with field point from 0.058 to 0.071 at 13 nm compared to design values ranging from 0.055 to 0.064.

The effects on figure of the stresses in the applied multilayer and the varying thickness of the tapered multilayers have been studied[5]. The thickness of the multilayer varies with radius of the primary due to the varying incidence angle. For 40 multilayer pairs having a center wavelength of 13 nm, the thickness increases with radius by 6 nm across the subaperture. While this value represent almost half of a wavelength change in figure, to first order it introduces a tilt error across the subaperture, which does not affect image quality. Finite element calculations using the stress analysis code ABAQUS indicate that induced stress from the applied multilayers cause a more complex figure change. Maximum deformations approaching one wave at 13 nm are indicated by this calculations. Figure errors due to fabrication are on the same order, and ray tracing results indicate that they can be mitigated by clocking the elements.

The new Schwarzschild imaging objective is incorporated into a vacuum environment containing the laser plasma source (LPS), condensing optics and required adjustment as shown in Figure 2. The soft x-rays are generated by impinging a laser beam onto a gold target, creating a 15 eV plasma. The plasma source is driven by a Lambda Physik PLX 250 KrF excimer laser emitting 0.6 Joule, 20 ns pulses at a 200 Hz repetition rate.

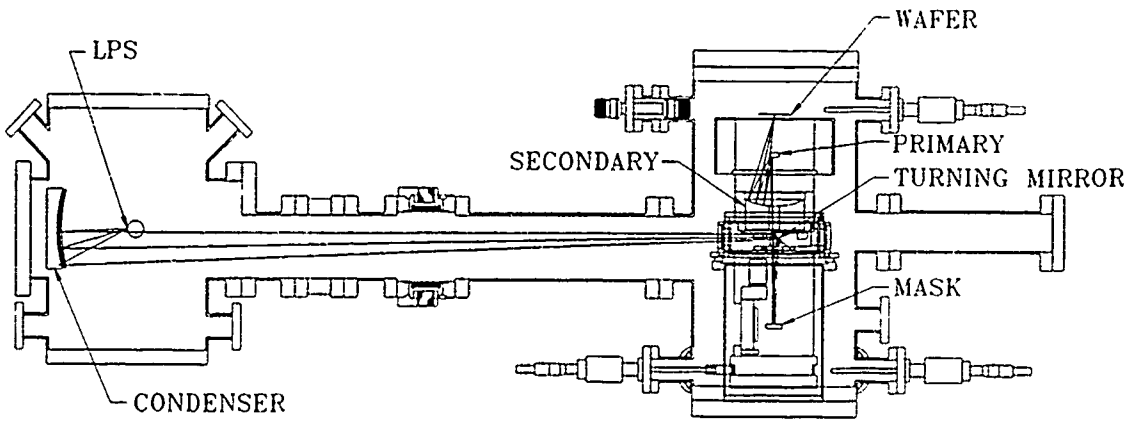

Figure 2. Sketch of 10x soft-x-ray imaging system.

The condensing system comprises an on-axis ellipsoidal collector located behind a decentered, 50 mm diameter aperture. The aperture protects the unused portion of the ellipsoid from LPS debris. Two ellipsoids have been fabricated having figure errors of 1/6 and 1/8 wave at HeNe wavelength throughout the 110 mm clear aperture. One focal point of the ellipsoid is placed precisely on the LPS using an alignment telescope, so that aberrations due to fabrication and alignment do not degrade image quality. The distance from the LPS to the center of the 50 mm aperture is 112.5 mm, which provides a 0.155 ster radian collection solid angle (2.5% of the available 2π ster radians) or an f/2.25 condenser aperture. This aperture is sufficient to provide kohler illumination over the 4 mm field of view in the mask plane. Three sites can be used on each ellipsoid as new surfaces are required. The second focal point is located in the entrance pupil of the Schwarzschild at an optical path length of 1500 mm. Alignment and focus of the condenser is observed on a scintillator located at the second focal plane. The resulting 13.3x condenser produces a 2 mm diameter image of the 150 μm source in the 4 mm entrance pupil of the Schwarzschild for a coherence factor of 0.5.

To illuminate a reflecting mask a turning mirror is aligned for a 45 degree angle of incidence, directing the x-rays onto the mask at 1.2 degrees. The x-rays reflect off of the mask and into the Schwarzschild, kinematically mounted on top of the turning mirror / mask assembly. This assembly gimbals about the turning mirror in two dimensions to direct the x-rays into the entrance pupil of the Schwarzschild. Since the aperture stop is embedded inside the objective, a surrogate objective, replicating the front end of the objective housing, is used for alignment. The back of the surrogate identifies the aperture plane. A scintillator is inserted in the aperture plane with a reticule marking the location of the decentered aperture.

The system contains five reflections which much be matched in center wavelength to maximize soft-x-ray throughput. Multilayer matching has been achieved in the turning mirror and mask to within one angstrom of the desired 134 angstrom center wavelength.

References:

1. H. Kinoshita, K. Kurihara, Y. Ishii and Y. Torii, J. Vac. Sci. Technol. **B7**, 1648 (1989)

2. J. E. Bjorkholm, J. Bokor, L. Eichner, R. R. Freeman, J. Gregus, T. E. Jewell, W. M. Mansfield, A. A. MacDowell, E. L. Raab, W. T. Silfvast, L. H. Szeto, D. M. Tennant, W. K. Waskiewicz, D. L. White, D. L. Windt, O. R. Wood, II, and J. H. Bruning, J. Vac. Sci. Technol. **B8**, 1509 (1990)

3. D. A. Tichenor, G. D. Kubiak, M. E. Malinowski, R. H. Stulen, S. J. Haney, K. W. Berger, L. A. Brown, R. R. Freeman, W. M. Mansfield, O. R. Wood II, D. M. Tennant, J. E. Bjorkholm, A. A. MacDowell, J. Bokor, T. E. Jewell, D. L. White, D. L. Windt, and W. K. Waskiewicz, Optics Letters **16**, 20 (1991)

4. D. A. Tichenor, G. D. Kubiak, M. E. Malinowski, R. H. Stulen, S. J. Haney, K. W. Berger, L. A. Brown, W. C. Sweatt, J. E. Bjorkholm, R. R. Freeman, M. D. Himel, A. A. MacDowell, D. M. Tennant, O. R. Wood, II, J. Bokor, T. E. Jewell, W. M. Mansfield, W. K. Waskiewicz, D. L. White and D. L. Windt, Applied Optics feature issue on Soft X-ray Projection Lithography, (1993).

5. R. R. Kola, D. L. Windt, W. K. Waskiewicz, B. E. Weir, R. Hull, G. K. Celler, C. A. Volkert, Appl. Phys. Lett. **60**, 3120 (1993).

Soft X-ray Projection Imaging using 32:1 Schwarzschild Optics

Hiroshi Nagata, Masayuki Ohtani, Katsuhiko Murakami and Tetsuya Oshino

Research Laboratory, Nikon Corporation,
1-6-3 Nishi-ohi, Shinagawa-ku, Tokyo 140, Japan
(03)3773-1111

Yukihiko Maejima, Toshihiko Tanaka, Takeo Watanabe, Yoshio Yamashita
and Nobufumi Atoda

SORTEC Corporation,
16-1 Wadai, Tsukuba-shi, Ibaraki 300-42, Japan
(0298)64-4550

X-ray projection lithography is expected as a candidate for VLSI production in the near future. To get a resolution of 0.1μm and wide exposure area simultaneously, reduction systems with aspherical mirrors are required[1,2], but the machining precision required to fabricate aspherical surfaces has not been achieved. Thus reduction systems with spherical mirrors[3-5] are preferable in current study of mounting and alignment of optical elements and resist process.

We designed and arranged a 32:1 reduction imaging system using Mo/Si-multilayer-coated Schwarzschild optics. The imaging experiment with a transmission mask was carried out using the synchrotron radiation (SR) light source in SORTEC[6]. Line-and-space patterns down to 0.1μm were fabricated in PMMA resist with an exposure of 100sec.

The experimental arrangement is shown in Fig.1. X-rays from the SR ring, operating at 1GeV and 200mA, passed through a Be filter, a quartz deflecting mirror and a polypropylene vacuum window, illuminated the transmission mask. The deflecting mirror was concave and deflecting angle was 8 degrees. Thus the SR light was focused on the mask and fitted to the numerical aperture of the Schwarzschild optics only in the horizontal direction.

The mask was made of Au on SiN membrane, and the line-and-space widths were between 10μm and 1μm. The reduction rate of the Schwarzschild optics was comparatively high, and the mask pattern was easily fabricated by conventional optical lithography.

The Schwarzschild optics was the same as used in the microscopic experiment[7,8], except the multilayer coating was Mo/Si to obtain high reflectivity at 13nm[9] instead of NiCr/C at 4.5nm. The designed specifications of resolution were 0.08μm for the diffraction limit at 13nm, 0.06μm for aberration within 30μm of image height, and 0.1μm for total resolution.

Figure 2 shows the scanning electron microscopic images of the projected pattens in PMMA resist. The thickness of the resist was 0.17μm and the exposure

time was 100sec. In Fig.2a, the projected patterns of 0.3μm were clearly shown to be independent of the line orientation, while the resolution of the 0.15μm patterns changed with line orientation. This was due to the difference in the numerical aperture of the X-rays, as mentioned above. Figure 2b shows enlarged patterns of the 0.15 and 0.1μm lines and spaces. The patterns are not sharp, but can still be distinguished down to 0.1μm.

As a result of this imaging experiment, we found that the projection optics worked very well, and almost diffraction-limited images down to 0.1μm were fabricated. Further experiments, for example, full aperture illumination and/or thinner resist process, will be conducted soon.

References

1. T.E.Jewell,J.M.Rodgers and K.P.Thompson, J.Vac.Sci.Technol.B8,1519 (1990).
2. K.Kurihara,H.Kinoshita,N.Takeuchi,T.Mizota,T.Haga and Y.Torii, J.Vac.Sci.Technol.B9,3189(1991).
3. H.Kinoshita,K.Kurihara,Y.Ishii and Y.Torii, J.Vac.Sci.Technol.B7, 1648(1989).
4. J.E.Bjorkholm,J.Bokor,L.Eichner,R.R.Freeman,J.Gregus,T.E.Jewell, W.M.Mansfield,A.A.MacDowell,E.L.Raab,W.T.Silfvast,L.H.Szeto, D.M.Tennant,W.K.Waskiewicz,D.L.White,D.L.Windt,O.R.Wood U and J.H.Bruning,J.Vac.Sci.Technol.B8,1509(1990).
5. D.A.Tichenor,G.D.Kubiak,M.E.Malinowski,R.H.Stulen,S.J.Haney, K.W.Berger,L.A.Brown,R.R.Freeman,W.M.Mansfield,O.R.Wood U, D.M.Tennant,J.E.Bjorkholm,A.A.MacDowell,J.Bokor,T.E.Jewell, D.L.White,D.L.Windt and W.K.Waskiewicz,Optics Letters 16,1557(1991).
6. M.Kodaira,N.Awaji,T.Kishimoto,H Usami and M.Watanabe,Jpn.J.Appl.Phys. 30,3043(1991).
7. K.Murakami,H.Nakamura,T.Oshino,M.Ohtani and H.Nagata,OSA Technical Digest on Soft-X-Ray Projection Lithography 8,79(1992).
8. K.Murakami,H.Nakamura,T.Oshino,M.Ohtani and H.Nagata,Jpn.J.Appl.Phys.31, L-1500(1992).
9. K.Murakami,H.Nakamura,T.Oshino,M.Ohtani and H.Nagata,Proc.SPIE 1742, (1992). (in printing)

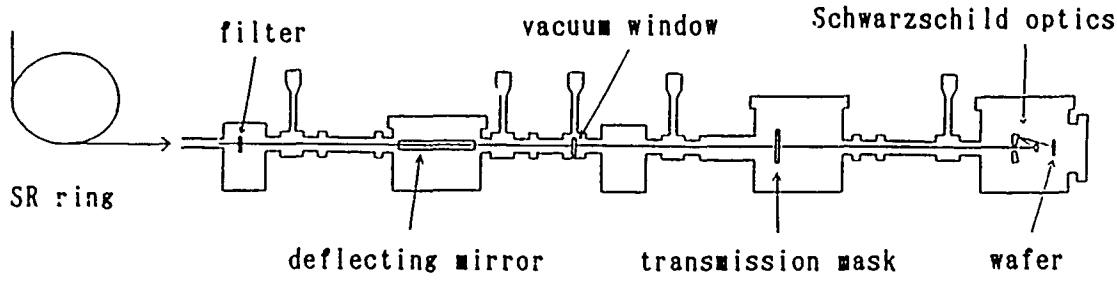

Figure 1. Experimental arrangement for soft X-ray projection imaging with synchrotron radiation.

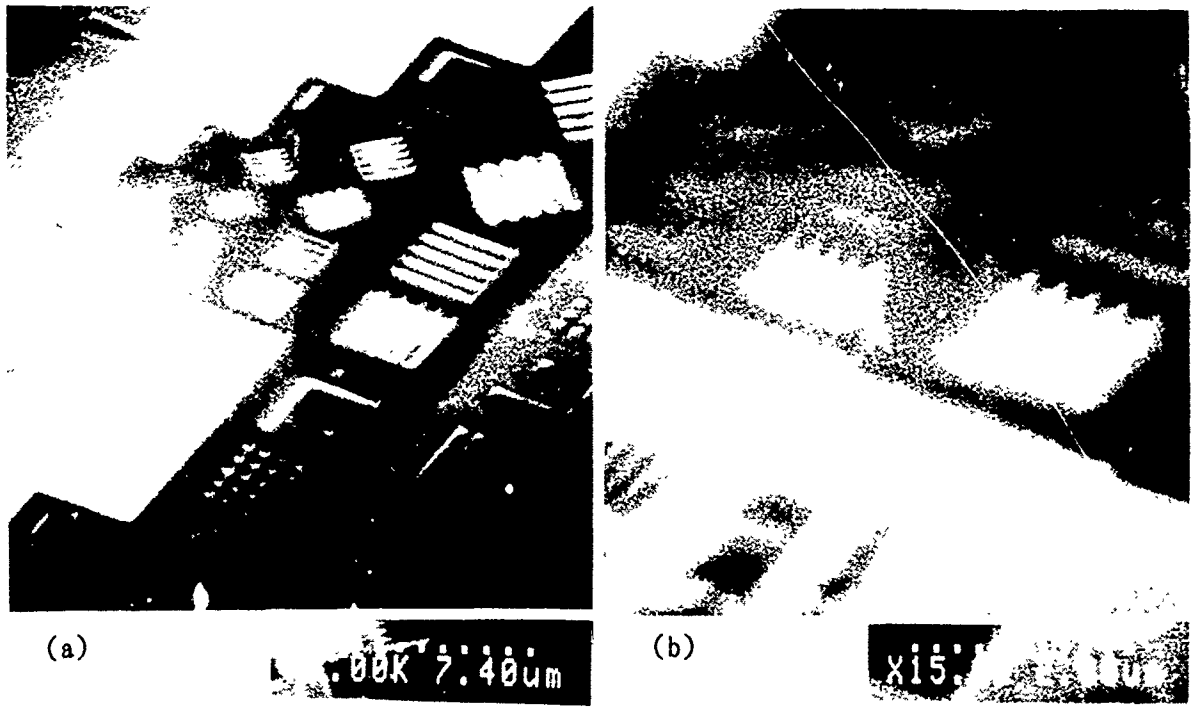

Figure 2. SEM images of the projected patterns. Line-and-space widths are (a) 0.3, 0.2, 0.15 and 0.1μm and (b) 0.15 and 0.1μm.

A New Surface Imaging Resist Technology for Soft-X-Ray Projection Lithography

A. A. MacDowell
AT&T Bell Laboratories, 510E Brookhaven National Laboratory, Upton, NY 11973 (516) 282-5334

O. R. Wood, II
AT&T Bell Laboratories, 101 Crawfords Corner Road, Holmdel NJ 07733-3030

J. M. Calvert, T. S. Koloski
Naval Research Laboratory, Center for Bio/Molecular Science & Engineering (Code 6900), 4555 Overlook Avenue, SW Washington, DC 20375-5348

Sub-quarter-micron features have been produced in a number of organic resists using soft-x-ray projection lithography (SXPL) at 14 nm, including a demonstration of 0.05 um lines and spaces in poly (methylmethacrylate) (PMMA).[1] Unfortunately, the opacity of conventional resists in the soft-x-ray region requires that the resist thickness be reduced to less than 200 nm;[2] in practice, 70 nm thick layers are often used. Such thin layers lead to several problems. First, spincoating pinhole-free layers becomes increasingly difficult at thicknesses below 100 nm. Second, the etch resistance of thin organic layers may not be sufficient for subsequent pattern transfer operations. Third, they are too thin to function as planarizing layers over pre-existing substrate topography. One solution has been to use a trilevel resist composed of a thin top PMMA imaging layer, an intermediate layer of germanium for etch resistance, and a thick hardbaked photoresist for planarization. While the trilevel approach has been successfully demonstrated for producing high resolution features with SXPL at 14 nm,[3] the complexity of this process makes it problematic for rapid acceptance in a production environment. An alternative approach, which circumvents the resist opacity issue, involves the use of so-called surface-imaging resists.[4] In a surface imaging resist, radiation-induced changes in a thin imaging layer lead to conversion of the exposed region to an etch resistant material.

In this talk, we describe soft-x-ray projection lithography using a true top-surface-imaging process, with an organosilane monolayer film as the primary imaging layer and electroless Ni as the etch resist layer.[5] Specifically, an x-ray sensitive self-assembled monolayer organosilane film was patterned using a 20:1 reduction Schwarzschild optic illuminated at 14 nm. Feature resolution has been demonstrated to linewidths as small as 0.15 μm with doses of 50 mJ/cm^2.

Our monolayer surface imaging approach, a ligand-based selective metallization process, is shown schematically in Fig. 1

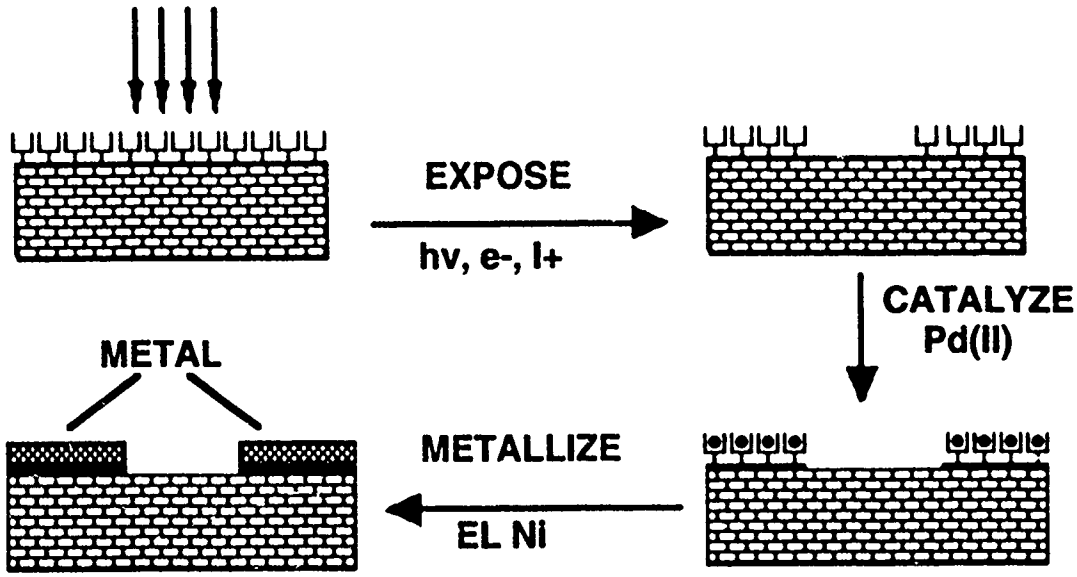

Figure 1. Schematic diagram illustrating a ligand-based selective metallization surface imaging resist process.

The general concept of the monolayer surface imaging approach is shown schematically in Fig. 1. In the first step, molecular self-assembly is used to produce a monolayer organosilane film containing metal ion binding functional groups (ligands) which are represented by the "goalpost" structures. In the second step of the process, the monolayer film is exposed to a sufficient dose of patterned radiation to impair the ligating ability of the film with regard to binding a metal complex catalyst. In the next step, the patterned surface is treated with an aqueous catalyst solution[6] based on $PbCl_4^{2-}$ for approximately 30 minutes to bind the catalyst only to the remaining intact ligand sites. Finally, immersion of the catalyzed surface in NIPOSIT™ 468 (Shipley Co., Marlborough, MA) borane-reduced electroless nickel bath results in deposition of nickel only in the unexposed regions of the film. A related approach was also investigated in which organosilane monolayer films containing halobenzyl ($-C_6H_4-CH_2X$, where X = Cl, I) groups[7] were irradiated to eliminate the halogen from the film. Subsequent treatment with a ligand containing nucleophilic reagent, such as the lithium salt of ethylenediamine or the cesium salt of a carboxylic acid, results in grafting a metal binding site onto the film.[7] This produces a surface equivalent to that shown in the upper right-hand corner of Fig. 1. After the grafting step, the catalysis and metallization steps are identical to those used in the first approach. An advantage of the second approach is that the x-ray photosensitivity of the halobenzyl film is approximately 100 times greater than for the intact ligand films (see below).

Soft-x-ray exposures were performed using 14 nm radiation from the undulator on the U13 beamline on the VUV storage ring at the National Synchrotron Light Source at Brookhaven National

Laboratory. The imaging system, a Mo/Si multilayer coated Schwarzschild camera providing 20X reduction, produced a roughly square image field, approximately 35 μm on a side.[1] The die was composed of four subfields, each of which contained a number of

a)

b)

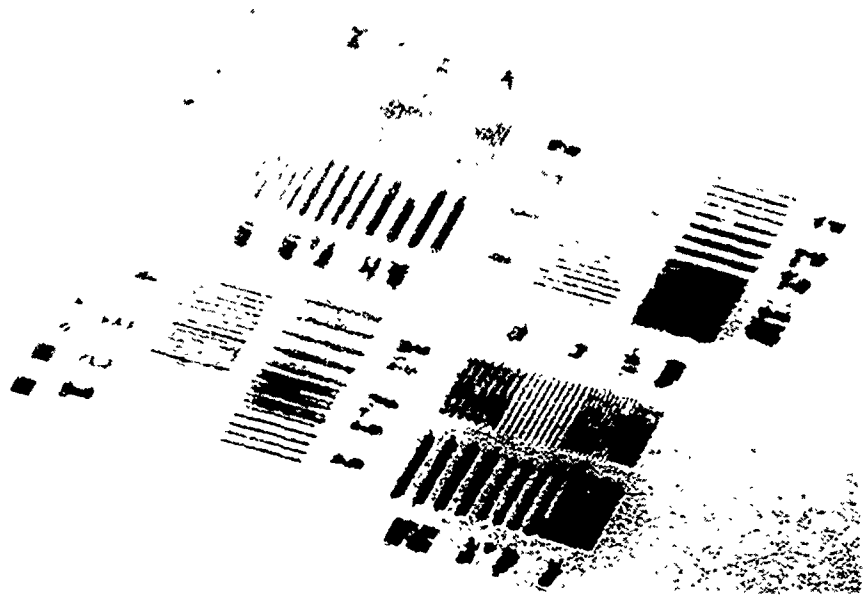

Figure 2. SEM micrograph of image of resolution test pattern produced by a 20X reduction Schwarzschild optic at 14 nm in (a) a 60 nm thick film of PMMA and (b) a metallized monolayer resist.

equal line and space patterns with widths varying from 0.5 μm to 0.05 μm. Exposures were performed in vacuum at 10^{-5} Torr.

Fig. 2 shows scanning electron micrographs of soft-x-ray images made using PMMA and the ligand-based selective metallization monolayer resist process. These micrographs were taken at approximately the same magnification to allow direct comparison of the overall imaging characteristics of the two resists. After exposure to 55 mJ/cm^2 of 14 nm radiation, PMMA was wet developed in a 1:2 mixture of MIBK:IPA for 60 seconds, followed by a 60 second rinse in IPA for 60 seconds. After exposure to 250 mJ/cm^2 of 14 nm radiation, the monolayer organosilane film containing a chlorobenzyl functional group on native oxide Si was selectively metallized using cesium salt grafting chemistry[6] in conjunction with electroless nickel plating, as described above. Examination of the PMMA image shows that lower resolution structures (feature sizes from 0.25 μm to 0.5 μm) in the upper left and lower right fields are reasonably well resolved and some, but not all, of the higher resolution structures in these fields are also discernible. There are several large defects in the image, all of which are replicated in the micrograph of the metallized monolayer, indicating that their origin was in the aerial image from the camera, and was not due to the resist process. Except for the graininess present in the metallized monolayer image, which will adversely affect features at the 0.15 μm size regime and below, the two images are comparable.

The aerial image should be accurately replicated as the latent image in the organosilane layer, due to the monomeric character of the film. Recent studies have shown that the Pd(II) catalyst is composed of colloidal particles whose diameters can be controlled to range between 50 - 100 Å, a dimension that is small compared to the lithographic feature size. Therefore, we believe that optimization of the electroless plating bath composition and/or process conditions to minimize deposit crystallinity is the critical issue in determining the ultimate resolution of this process.

1. J. E. Bjorkholm, et al., J. Vac. Sci. Technol. B **8**, 1509 (1990).
2. G. N. Taylor, R. S. Hutton, D. L. Windt, and W. M. Mansfield, Proc. SPIE, **1343**, 258 (1990).
3. D. W. Berreman, et al., Appl. Phys. Lett. **54**, 2180 (1990).
4. G. N. Taylor, L. E. Stillwagon, and T. Venkatesan, J. Electrochem. Soc. **131**, 1658 (1984).
5. J. M. Calvert, et al. Solid State Technol. **34**, 77 (1991).
6. W. J. Dressick, et al., Mat. Res. Soc. Symp. Proc. **260**, 659 (1992).
7. J. M. Calvert, T. S. Koloski, W. J. Dressick, C. L. Dulcey, M. C. Peckerar, F. Cerrina, J. W. Taylor, D. Suh, O. R. Wood, II, A. A. MacDowell and R. M. D'Souza, Proc. SPIE **1924**, (1993), To be published.

High-Resolution Imaging of Laser-Produced Plasmas at a Wavelength of 130 Å using a Normal Incidence Multilayer-Mirror Microscope

J. F. Seely, G. E. Holland, and J. V. Giasson
E. O. Hulburt Center for Space Research
Naval Research Laboratory, Washington DC 20375-5352
(202)767-3529

Laser-produced plasmas were recently imaged at a wavelength of 44 Å using a spherical multilayer-coated mirror operating near normal incidence, and emission features were recorded with a spatial resolution of 40 μm.[1] In order to produce images with better resolution, we have developed a microscope consisting of two spherical mirrors in a Cassegrain-type optical configuration. Spherical optical figure was chosen because of the demonstrated low surface roughness and high optical figure accuracy of previously fabricated mirrors. The spherical aberrations of the concave primary mirror and the convex secondary mirror tend to cancel, and the radii of curvature of the two mirrors and the mirror separation were chosen to minimize the overall spherical aberration of the optical system.

The optical layout is shown schematically in Fig. 1. The primary and secondary mirrors, filters, and camera were housed in a vacuum chamber that was attached to the target chamber of the 24-beam Omega laser. The primary mirror was positioned 170 cm from the target, was 9 cm in diameter, and had a radius of curvature of 110 cm. The secondary mirror was positioned 50 cm from the primary mirror and was 3.1 cm in diameter. Two different secondary mirrors had radii of curvature of 150 cm and 80 cm and produced images with magnifications of 0.8 or 2.2, respectively.

The radius of curvature (150 cm) of one secondary mirror was chosen to produce an image just behind the primary mirror with a magnification of 0.8. Shown in Fig. 2(a) is the calculated image of an on-axis point object 170 cm from the primary mirror, and the size of the focal spot is less than 0.1 μm. This small size is the result of the cancellation of the spherical aberrations of the concave primary mirror and the convex secondary mirror. Targets that were irradiated by the Omega laser were of order 1 mm in size, and the case of a point object 0.5 mm above the optical axis is shown in Fig. 2(b). The focal spot is 0.5 μm in size. The two focal spots shown in Fig. 2(a) and (b) fall at the same distance behind the primary, and this implies that the image has negligible curvature. The dashed lines in Fig. 2(b) indicate extreme off-axis rays that were obstructed by the hole in the primary mirror.

The mirror substrates, fabricated by General Optics, were super-polished fused quartz with optical figure accuracy of λ/10 and surface roughness of 1 Å. The mirror coatings were sputter deposited by Ovonic Synthetic Materials and

consisted of 40 periods of molybdenum and silicon. The intention was to image the intense transition of the sodium-like niobium ion Nb^{30+} at a wavelength of 131.69 Å. This transition had been observed in the spectrum of a laser-produced plasma recorded by a grazing-incidence spectrograph (see Fig. 3(a)). A multilayer mirror was characterized using synchrotron radiation and nad peak normal-incidence reflectance of 59% at a wavelength of 130 Å.

The calculations of the reflectance were performed using the computational model described in Ref. 2. Two parameters were varied in the calculation, the period thickness and the interfacial roughness parameter, and the inferred values were 66.9 Å and 8 Å, respectively. The calculated normal-incidence reflectance profile is shown in Fig. 3 (b), and the reflectance at the wavelength (131.69 Å) of the Nb^{30+} transition is 40%. Filters consisitng of 3 μm silicon and 1 μm beryllium blocked the intense backscattered laser light of wavelength 3510 Å and other plasma radiation outside the reflectance waveband of the multilayer mirrors. The transmittances of the silicon and beryllium filters were 1% and 20% at a wavelength of 130 Å, respectively.

The microscope was used to image a variety of laser-irradiated targets. Shown in Fig. 4 is the image of a 1 mm niobium wire that was recorded using the secondary mirror with 80 cm radius of curvature and 2.2 magnification. A ring of plastic was fitted around the wire near the tip, and the width of the plastic ring was approximately 0.5 mm. Emission was observed from the focal spots of the laser beams incident on the niobium wire and on the plastic ring. The emission from the plastic was presumably from higher-atomic-number impurities in the plastic or contaminants on the surface of the plastic. A particularly interesting focal spot appears at the location indicated by A in Fig. 4. This focal spot was apparently viewed on edge, and the width of the emission region is 25 μm on the film. The edges of this and other sharp features indicate a spatial resolution of 10 μm in the film plane which corresponds to 5 μm spatial resolution in the target plane. Since the target was 170 cm from the primary mirror, this is equivalent to a resolution of 0.6 arcsec. Integrating over the entire area of a typical image, the total number of photons incident on the film from the laser-irradiated target was approximately 3×10^{7}, and the corresponding energy radiated by the target into 4π solid angle was approximately 5×10^{-3} J in the 128-132 Å waveband.

The high exposure levels achieved in the wavelength region 128 Å to 132 Å indicate that a similar microscope may be operated at shorter wavelengths. In the present experiment, the product of the reflectances of the two multilayer mirrors and the transmittances of the silicon and beryllium filters was 5×10^{-4}. In the wavelength region 34 Å to 50 Å, for example, W/B_4C multilayer coatings have been fabricated with measured reflectances of 2%, and a thin titanium or tin filter has transmittance of 50%. Thus the product of the reflectances of two multilayer mirrors and the transmittances of two filters would be 1×10^{-4} in the 34 Å to 50 Å wavelength region. Grazing-incidence spectra indicate that laser-irradiated targets are typically much brighter in the shorter wavelength regions, and a two-mirror microscope operating in the 34-50 Å region seems feasible.

1. C. M. Brown, U. Feldman, J. F. Seely, M. C. Richardson, H. Chen, J. H. Underwood, and A. Zigler, "Imaging of laser-produced plasmas at 44 Å using a multilayer mirror", Opt. Commun. 68, 190-195 (1988).
2. J. F. Seely, M. F. Kowalski, W. R. Hunter, J. C. Rife, T. W. Barbee, G. E. Holland, C. N. Boyer, and C. M. Brown, "On-blaze operation of a Mo/Si multilayer-coated, concave diffraction grating in the 136-142 Å wavelength region and near normal incidence", Applied Optics (in press).

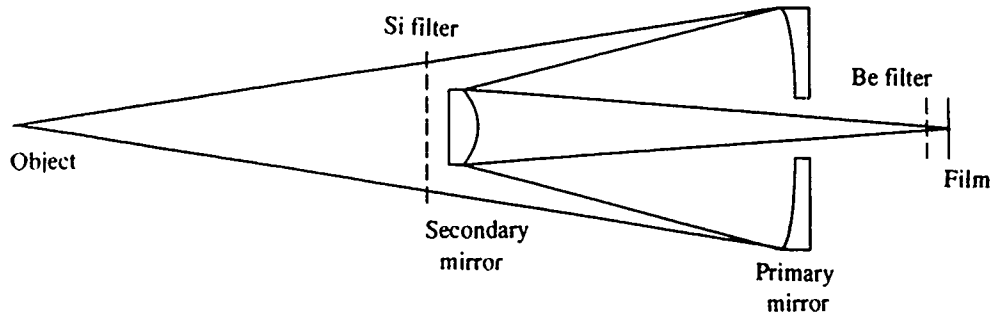

Figure 1

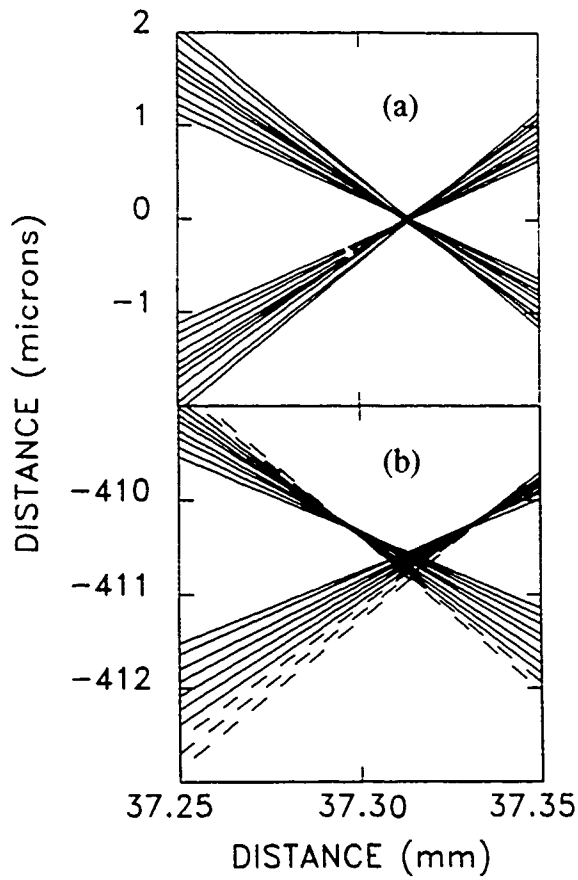

Figure 2

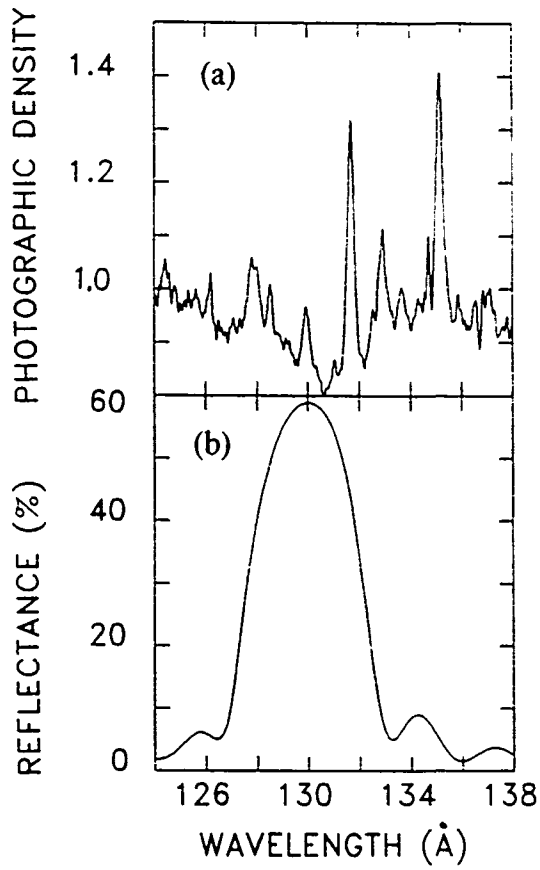

Figure 3

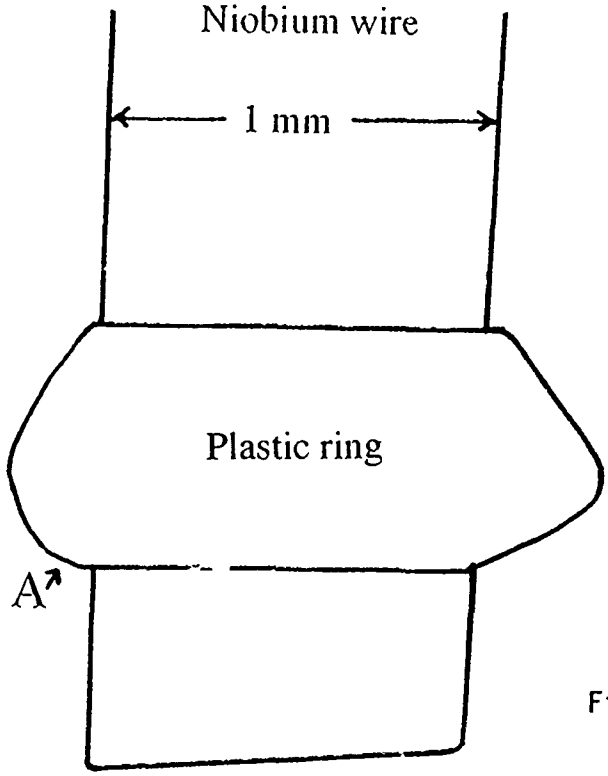

Figure 4

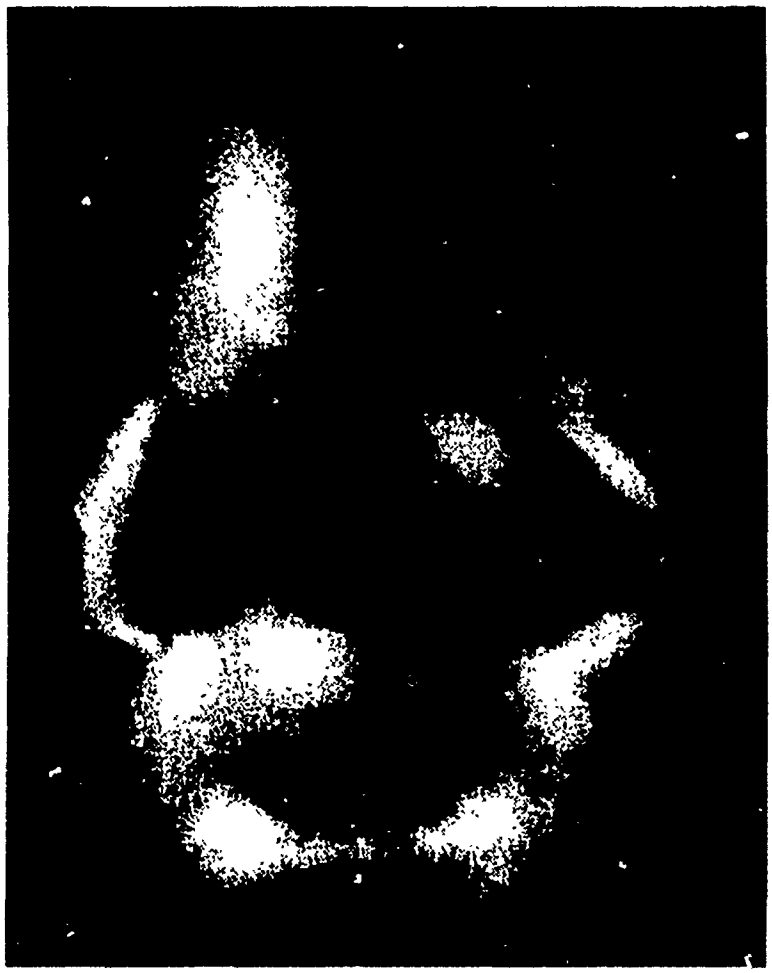

Optical Metrology

TuB 1:00pm–3:10pm
Bonsai II & III

Frits Zernike, Jr., *Presider*
SVG Lithography Systems, Inc.

Cost of Ownership for Soft X-ray Projection Lithography

William H. Arnold and Kathleen Early
Integrated Technology Division
Advanced Micro Devices
Sunnyvale, CA 94088

This paper explores the projected cost of ownership for a soft x-ray projection lithography process. The analysis includes the cost of capital equipment (exposure tool and resist processing), resist materials, and masks, as well as the economics associated with tool productivity and utilization. There is a particular focus on the impact of the cost of the masks, as it apr' · different IC product types and their volumes. Also studied are the tradeoff of system thr(·, with required resist dose and the costs associated with multilayer resist systems.

The results of the calculations are stated in terms of dollars per wafer level exposed. These will be compared with current cost estimates for optical lithography processes in order to frame the problem in a realistic way.

Title to be Announced

John H. Bruning
GCA Tropel
60 O'Connor Road
Fairport, NY 14450

Optic Fabrication and Metrology for Soft X-Ray Projection Lithography

Marc D. Himel
AT&T Bell Laboratories
101 Crawfords Corner Road
Holmdel, NJ 07733
(908) 949-6675

Introduction

One of the many technology areas that lie on the critical-path to the success of soft X-ray projection lithography (SXPL) is the fabrication and metrology of aspheric mirrors. I will review the progress of our collaboration with a number of companies to determine if the mirror fabrication and metrology technologies can be developed so that SXPL can meet the early next century demand for 0.1 μm design rule devices. The figure and finish tolerances for these mirrors are well beyond the current state-of-the-art for aspheres and even beyond industry's capability to fabricate spheres. To achieve the desired imaging capability will require mirrors with subnanometer figure errors over the full spatial frequency bandwidth, from 10 nm to 250 mm. Although exact full bandwidth tolerances have not been determined, we have estimated that the nanoscale rms roughness (as measured over a bandwidth of 10 nm to 1.0 μm) must be less than 0.1 - 0.2 nm so that high reflectivity multilayers can be attained. Specifications for the figure errors of a 5X reduction system being developed by GCA/Tropel range from 1.0 to 3.0 nm PV (depending on the mirror) for a 36 term Zernike polynomial fit. Although we have not yet estimated the specification for spatial frequencies between 1.0 μm and 25 mm, there is evidence that they could have a significant effect on imaging performance at X-ray wavelengths near 14 nm.[1]

Metrology

To meet the above fabrication requirements, it is necessary to have a full bandwidth metrology capability for the evaluation of spheres and aspheres during the fabrication process. We envision developing a capability that covers four frequency bandwidths: figure, using visible light interferometry; mid-spatial frequencies, using a Bauer optical profiler; microroughness, using a Wyko Topo or similar profiler; and nanoscale roughness, using force microscopes. Each of these tools must be developed to measure coated and uncoated aspherical surfaces and there must also be enough overlap in the measured bandwidth to allow for metrology cross checks. The bandwidths we would like to achieve for power spectral density measurements are shown below:

Metrology tool	Bandwidth
Interferometer	5.0 mm - Full Aperture
Bauer optical profiler	300 μm - 50 mm
Wyko Topo/Zygo Maxim	1.0 μm - 3.0 mm
Atomic force microscope	10 nm - 10 μm

At the present time, we do not see any major problems achieving the desired capability for measuring the nanoscale and microscale finish errors of curved optics. We do, however, anticipate that making measurements of figure and mid-frequency errors with the desired accuracy will be much more difficult.

To date, the best figure measurements we have seen were recorded with a specialized interferometer designed and built by GCA/Tropel as part of the development of our 5X imaging system. That interferometer has achieved a 3σ reproducibility of 1.2 nm PV (36 term Zernike fit) for the measurement of a sphere, which is approaching our estimated accuracy requirements. As absolute accuracy is very hard to determine at these levels, we hope to develop metrology crosschecks for the figure measurements by extending the measurement bandwidth of the Bauer optical profiler to full figure metrology and to develop an X-ray metrology tool capable of 1.0 nm reproducibility. Our candidates for the at-wavelength test include knife-edge, scanned grating, and shearing interferometry.

Substrate Fabrication

In conjunction with developing the necessary metrology techniques, we must also be able to fabricate the mirror substrates. The figuring method must be able to meet the full bandwidth error tolerances for the fabrication of high order aspheres with a few microns of departure from the base sphere. We are concentrating our efforts on two techniques: controlled deposition of Mo/Si multilayer coatings and ion-beam figuring. With controlled deposition, an additive process, we plan to develop a multilayer coating process that will allow us to deposit the desired profile. Once the desired figure has been obtained, a highly reflective Mo/Si multilayer coating would be deposited to bring the reflectivity to 60% over the entire clear aperture. One of the main advantages of this method is that we know that we can deposit high reflectivity coatings on top of another Mo/Si multilayer. Ion beam figuring, a subtractive process, is attractive because it can be computer controlled and it is an iterative technique that should converge rather quickly to the desired figure. Its main disadvantage is that it requires smooth surfaces with little or no sub-surface damage or else additional roughness may be induced by the milling process, which would reduce the soft X-ray reflectivity of the multilayer coatings.

Conclusion

We are in the process of developing and evaluating potential fabrication and metrology techniques for the production of high accuracy mirrors for SXPL. Although the industry euphemism is "if you can measure it, you can fabricate it," the fabrication requirements for these aspheres are so far beyond the current state-of-the-art that this assumption may no longer be valid. Although recent advances show much promise, significant efforts are still needed to meet industry demands.

Acknowledgements

This project is funded in part by a Cooperative Agreement with the National Institute of Standards and Technology as part of their Advanced Technology Program.

References

1. K. L. Lewotsky, A. Kotha, and J. E. Harvey, "Performance Limitations of Imaging Microscopes for Soft X-ray Applications," Proceedings of the 1992 SPIE Annual Meeting.

SURFACE METROLOGY OF SOFT X-RAY OPTICS

T. Vorburger, T. McWaid, J. Fu, C.J. Evans,
W.T. Estler, and R.E. Parks
Precision Engineering Division
National Institute of Standards and Technology
Gaithersburg, MD 20899 USA

The reflectivity and scattering of mirrors used for x-ray optics at a wavelength of 13.6 nm depend on spatial wavelengths of the surface topography ranging from atomic dimensions to the full aperture of the mirror. Accordingly, we are developing measurement and calibration approaches that will span over 8 orders of magnitude of spatial wavelength from 1 nm to 150 mm. As shown in Fig. 1, the array of profiling techniques in our laboratory includes scanning tunneling microscopy, atomic force microscopy, stylus profiling, and phase measuring interferometry for both finish and figure. In addition, a calibrated stylus instrument produces measurements of surface finish profile with good resolution and accuracy. Thus, NIST is developing the capability to provide continuous power spectral information over the full bandwidth. The overlapping spatial wavelength regimes of the various approaches enable us to test any methods divergence between them.

For surface finish measurements, we have developed a long-range STM with a lateral range of 600 μm and a lateral resolution of 1 nm. The rms vertical resolution is approximately 0.03 nm. This instrument has been used to measure x-ray multilayer test specimens over several fields of view. In addition, measurements with this instrument have been compared with the interferometric microscope, the stylus profiler, and an atomic force microscope for the same surface features, including a square-grid calibration pattern, an isolated surface scratch, and an isolated single point defect. Relocation of the same surface features in the field of view of the various techniques was achieved by "road mapping" the surface.

We have also acquired a stand-alone atomic force microscope which may be used to measure insulating surfaces. It may also be positioned directly on large optics for surface finish testing. Measurements with the AFM of superpolished silicon yield rms roughness values of approximately 0.3 nm over a field of view of several micrometers.

In the regime normally considered figure metrology, measurements will be needed of both bare substrates and coated optics. For this reason, our program focuses initially on visible light interferometry. Figure tolerances required for soft x-ray projection lithography optics exceeded NIST's calibration capability for flats, let alone off-axis aspheres. Thus, our program started with flat calibration. Full aperture calibration of 150 mm flats is now available with 5 nm two sigma uncertainty; uncertainties less than 1 nm are obtained on individual profiles. In addition, our measurement of single profiles on an optical flat agree with results obtained by United Technology Optical Systems and Brookhaven National Laboratory to better than 4 nm peak-to-valley.

The lessons and techniques learned from flats are now being applied to spheres, and techniques to allow measurement of aspheres with respect to spherical reference optics developed. In particular, we have developed an algorithm for correcting the fringe-density-induced errors in phase measuring interferometry of steep aspheres. Initial measurements of surface profiles with 5 μm deviation from a best fit sphere showed an accuracy improvement by about a factor of 5 to approximately 10 nm (P-V) using the current version of the algorithm.

The measurement of the surface power spectral density with these types of instruments is related to the performance of the x-ray optical surfaces for making high quality lithographic images. Power spectra must be measured over a wide dynamic range and with reasonably high accuracy. Therefore, we are developing a calibrated atomic force microscope with displacement measuring interferometers to calibrate motion in all three directions.

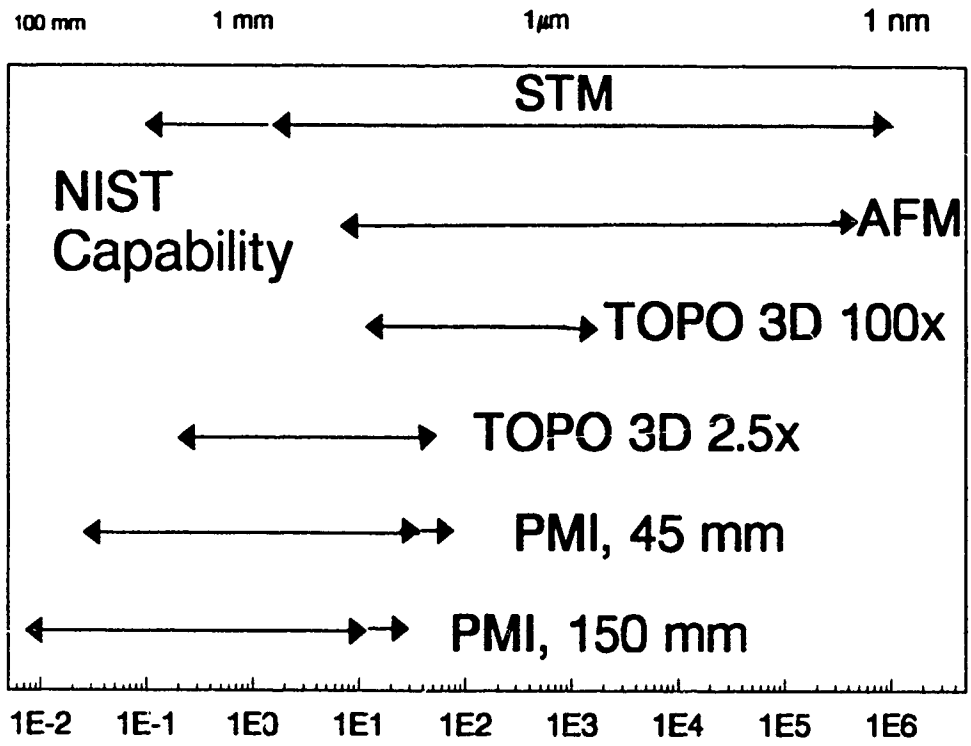

FIGURE 1: NIST capabilities for surface topography measurement spanning about eight orders of magnitude of spatial frequency (or spatial wavelength from full apertures of 150 mm to a fraction of the illuminating wavelength).

X-Ray Metrology

TuC 3:40pm–4:30pm
Bonsai II & III

David T. Attwood, *Presider*
Lawrence Berkeley Laboratory

Point Diffraction Interferometry at Soft X-ray Wavelengths

Gary E. Sommargren
Lawrence Livermore National Laboratory
University of California
Livermore, CA 94550

Ralph Hostetler
AlliedSignal Technical Services
Livermore, CA 94550

To achieve the image performance necessary for soft x-ray projection lithography, interferometric testing at the design wavelength is required to accurately characterize the wavefront of the imaging system. The wavefront depends not only on the surface figure of the individual optics and on their relative alignment, but also on aperture dependent phase shifts induced by the resonant multilayer coatings on the optical surfaces. This paper describes the design and lithographic fabrication of an array of point diffraction interferometers on a Si_3N_4 membrane that has been over-coated with a spatially graded absorbing film to provide fringe contrast control. Experimental results using a visible light analogue (larger pinholes and different absorption gradient) will be presented.

Beamline Design for at Wavelength Interferometry

K. Jackson, R. Beguiristain, M. Koike, and D. Attwood
Center for X-ray Optics
Lawrence Berkeley Laboratory
Berkeley, Ca. 94720
(510)-486-6894
(510)-486-4550

G. Sommargren
Lawrence Livermore National Laboratory
P.O. Box 808
Livermore, Ca. 94550

Introduction

A facility for research associated with the pursuit of extreme ultraviolet (EUV) and soft x-ray (SXR) projection lithography is proposed. The facility would be based on unique opportunities for research in science, and technology due to the availability of high-brightness, partially coherent radiation at wavelengths extending from 140 Å to 40 Å from an undulator at the Advanced Light Source (ALS). The large flux of radiation from the undulator poses serious problems for the optical components in the beamline. A major aspect of the research proposed herein is to develop a facility which permits the detailed characterization of complex, high-numerical-aperture multilayer coated optical surfaces with regard to their deviation from ideal as-prescribed shapes.

Spatially Coherent Undulator Radiation for at Wavelength Interferometry

Ideal spectral coverage for an at -wavelength x-ray lithography undulator at the ALS is from 40 Å to 200 Å, a wavelength region ideally covered by a U8 undulator. The desired bandwidth for this undulator is largely set by the anticipated reflection bandwidth of multilayer coatings, which is typically 2-3%. With a 8-cm period undulator at the ALS, having an overall length of 4.5 meters, it would have 5[illegible] periods (N magnetic cycles), thus giving a natural relative bandwidth of about 2%, e.g. $\Delta\lambda/\lambda$ approx. equal to 1/N, which very nicely fits our needs for optical testing. For experiments which probe a narrower spectral bandwidth a monochromator will be incorporated into the beamline. Relative bandwidths of 10^{-3} or less are easily achieved with varied line space grating monochromators, which offer other advantages for these type facilities (fixed entrance and exit slits over the entire tuning range, minimal moving parts and costs). Monochromators of this design have been designed and fielded by J. Underwood M. Koike achieving the desired performance.

Spatial coherence of this undulator radiation derives largely from the small phase space (source size-angle product) of the ALS electron beam, so small that it appears to be a point source, or at least nearly so. This is the major advantage of the ALS compared to all existing synchrotron radiation facilities, and x-ray plasma sources that might be considered for this task. In practice a water cooled pinhole will be placed in the beam to assure full spatial coherence. Longitudinal (temporal) coherence for this radiation, $\lambda^2/\Delta\lambda$, would be about 10 microns in the monochromatized case, and thus requires careful attention in the optical design.

Table 2 Performance of a 8 cm period undulator at the Advanced Light Source

Wavelength	130Å	70Å
$\Delta\lambda/\lambda = 1/N$	0.02	0.02
K	1.9	1.01
Total Power* (watts)	179	50
Power* in Central Cone (watts)	0.93	1.0
Coherent Power** (mwatts)	7	2

* All of the above table entries are for the fundamental n=1 of the undulator

** Defined as spatially coherent $\mathbf{d} \cdot \theta = \lambda/2\pi$, with a coherence length $\ell_c = \lambda^2/2\,\Delta\lambda = 0.5\mu m$.

For lithography it is desirable to have a source with high power at 130Å and 70Å. This region can be covered at the ALS by a undulator with a 8 cm period. Table 2 compares the performance of the undulator at 130Å and 70Å. The wavelength of 130Å (95eV) is where the highest reflectivity multilayer mirrors operate, with reflection efficiency of 60%. At 70Å (175eV) another multilayer mirror system is available. The tuning range of the undulator should extend at least to the carbon absorption edge at 44Å. 44Å is the practical limit for multilayer coatings because of the fabrication issues involved in such thin layers (10Å).

An 8.0 cm device can easily cover the two wavelengths of interest in projection x-ray lithography (130Å, and 70Å). The total output power of a U8 undulator is 180W. There is one disadvantage with the U8, it cannot reach the carbon K edge using only the fundamental radiation. For the interferometric characterization optics we are more concerned with the amount of the radiation in the central cone which is spatially coherent . The low emittance , high brightness, ALS electron beam is a excellent source of partially coherent EUV/SXR radiation . The amount of power in the central cone for the fundamental n=1, which is transversely (spatially) coherent is given in table 2.

Beamline Design

Our goal is to provide a beamline, optimized for storage ring operation at 1.5 GeV and up to 400 mA of electron current. The beamline must be able to accommodate up to three branchlines for future expansion. It is possible to share the undulator beam either by cutting the emerging beam spatially so that all stations are served simultaneously (spatial sharing) or by arranging that all stations receive the beam when it is required (time sharing). We have chosen time-share between the three branchlines using a water cooled "mirror". A diagram showing major beamline subsystems is shown in Figure 1. The "front end" contains photon shutters, fast-closing gate valve(s), beam-defining apertures, and photon beam position monitors.

The optical performance of the beamline is dominated by the beam-defining aperture. The rectangular aperture is adjusted to minimize thermal loading of the downstream beamline optics. The aperture can also be used to select off-axis radiation, for example, the undulator 2nd harmonic, for use in the branchline. Each of blades must be able to withstand the full thermal loading potential of the undulator at a minimum gap of 640 W. The minimum aperture size is 100 μm x 100 μm and can be scanned over the full beam. Beyond the mirror tank a second pinhole acts as spatial filter to select the coherent fraction of the radiation. The beam exiting the aperture impinges on a water

coherent fraction of the radiation. The beam exiting the aperture impinges on a water cooled pop-up mirror. The coating on this mirror is designed to absorb the unwanted higher-order harmonics. For at-wavelength interferometry, a multilayer coating tuned to 130 Å would be the ideal choice. However thermal loading may prohibit this choice. The Kirkpatrick-Baez system focuses radiation into the entrance slits of a variable line space grating (VLS) monochromator. The output of the monochromator is provided to a pinhole to preserve the spatial coherence of the radiation). Radiation from the monochromator is then focused into the interferometer endstation.

Figure 1. Interferometer beamline layout showing major subsystems

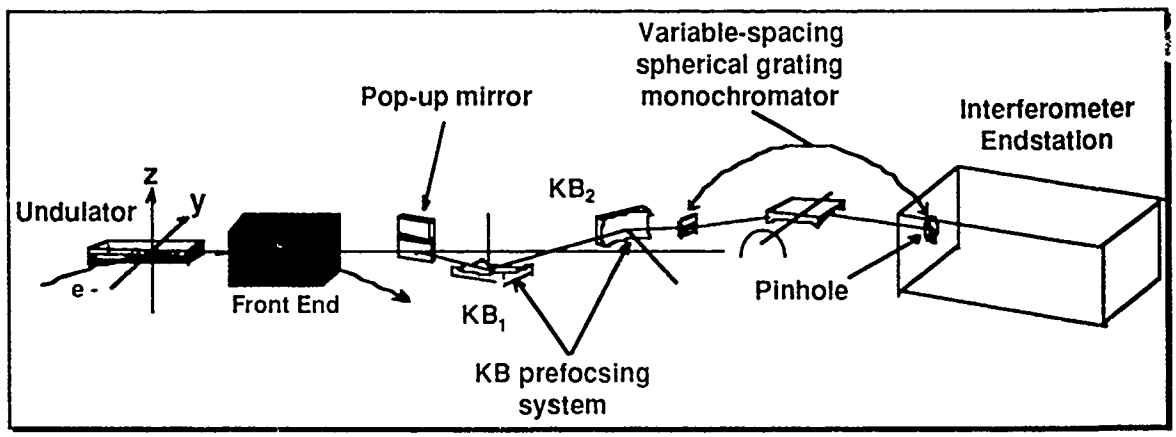

Tuesday, May 11, 1993

Poster Session 1

TuD 4:30pm–6:00pm
DeAnza III

The New Reflectometry Facility at the National Institute of Standards and Technology

C. Tarrio, R. N. Watts, T. B. Lucatorto,
Division of Electron and Optical Physics, Physics Laboratory, National Institute of Standards and Technology, Gaithersburg, MD 20899
(301) 975-3737

M. Haass, T. A. Calcott and J. Jia
Department of Physics and Astronomy, University of Tennessee, Knoxville, TN 37996
(615) 974-7848

The National Institute of Standards and Technology (NIST), as part of its soft x-ray metrology program, is constructing a new reflectometry beamline designed to improve our XUV measurement service. The new facility, intended primarily to characterize soft x-ray multilayer optics and to measure the optical properties of materials, consists of a newly commissioned varied line-spaced grating monochromator and a new reflectometry chamber currently under construction. The monochromator is designed to cover the 3.5 - 40 nm region of the spectrum with high throughput, a resolving power of 100 to 2000, and a spot size of 0.5 mm x 0.5 mm. In addition, the reflectometer is designed to measure the specular and non-specular reflectivities of optics up to 35 cm in diameter at any orientation with respect to the incoming x-ray beam. In this talk, we describe the optical properties and the performance of the new monochromator and discuss the capabilities of a hybrid reflectometer consisting of the newly commissioned monochromator and the existing reflectometer chamber already in use at NIST.

SPECIFYING THE SURFACE FINISH OF X-RAY MIRRORS

E. L. Church
Bldg. 65N, US ARDEC, Dover NJ 07801
201 724 7317

P. Z. Takacs
Bldg. 535, Brookhaven National Laboratory
Upton NY 11973
516 282 2824

ABSTRACT

Our measurements of synchrotron x-ray mirrors indicate that the power spectral densities of their finish errors have inverse power-law or fractal forms, rather than being flat at low frequencies as is usually assumed. This paper reviews these data and discusses how this apparent divergent behavior leads to finite but unconventional effects in imaging. Results are then used to develop more rational and realistic surface-finish specifications.

INTRODUCTION

Because of the short radiation wavelength involved, the performance of normal-incidence x-ray mirrors is particularly sensitive to shape errors in their manufacture. These errors are divided into two classes: figure and finish, which occupy different but overlapping regions in spatial-frequency space.

Figure errors are the low-frequency errors left by the shaping process. They are expressed in terms of Zernike polynomials, and their effects on image quality are described deterministically. Finish errors, on the other hand, are the errors left by the polishing process, which extend over a much wider range of spatial frequencies, and are described statistically. In particular, their effects on the figure-aberrated image depends on the shape and magnitude of the two-dimensional power spectral density of the finish errors, $S_2(\underset{\sim}{f})$.

The spectra of figure and two types of finish errors are sketched below:

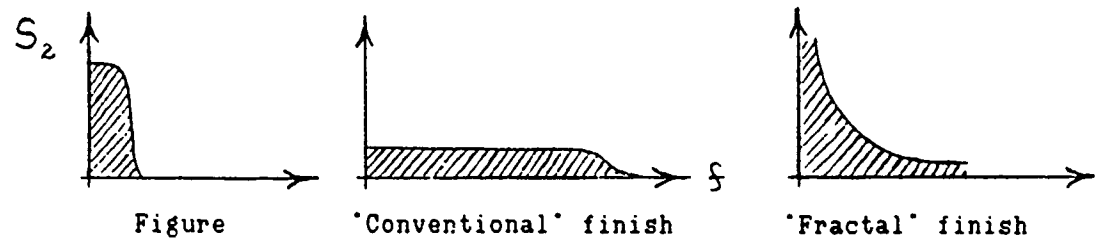

(1)

The spectrum of conventional finish errors is flat at low frequencies while the that of fractal finish diverges.

CONVENTIONAL SURFACE FINISH

Since conventional finish lies mainly at high frequencies, its principal effect on imaging is to scatter intensity out of the image core, which leaves the shape of the core unchanged, but lowers its overall intensity by the well-

known Strehl factor:

$$\text{Strehl factor} = e^{-(4\pi\sigma/\lambda)^2} . \qquad (2)$$

Here σ is the root-mean-square (rms) value of the finish roughness, which, in frequency space, is given by the volume under the finish power spectral density:

$$\sigma^2 = \int d\underset{\sim}{f}\, S_2(\underset{\sim}{f}) . \qquad (3)$$

In the case of conventional finish this quantity is finite and represents an intrinsic property of the surface finish.

FRACTAL SURFACE FINISH

Our measurements of the finish spectra of x-ray synchrotron mirrors shows that they are not flat at low frequencies but tend to diverge in an inverse-power-law or fractal way.

In retrospect, this form is not unexpected for highly-finished surfaces since it is the only mathematically-permissible form for a process that does not involve unique length scales -- and unique length scales are expected to be absent, by definition, for 'good' polishing processes. In the modern metaphor, fractal finish is an 'attractor' for random polishing techniques.

In the discussion below we use the isotropic form

$$S_2(\underset{\sim}{f}) = K' / f^{n+1} \qquad (4)$$

where K' is the spectral strength and $1 < n < 3$ is a number called the spectral index. Note that if we attempt to evaluate the rms roughness of a fractal surface using Eq 3 we get an indeterminate result because of the divergence of the fractal spectrum at low frequencies.

EFFECTS ON IMAGING

Surface shape errors affect imaging by introducing 'random' phase modulation in the imaging wavefront. The simplest way of exploring such effects is to use the well-known Huygens-Fresnel diffraction formalism to express the ensemble-average image intensity distribution in terms of the power spectrum of the finish errors. Because of space limitations, we consider here only two effects of finish on the image -- the smooth-surface forms of the on-axis Strehl factor (which we denote by Strehl(0)) and the Hopkins factor.

THE ON-AXIS STREHL FACTOR

This is the factor which reduces the on-axis image intensity due to the presence of imperfect surface finish. Its general form is:

$$\text{General Strehl}(0) = 1 - \left(\frac{4\pi}{\lambda}\right)^2 \int d\underset{\sim}{f}\, S_2(f) \left[1 - \left\{\frac{J_1(\pi D_0 f)}{\pi D_0 f/2}\right\}^2\right] . \quad (5)$$

In the case of conventional finish the major contribution to the integrand comes from high frequencies where the J_1 term can be neglected, so that

$$\text{Conventional Strehl}(0) = 1 - \left(\frac{4\pi}{\lambda}\right)^2 \sigma^2 \quad , \quad (6)$$

which is, as expected, just the smooth-surface limit of Eq 2.

In the case of fractal spectra, Eq 4, the presence of the J_1 term is no longer negligible, but plays the important role of killing the fractal divergence at low frequencies. The result is the finite expression

$$\text{Fractal Strehl}(0) = 1 - \left(\frac{4\pi}{\lambda}\right)^2 K' D_0^{m-1} \cdot \frac{32\,\pi^{m-1/2}}{(m+1)^2(m+3)} \left| \frac{\Gamma\left(\frac{2+m}{2}\right)\Gamma\left(\frac{1-m}{2}\right)}{\Gamma^2\left(\frac{1+m}{2}\right)} \right| \quad (7)$$

where D_0 is the diameter of the mirror. The practical use of this expression is illustrated later.

THE HOPKINS FACTOR

The Hopkins factor is the factor which reduces the spatial-frequency content of the image -- the system OTF -- due to the presence of imperfect surface finish. Its general form is:

$$\text{General Hopkins}(f') = 1 - \left(\frac{4\pi}{\lambda}\right)^2 \int d\underset{\sim}{f}\, S_2(f) \left[1 - J_0\left(2\pi D_0 f \frac{f'}{f_0}\right)\right] \quad (8)$$

where f' is the spatial frequency in the image plane and $f_0 = 2NA/\lambda$ is its value at the incoherent cut-off of the system. Note that this expression is the same as Eq 5 except for a different form of the killing factor in the square brackets.

In the case of conventional surface finish, the J_0 term in those brackets can also be neglected, except for extremely low image frequencies, so that

$$\text{Conventional Hopkins}(f') = 1 - \left(\frac{4\pi}{\lambda}\right)^2 \sigma^2 \quad , \quad (9)$$

which is identical with the conventional Strehl factor under the same conditions, Eq 6.

The fact that the conventional Hopkins factor is independent of image frequency corresponds to the fact that conventional finish errors reduce the intensity of the image core but do not change its shape.

In the case of fractal finish we get the different result:

$$\text{Fractal Hopkins}(f') = 1 - \left(\frac{4\pi}{\lambda}\right)^2 K' D_0^{m-1} \cdot \pi^m \left| \frac{\Gamma\left(\frac{1-m}{2}\right)}{\Gamma\left(\frac{1+m}{2}\right)} \right| \left(\frac{f'}{f_0}\right)^{m-1} . \qquad (10)$$

This indicates a preferential attenuation of higher image frequencies, which corresponds to a broadening as well as lowering of the image core.

ILLUSTRATIONS

Equations 7 and 10 are pieces of a larger Rosetta stone for translating performance requirements on the image intensity distribution into specifications on finish parameters that can be measured in the metrology laboratory. For example, we consider the case of a source of 140-Ångstrom (14 nm) radiation imaged by a mirror with a diameter D_0 = 10 cm.

In the case of conventional surface finish, the requirements that

$$\text{On-axis Strehl, Hopkins factors each} \geqslant 0.8 \qquad (11)$$

translate to the same condition on the rms finish error, namely:

$$\sigma \leqslant 4.98 \text{ Å} = 4.98 \times 10^{-10} \text{ m} . \qquad (12)$$

In the case of fractal surfaces the Strehl requirement leads to a condition on a combination of the finish parameters n and K' . If we take the nominal value of n = 4/3 , we find

$$\text{Strehl}(0)\text{-based limit:} \quad K'(n = 4/3) \leqslant 2.14 \times 10^{-20} \text{ m}^{5/3} . \qquad (13)$$

In the case of the fractal surfaces the Hopkins factor depends on the spatial frequency f' as well. If we require that factor to be greater than 0.8 at half the incoherent cutoff, we find essentially the same condition:

$$\text{Hopkins}(f_0/2)\text{-based limit:} \quad K'(n = 4/3) \leqslant 2.01 \times 10^{-20} \text{ m}^{5/3} . \qquad (14)$$

The values in Eqs 13 and 14 can be compared with $K' = 54.9 \times 10^{-20}$ $m^{5/3}$ that we have measured for a particular silicon mirror at Brookhaven. This n = 4/3 mirror, then, has a spectrum that is $\sim$ 27 times too large to satisfy these requirements. That is, it is too 'rough' by a factor of $\sqrt{27} \sim 5$.

ADDITIONAL INFORMATION

The presented version of this paper will include illustrations and extensions of this work that have had to be omitted in this short summary.

FEL Sources For Soft X-Ray Projection Lithography On The Duke 1 GeV Storage Ring

Lewis E. Johnson and John M. J. Madey

FEL Laboratory, Physics Department, Duke University
LaSalle Street Extension, Durham, NC 27706
Telephone: (919)-660-2644; Fax: (919)-660-2671

The Free Electron Laser has been proposed as a source to extend projection lithography to even greater resolution[1]. The envisioned high power, coherence and wavelength tunabality of these sources make the FEL a welcome radiation source to overcome some of the limitation with optics and resist technology that plague the current sources. The narrow line width imposed by the FEL should generate a steeper step in resist. Moreover, the higher power should allow us to explore regions in the resist once currently of reach.

Current radiation sources used for projection lithography yield output powers between 2-7mW in a .1% bandwidth[2]. The Duke FELs offer 1-3 orders of magnitude greater power with an extended range of wavelength tuning not accessable with current sources. The Duke FEL facility will host the first UV-VUV FEL to come on-line in this country.

The OK-4 FEL first lased in the former Soviet Union. The Duke FEL facility will be the new home to the device in the summer of 1993. Driven by the Duke 1 GeV storage ring, the OK-4 will possess an average power of 2.5 - 30 watts and a peak power of 10 - 80 kW in a 7-30 psec bursts. The OK-4 will cover the range from 30 - 400 nm. The NIST undulator acquired from the National Institute of Science and Technology sits on the storage ring now awaiting commissioning. The NIST undulator, although not a true FEL, possess a very tight BW(.2%) due to the nature of the Storage Ring. This quasi-Coherent source will puts out 40mW of average power and 1.5 kW of peak power. It's tunability is between 37-210Å.

The facility will also house the world's first soft x-ray FEL. Due to the lack of highly reflecting resonator optics in the 40-50Å range the last FEL utilizes a phase Displacement scheme[3]. It consists of a constant period spontaneous radiator followed by an inverse tapered undulator. Utilizing this scheme it will be possible to extract 10 watts average power of 40-50Å radiation in a .1%BW. Peak power from a 7-30 psec burst will approach 370kW.

These FEL radiation sources have the possibility to further not only lithography, but biological imaging and radiation damage studies to new levels.

1. B. Newnam, "Development of free-electron lasers for XUV projection lithography," in *Free Electron Lasers and Applications*, SPIE Vol. 1227, 116-127 (1990).

2. ibid.

3. N. M. Kroll, P. L. Mortor , and M. N. Rosenbluth, " Free-Electron Lasers with Variable Parameter Wigglers," *IEEE J. Quantum Electron.*, vol. QE-17, pp. 1436-1468, Aug. 1981

Soft X-ray Conversions Efficiencies from Laser-Produced Plasmas for Soft X-ray Projection Lithography Sources

R. C. Spitzer*, R. L. Kauffman, T. Orzechowski, D. W. Phillion, and C. Cerjan

Lawrence Livermore National Laboratory

Soft x-ray projection lithography (SXPL) systems are designed to operate with narrow bandwidths around 130Å, where the highest reflectivity mirrors have been demonstrated[1]. Several different sources are under consideration. One possibility is the laser-produced plasma, in which intense visible laser light incident on a solid metal surface in vacuum generates an x-ray emitting plasma. An important question is whether sufficient x-ray radiation is generated at 130Å. Although much work has been performed at the very high laser intensities used in fusion applications, no experiments existed at the pulse widths and intensities necessary for SXPL systems. In this work a comprehensive soft x-ray database for laser plasma lithographic sources was developed. We determined the *absolute* conversion efficiency from laser light into x-rays for various target materials, laser wavelengths (1.064μm & 532nm),pulse lengths (7.5-30ns), incident intensities(1×10^{9}W/cm^{2} - 1×10^{13}W/cm), and spot sizes(15μm-2mm).

The conversion efficiency as a function of target material, shown in Fig. 1, is found to display periodic variations with atomic number. For our x-ray wavelength region, the best material is Sn, with a measured conversion efficiency greater than 1% into a 3Å bandwidth at 130Å. Higher values have been obtained by optimizing the laser parameters. This conversion efficiency meets the necessary system requirements and establishes laser produced plasmas as viable SXPL sources.

Spectral measurements indicate that Sn is advantageous due to a sharp peak which concentrates energy into a narrow band. This feature has been ascribed to transitions within multiply ionized Sn atoms present in the plasma. Other materials such as Au also have transitions in the region of interest but with much broader widths than the SXPL bandwidth.

1. N. M. Ceglio and A. M. Hawryluk, "Soft x-ray Projection Lithography System Design," OSA Proceedings on Soft X-ray Projection Lithography Vol 12, J. Bokor, Ed. (OSA Washington, D. C., 1991), p.5.

*Visiting Scientist from Brigham Young University.

This work was performed under the auspices of the U.S. Department of Energy by Lawrence Livermore National Laboratory under contract No. W-7405-Eng-48.

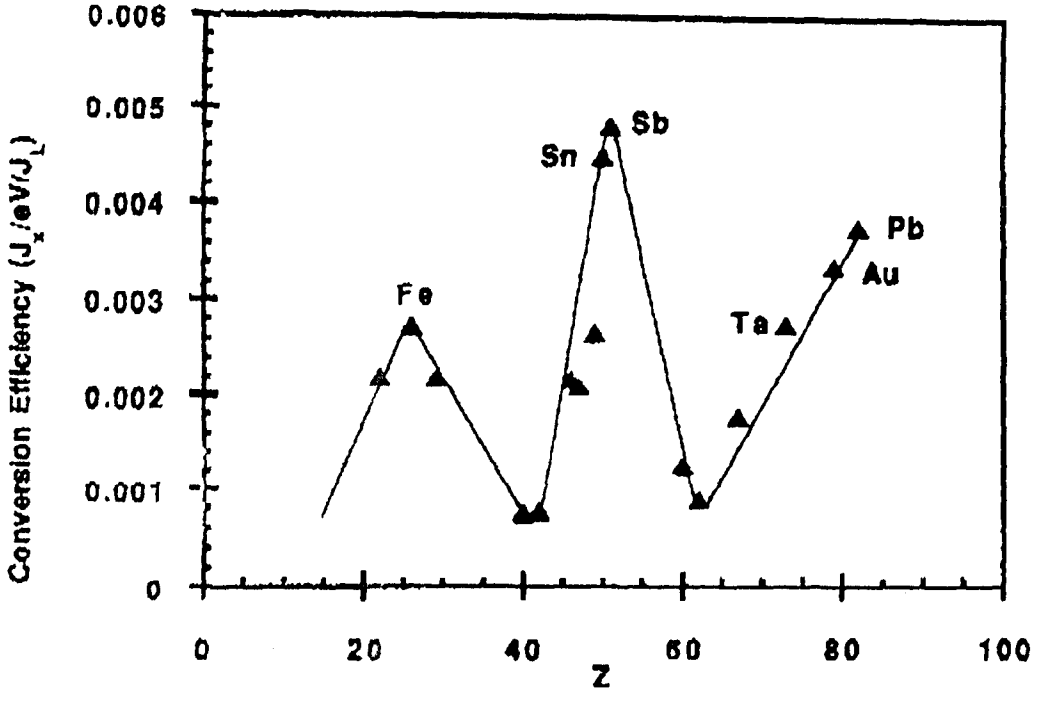

Figure 1. The dependence of the conversion efficiency at 128.3Å on atomic number of the target material. All of the data are obtained using 532nm light with an incident intensity of $1x10^{11}W/cm^2$ and a spot size of 160μm.

Thermal distortion effects on optical substrates that reduce coherence properties of Undulator beamlines

Raul Beguiristain
Center for X-Ray Optics
Lawrence Berkeley Laboratory

A long undulator installed at the ALS, a low emittance storage ring, generates quasi-monochromatic beams of high brightness and improved coherence properties that could be used for "at wavelength" interferometry for x-ray projection lithography experiments. However, the heat load produced by intense beams impinging on mirrors and gratings can deform their surfaces considerably, and thus, degrade the coherence and brightness qualities and overall performance of the beamline. It is therefore necessary to accurately describe the surfaces of the distorted mirrors and gratings to ensure that the brightness and coherence properties of the undulator radiation are preserved through the beamline.

A few stringent cases taking wide apertures and high undulator K values corresponding to high heat loads on water cooled and non-water cooled mirror and grating substrates were analyzed. The distorted surfaces of these substrates are described by a polynomial fit to the results from runs of the ANSYS[1] computer code, a commercially available finite element analysis method for heat transfer and stress analysis, and are used in further ray tracing and may be implemented into active adaptive optics schemes in the future. Figure 1 shows the surface of a typical distorted first mirror water cooled substrate that can be describe as a polynomial of the form $z=\sum_{i,j} a_{ij}\, x^i\, y^j$, the slope of this substrate at the edge of the central cone of usefull radiation is 2.5 microradians.

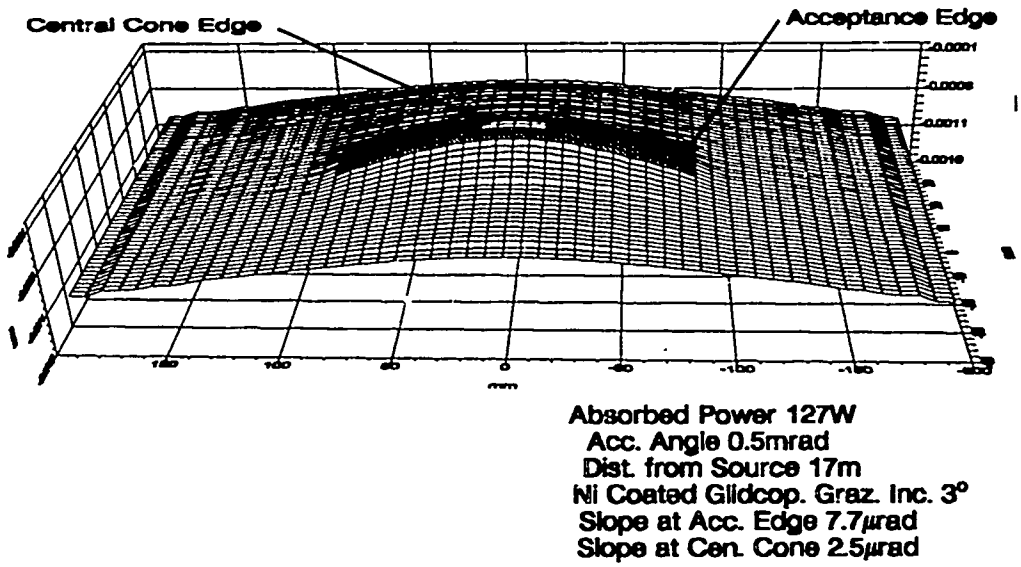

Figure1: *Top surface of a distorted water cooled 1st. mirror substrate of an undulator beamline*

Acknowledgment: The work on x-ray lithography is supported by the Defense Advanced Research Projects Agency, U.S. Department of Defense.

References:

1) ANSYS is a registered trademark of Swanson Analysis Systems,Inc., Houston, Pennsylvania.

Monochromator Optics for Coherent Illumination of an Undulator Beamline

Masato Koike

Center for X-ray Optics, Lawrence Berkeley Laboratory, University of California,
1 Cyclotron Road MS 2-400, Berkeley, California 94720
(510)486-4131

An undulator having a long, periodic magnetic structure installed at a low emittance storage ring generates quasi-monochromatic, narrowly collimated, and partially coherent radiation. However, undulators currently operated and even those planed at third-generation synchrotron sources still do not provide a narrow bandwidth and a low emittance enough to meet spatial and temporal coherence requirements for experiments such as soft X-ray interferometry, holography, and scanning microscopy. This paper presents a beamline design which comprises a variable-spacing spherical grating monochromator with a Kirkpatrick–Baez (KB) prefocusing system to deliver a spatially and temporally coherent flux into an end station without sacrificing throughput for the coherent flux radiated from the undulator.

In the following design, the machine parameters for the U-3.9 undulator[1] of the Advanced Light Source (ALS) at Lawrence Berkeley Laboratory were used: $\sigma_y = 0.330$ mm, $\sigma_z = 0.063$ mm, $\sigma'_y = 0.030$ mrad, $\sigma'_z = 0.016$ mrad. Here, σ_y (σ_z) and σ'_y (σ'_z) are the rms horizontal (vertical) electron beam size and beam divergence, respectively. The design parameters were optimized to deliver only the spatially coherent flux radiated from the central cone of the undulator through a pinhole and a beam–defining aperture placed in front of the end station. The designed system is schematically shown in Figure 1. The first mirror is a pop-up plane mirror for switching the incoming beam to the other station as well as for reducing heat load on the optics to follow. The

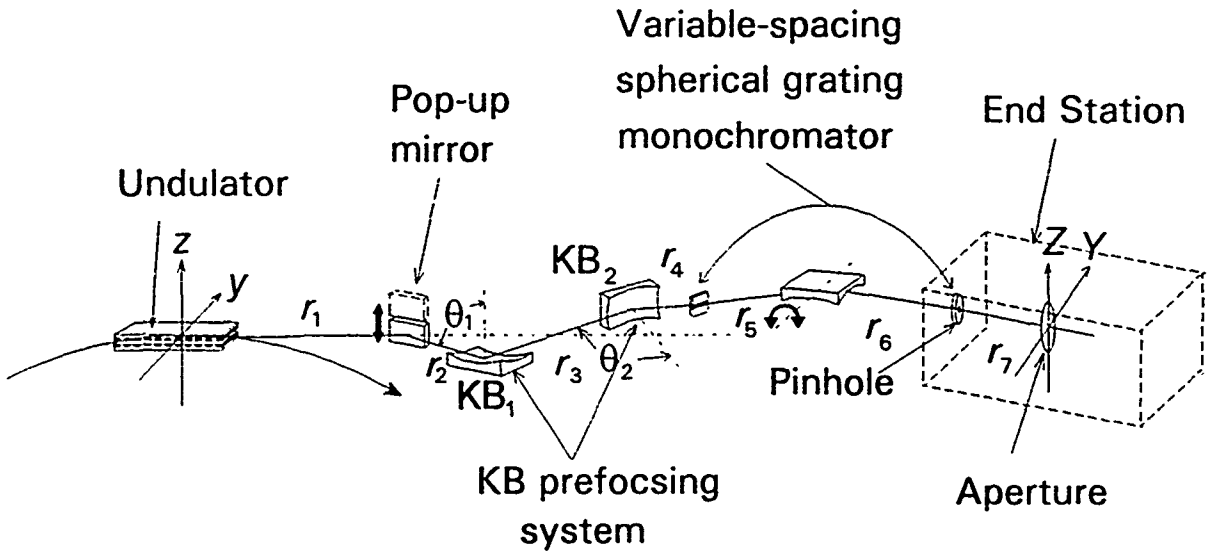

Figure 1. Beamline optics consisting of a pop-up mirror, a Kirkpatrick-Baez (KB) prefocusing system, a variable spacing spherical grating monochromator, and an end station.

KB prefocus system consists of the vertical-folding (KB_1) and horizontal-folding (KB_2) spherical mirrors which focus the source image vertically on the entrance slit of the monochromator and horizontally on the exit slit (pinhole), respectively. The monochromator is a 174° constant-deviation type equipped with a 38-m, 300-grooves/mm spherical grating with variable spacing. The other parameters (refer to Fig.1) are: distances r_1 = 16.9 m, r_2 = 4.0 m, r_3 = 3.0 m, r_4 = 5.0 m, r_5 = 1.914 m, r_6 =1.914 m, and r_7 = 1.0 m; angles of incidence at the KB mirrors $\theta_1 = \theta_2 = 87.0°$; radius of curvature of the KB_1 (or KB_2) mirror = 221 m (or 183 m); entrance slit width = 23μm; pin hole diameter = 30μm; and aperture diameter = 100μm. To determine the ruling parameters for the variable spacing grooves that minimize the aberrationS of the monochromator, we applied a damped least squares method to the merit function which represents the rms spread of the spots averaged over a given wavelength range[2]. The ruling parameters of the ruled grating with variable spacing and straight grooves are defined by the coefficients σ_0, $2a$, $6b$, and $4c$ in a cubic expression, $\sigma_n = \sigma_0 + 2an + 6bn^2 + 4cn^3$, for the groove spacing σ_n between the nth and $(n+1)$ th grooves. The ruling parameters thus obtained are : $\sigma_0 = 3.333333 \times 10^{-3} + a - b$ mm, $2a = 2.514256 \times 10^{-9}$ mm, $6b = -1.280905 \times 10^{-14}$ mm, $4c = 1.050669 \times 10^{-20}$ mm. The estimated range of resolution for a wavelength range of 20 - 50 Å is 500 - 1000 in +1st order.

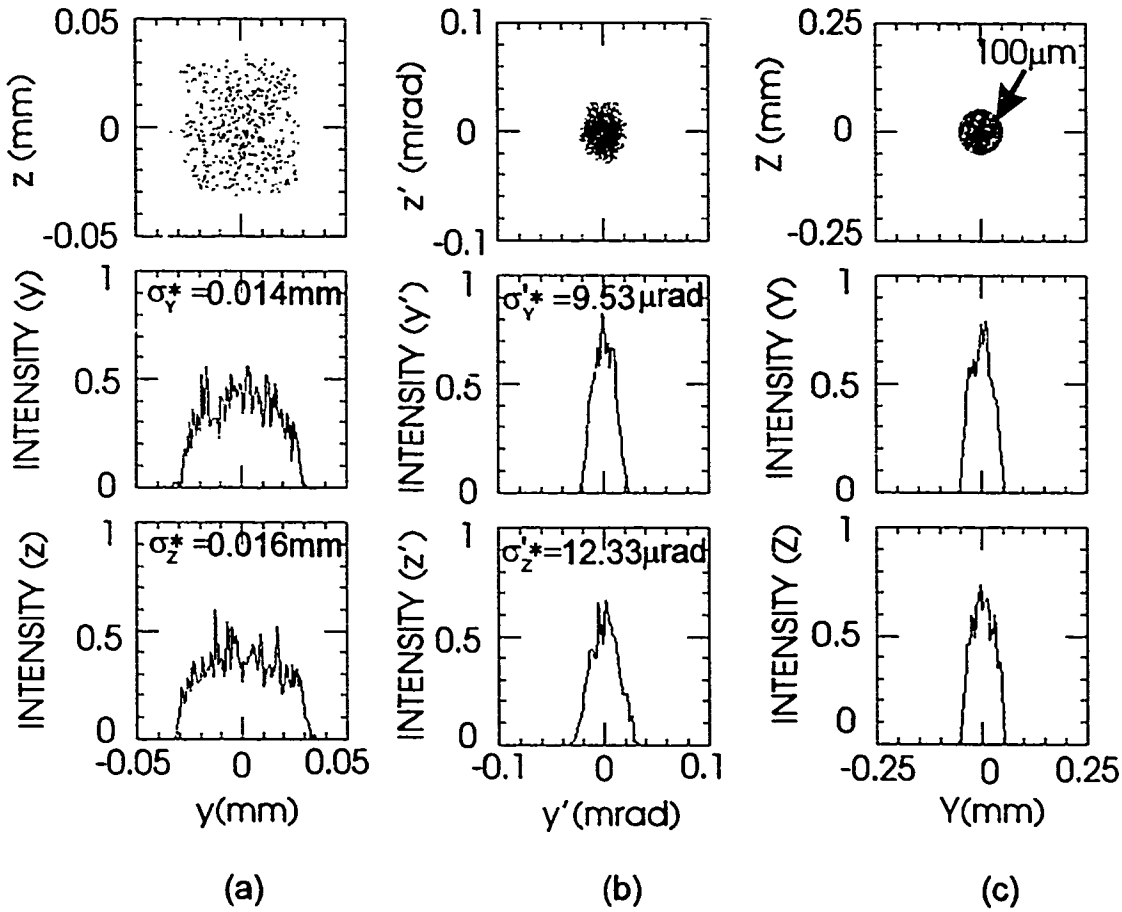

Fig. 2. Spot diagrams and image profiles formed by the through rays in the source plane (center of the undulator) in the real (a) and the phase space (b) and in the aperture plane in the real space (c).

The designed system was evaluated by exact ray tracing. Figure 2 shows spot diagrams and image profiles formed by the through rays in the source plane (center of the undulator) in the real (a) and the phase space (b) and in the aperture plane in the real space (c). By through rays we mean the rays which pass through both the pinhole and the aperture . We assumed the U-3.9 undulator tuned at the wavelength region of λ= 24±0.012Å. To generate the rays which simulate the radiation in the central cone, use was made of a simulation code[3]. The rms source size (σ^*_y, σ^*_z) and beam divergence (σ'^*_y, σ'^*_z) for the through rays are shown in the image profile frames. The effective emittance ε^*_y and ε^*_z ($\varepsilon^*_i = 4\pi\sigma^*_i\sigma'^*_i$, $i = y, z$) compatible with the through rays are 16 Årad and 25 Årad, respectively. These values are fairly close to those of the spatial coherence criterion $\varepsilon^*_i \leq \lambda$. The geometrical throughput of the overall system is 0.2% at 24Å, which also well coincides with the analytically estimated percentage of the coherent flux in the central cone. When spatial and angular instabilities occur in the electron beam, the throughput is expected to decrease by 35 % (or 42 %) for a spatial deviation of one σ_y (or one σ_z) and by 21 % (or 7 %) for an angular deflection of one σ'_y (or one σ'_z). However, the effective emittance still remains to lie in a range of 16 - 26 Årad.

The work on X-ray lithography is supported by the Defense Advanced Research Projects Agency, U. S. Department of Defense.

References:

1) *An ALS handbook,* Lawrence Berkeley Laboratory report PUB-643 Rev. 2 (Lawrence Berkeley Lab., Berkeley , 1989).
2) T. Namioka and M. Koike, Nucl. Instr. and Meth. **A319**, 219 (1992).
3) M. Koike, Nucl. Instr. and Meth. **A319**, 135 (1992).

Printing a 500Å Period Grating Using X-Ray Interference

Max Wei*,† and Erik Anderson*

*Center for X-Ray Optics, Lawrence Berkeley Laboratory
University of California, Berkeley, CA 94720. Tel. (510) 486-4041

†Department of Electrical Engineering and Computer Science
University of California, Berkeley. CA 94720

Recently a great deal of attention has been directed towards developing, analyzing, and fabricating a new generation of electronic devices which depend upon and attempt to exploit quantum effects [1-3]. Such devices, known as quantum effect devices, exhibit transport characteristics which are described by quantum mechanics and not by macroscopic averaged quantities. Quantum effect devices are required to be much smaller in size than typical microelectronic devices. A major issue in the fabrication of these devices is the ability to write fine patterns of less than 0.05 μm pitch. Some candidate technologies which have been explored include electron beams, x-rays, and focused ion beams [4]. Electron beam lithography has been the most commonly used method thus far to produce features at this length scale, but is limited by the proximity effect. In this work, we choose to pursue a two grating x-ray interference technique as a method to produce finely spaced lines and spaces. X-rays are not limited by the proximity effect and thus a higher contrast resist pattern can be expected.

The x-ray interference technique consists of two linear transmission gratings. Incoming x-ray radiation is split into two paths by the first grating and recombined by the second grating to form a 500Å period fringe pattern (Figure1) which is recorded in photoresist. In general, such a configuration forms a pattern of fringe spacing p/2n (period p/n), where p is the period of the second grating and n is the order of the diffracted radiation which recombines. Thus 250Å lines and spaces are expected for a recombiner grating of period of p=1000Å and for n=2. This technique has the advantage of being able to produce a finely patterned structure over a relatively large area without stringent coherence requirements on the x-ray source. This method has been successfully applied in the past at deep ultraviolet wavelengths to produce below 1000Å period gratings.

This pattern can then be utilized to form a grating gate (Figure 2) of a modulation doped field effect transistor (MODFET). In MODFET devices, electrons are confined to move in two dimensions with extremely high mobility [5]. Applying a voltage to the grating gate thus imposes an additional periodic potential upon the electrons. If the period of such a grating gate approaches the Fermi wavelength of the electron gas, electron wave Bragg reflection is expected

at certain electron energies, giving successive dips in the drain to source current as a function of applied gate voltage. The Fermi wavelength is typically 400-500Å for a GaAs MODFET.

X-ray transmission gratings have been fabricated by electron beam lithography, using a similar process that has been employed to fabricate Fresnel zone plates [6]. After patterning with electron beam lithography, nickel is electroplated on to a silicon nitride substrate. We have fabricated 1000Å period gratings with nickel thickness of 1000Å. A major issue here is the grating line to space aspect ratio. Greater aspect ratios improve grating efficiency and are thus needed to achieve reasonable exposure times. Two plots of grating efficiencies are shown in Figure 3. These efficiencies are based on rigorous electromagnetic calculations. For a grating thickness of 1500Å, we see that 10% of the incident power is diffracted into 1st order and 1% into 3rd order for 0.5 linewidth fraction gratings. We have measured the grating efficiency of a 1000Å thick grating (Figure 4) and it agrees well with the calculated values.

The source that is used in our experiment is the X1A beamline at the National Synchrotron Light Source which provides a partially coherent source of x-rays [7]. At an incident wavelength of 20Å the measured flux is 1.5×10^6 photons/second-μm^2 and an exposure time of 2 hours is expected.

A method for producing a 500Å period grating using x-ray interference has been described. Such a finely spaced grating is difficult to produce using other fabrication methods and is at or beyond the current limits of electron beam lithography. Our technique uses two transmission gratings in a grating interferometer geometry to record an x-ray fringe pattern in photoresist. Periods of 500Å and below are interesting because they approach the electron Fermi wavelength in GaAs/AlGaAs modulation doped heterostructures. We propose to use this technique to fabricate the gate of a grating gate modulation doped field effect transistor. In such a device, the electron transport is expected to be strongly influenced by varying the gate voltage.

REFERENCES

1. F. Capasso, *Physics of Quantum Electron Devices*, Springer-Verlag, New York, NY (1990).
2. N. Tsudaka, A.D. Wieck, and K. Ploog, Appl. Phys. Lett. **56**, 2527 (1990).
3. K. Ismail, W. Chu, D.A. Antoniadas, and H.I. Smith, Appl. Phys. Lett. **52**, 1071 (1988).
4. R. Dingle, H.L. Stormer, A.C. Gossard, and W. Wiegmann, Appl. Phys. Lett. **33**, 665 (1978).
5. M.A. Reed and W.P. Kirk, *Nanostructure Physics and Fabrication*, Academic Press, Boston (1989).
6. Y. Vladimirsky, D. Kern, T.H.P Chang, D. Attwood, et. al. , J. Vac. Sci. Technol. **B6**,311 (1988).
7. H. Rarback, C. Buckley, H. Ade, F. Camilo et. al., J. X-Ray Sci. Technol. **2**, 274 (1990).

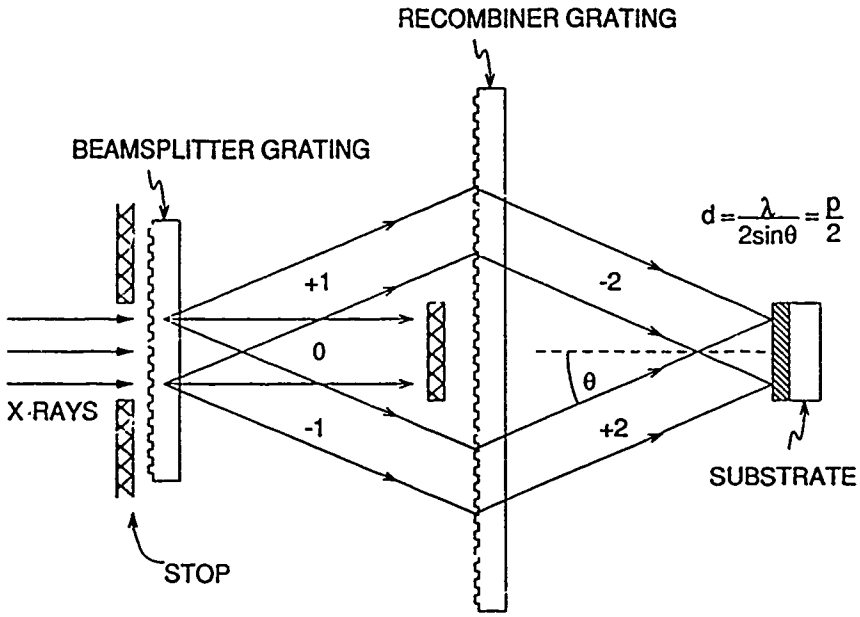

Figure 1. Two grating x-ray interference configuration.

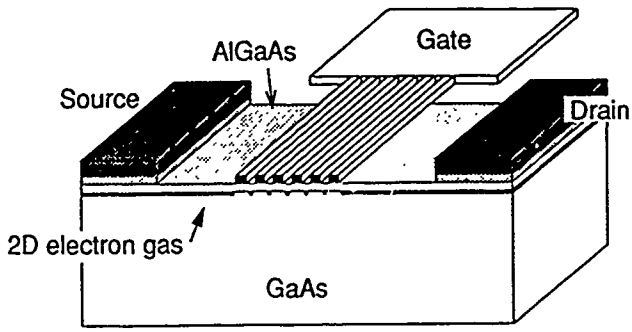

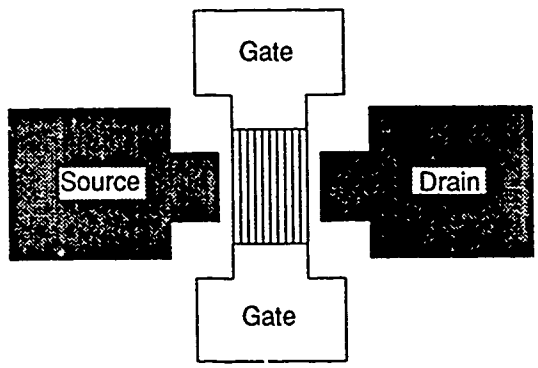

Figure 2. Grating Gate Modulation Doped Field Effect Transistor

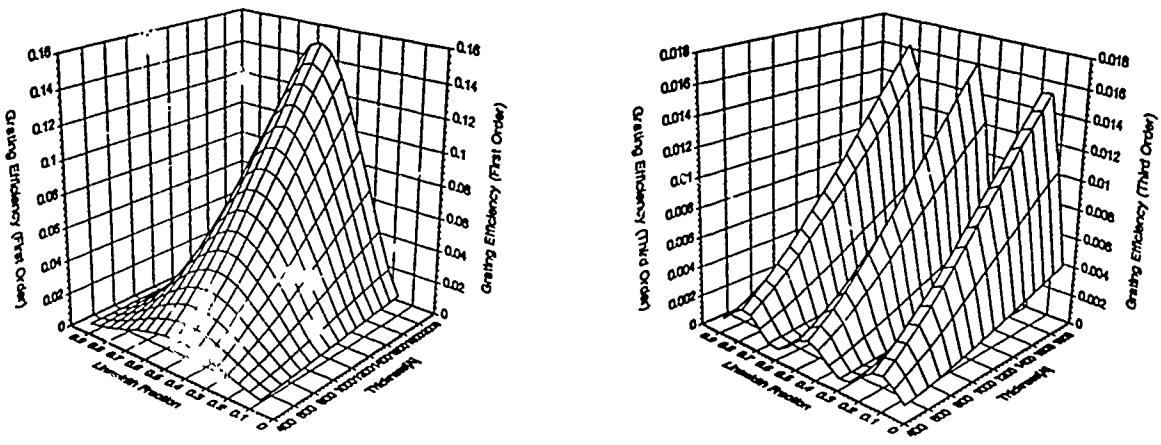

(a) (b)

Figure 3. Calculated Grating Efficiencies for 1000Å Period Transmission Gratings. (a) First Order Efficiency (b) Third Order Efficiency.

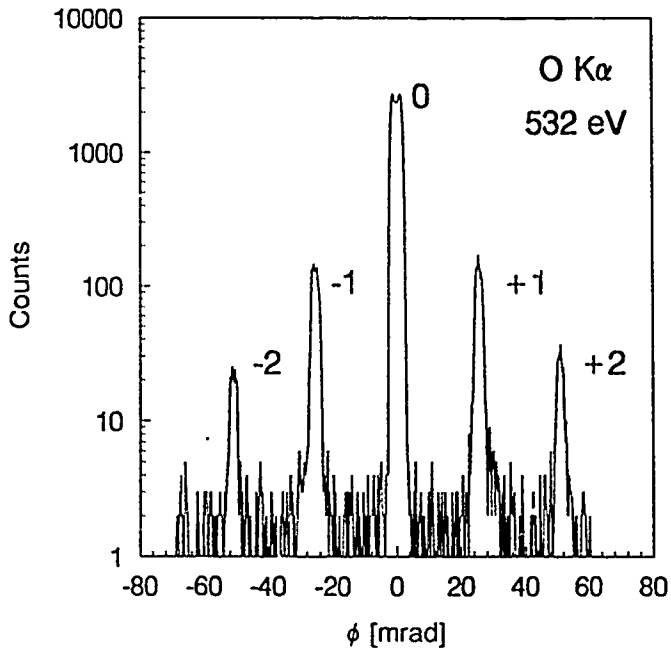

Figure 4. Measured Grating Spectrum for 1000Å Period Transmission Grating

Manufacture and Characterization of Holographic Diffraction Gratings for Soft X-Rays

Alexander Irtel von Brenndorff

Georg-August-Universität Göttingen, Forschungseinrichtung Röntgenphysik,
Geiststraße 11, W-3400 Göttingen, Germany
and
Lawrence Berkeley Laboratory, Center for X-Ray Optics,
1 Cyclotron Rd 2-400, Berkeley, CA 94720
phone: (510) 486-4079

In this paper, a manufacturing process for laminar gratings is described and the effects of variations of this process on the surface roughness are studied using a STM.

The grating pattern is created by exposing the interference fringes of two coherent plane wave fronts of laser light into a photo resist [1](Fig. 1a). The resist pattern is then transferred into a thin layer of SiO_2 by reactive ion etching (RIE). The SiO_2 layer is etched in a CF_4 plasma down to a Cr etch stop layer (Fig. 1b). Then, the photo resist is removed in a O_2 plasma (Fig. 1c) and the grating is coated with a material of high reflectivity for soft x-rays (Fig. 1d). The step height of the grating is given by the thickness of the SiO_2 layer and can be optimized for any wave length.

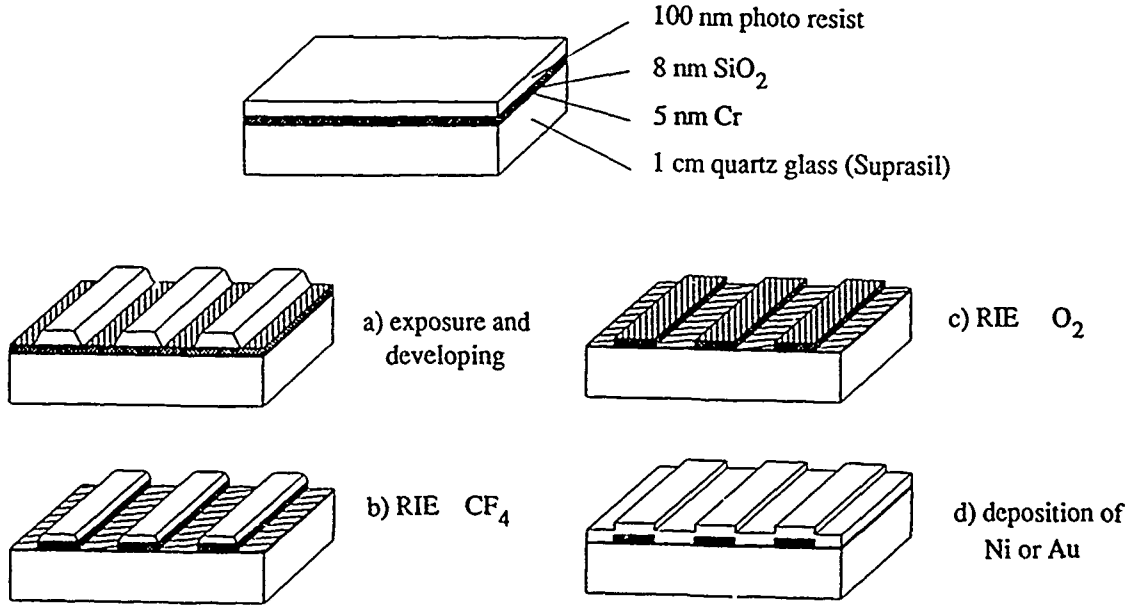

Fig. 1: manufacturing process for laminar gratings [2].

Using the process described above, gratings for the Göttingen x-ray microscopy beam line [3] with a line density of 600 lines/mm and a step height of 8 nm have been made [2]. A SEM image of an etched grating is shown in figure 2.

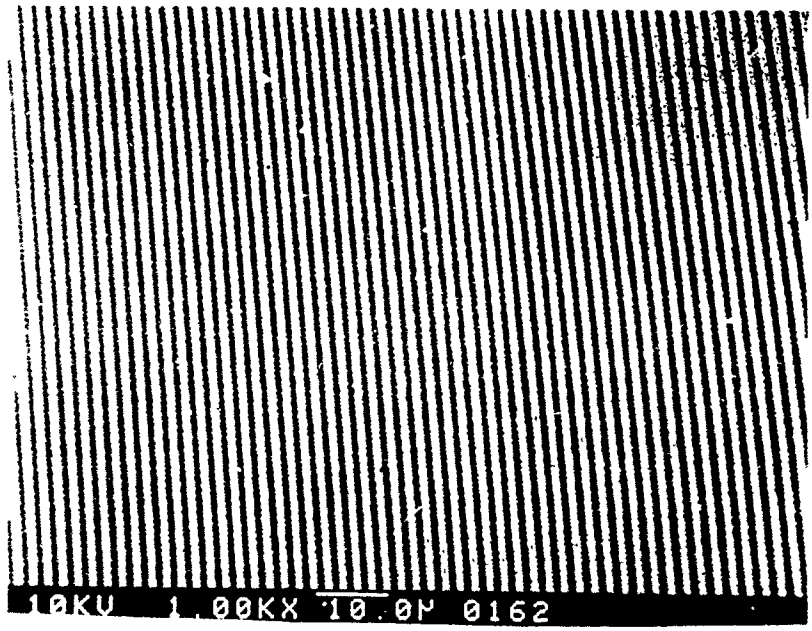

Fig. 2: SEM image of a etched grating. One can see the light SiO_2 lines on the dark Cr layer. Magnification 1000 x.

During manufacture, it is necessary to enhance the adhesion of the photo resist on the SiO_2 layer. One method is to evaporate a mono-molecular layer of Hexamethyldisilazan (HMDS) onto the substrate before spin coating the substrate. Another method is to put the substrate into an Ar plasma before spin coating. Both methods were applied. Then, the etched gratings are coated with either Au or Ni using evaporation techniques as well as sputtering techniques. The surfaces of these gratings were studied using a STM [4].

Fig. 3 shows the STM image of a nickel grating. HMDS was used to enhance the adhesion between the photo resist and the SiO_2 layer. The surface in the groove is smoother than on the land where the photo resist had to be removed in an O_2 plasma. Fig. 4 shows the STM image of a gold grating. In this case, no HMDS was used during manufacture, and instead the substrate was put into an Ar plasma before spin coating with photo resist. One can see an equally smooth surface in the groove as well as on the land. The photo resist was completely removed from the surface so that the roughness on the land was minimized.

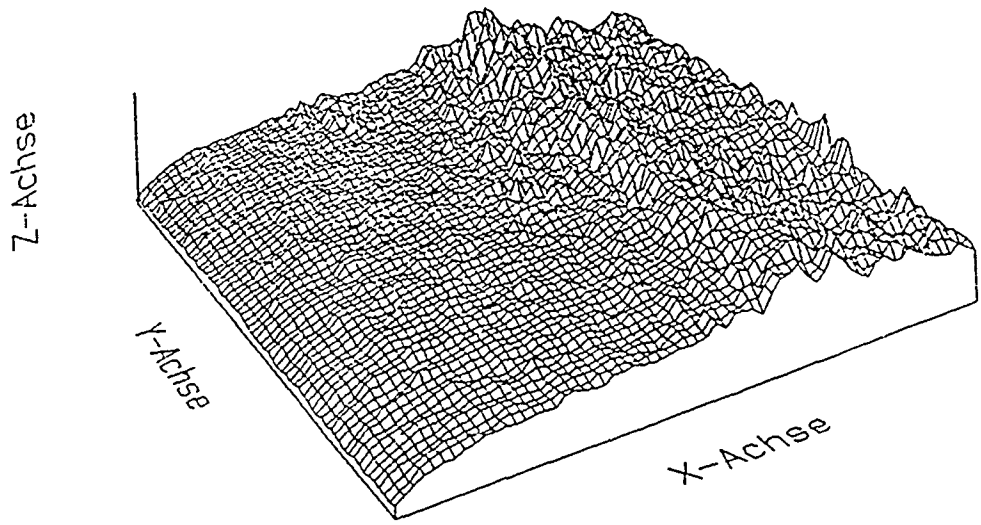

Fig. 3: STM image of a nickel grating. The image was taken in "constant-current-mode". HMDS was used to enhance the adhesion of the photo resist. The area is 1.0 x 1.0 μm^2 large.

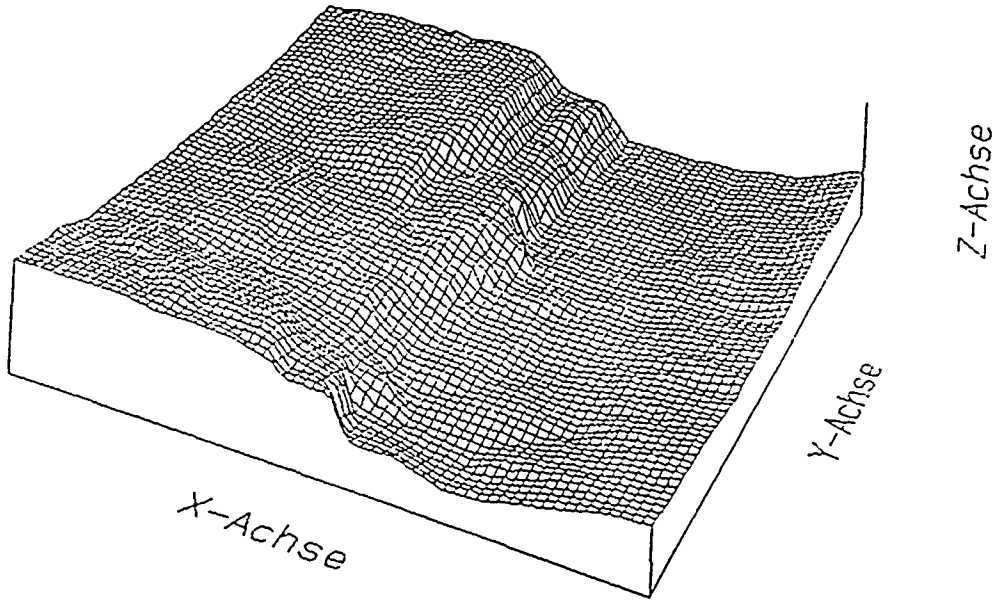

Fig. 4: STM image of a gold grating. The image was taken in "constant-current-mode". No HMDS was used during manufacture. The area is 0.6 x 0.6 μm^2 large.

Efficiency measurements at a laboratory x-ray source in Göttingen [5] proved high absolute efficiencies up to 11.4% in the $+1^{st}$ diffraction order and up to 10.1% in the -1^{st} order at the wave length $\lambda = 44.7$ Å. The nickel gratings show a higher efficiency than the gold gratings. There are no significant differences in the efficiency of gratings that were coated with evaporation or sputtering techniques.

Acknowledgments: I thank Dipl.-Phys. C. Burandt and Dipl.-Phys. M. Wenderoth from the 4. Physikalisches Institut of the University of Göttingen for their collaboration with the STM.

References

[1] G. Schmahl and D. Rudolph, Holographic Diffraction Gratings, in: E. Wolf (ed.), Progress in Optics XIV, 195-244, North-Holland (1976)

[2] A. Irtel von Brenndorff, Diplomarbeit in Physik, Universität Göttingen (1992)

[3] D. Rudolph et al., The Göttingen X-Ray Microscope and X-Ray Microscopy Experiments at the BESSY Storage Ring, in: X-Ray Microscopy, G. Schmahl and D. Rudolph (eds.), Springer Series in Optical Sciences 43, 192-202, Springer Verlag, Berlin (1984).

[4] R. Paucksch, Diplomarbeit in Physik, Universität Göttingen (1990)

[5] B. Niemann, Annals of the New York Academy of Sciences 342, 81-93, (1980)

Modeling Soft X-Ray Projection Lithography

Bernice M. Lum
University of California, Cory Hall Box 167
Berkeley California 94720 &
Center for X-ray Optics, Lawrence Berkeley Laboratory
(510) 642-8897

Andrew R. Neureuther
Department of Electrical Engineering & Computer Sciences and
The Electronics Research Laboratory
University of California, Berkeley California 94720
(510) 642-4590

Glenn D. Kubiak
Sandia National Labs, Livermore, California 94551-0969
(510) 294-3375

Resist models to support resist line-edge profile simulation are being developed for soft x-ray projection lithography. Models for resist exposure, post-exposure bake kinetics, and dissolution surface etching as well as exposure tool imaging are key to balancing tradeoffs between lithographic materials and exposure systems. The SAMPLE lithography simulation program is well suited for supporting the development of this new soft x-ray projection lithography technology once the materials and imaging models are extended.

The goal is to support researchers with qualitative models for promising new materials as well as commonly used standard materials such as Hoechst AZ PN114 (RAY-PN) and PMMA. The approach is to interpret through data analysis measured data on thickness remaining versus exposure dose using the menu of resist dissolution models available in SAMPLE. The initial effort is to screen potential materials and interpret existing data. Promising materials such as the generic AT&T t-BOC, IBM APEX-E, and OCG CAMP-6 will be investigated and models implemented. Methods for directly measuring resist dissolution for materials with high absorption constants and small exposure areas will be explored. For deep-UV resist materials, measurements of resist sensitivities at 13 nm are being correlated with the resist sensitivities at 248 nm scaled by the ratio of the absorption constants.

Research supported by DARPA BG91-285, Advanced X-ray Lithography Program

Image Simulation for Soft-X-ray Projection Printing

Derek C. Lee
The Electronics Research Laboratory, University of California,
Cory Hall Box 21, Berkeley California 94720 &
Center for X-ray Optics, Lawrence Berkeley Laboratory
Berkeley, California 94720
(510) 642-8897

Andrew R. Neureuther
Department of Electrical Engineering & Computer Sciences and
The Electronics Research Laboratory
University of California, Berkeley 94720
(510) 642-4590

SPLAT has been useful in exploring the deviations of optimal image quality from that of limits of diffraction limited optics in projection x-ray lithography proto-type systems. This was accomplished through modifying the aberration options in SPLAT to accept detailed optical system wavefront data from CodeV. This allows feedback from the as built and as coated soft x-ray elements on the resulting imaged quality.

SPLAT (Simulation of Projection Lens Aberrations via TCCs) is based on Hopkins theory of partially coherent imaging[1], which uses transmission cross-coefficients (TCCs) to calculate the image intensity pattern from the Fourier transform of the object (mask) transmission. Aberrations are included by integrating the optical path difference over the lens elements in calculating TCCs. At suggestion of O. Wood of At&T, extensions were made to encompass the detailed wavefront data synthesized via CodeV from lens element data. Initially, 37 Zernike polynomials were used. However, it was found that using only 37 terms produced smoothing which made the image quality over optimistic.

In a more rigorous approach SPLAT was modified to utilize the detailed wavefront map from CodeV. This map is available as fringe measurements on a rectangular grid and 64x64 point were typically used. This data representation and integration routine of SPLAT were modified for this map. A table lookup approach with a rectangular or triangular grid is used in integration. The undulated source also presented problems as a thin arc. SPLAT is currently being extended to include the effect of amplitude reduction from reflections in the optical system.

At x-ray wavelengths (13 nm) the surface figure errors of the multi-layer mirrors introduces significant wave aberrations which can severely distort the image. A pupilmap of the optical system used by O. Wodd, et al. at AT&T Bell Laboratories is shown in figure 1. Experimentally observed images with lower contrast, spatial shifts, and asymmetries were in agreement with those predicted by SPLAT. The resultant intensity profile generated by SPLAT can be used by SAMPLE-3D, an optical projection printing simulator.

† Research supported by the Semiconductor Research Corporation via SEMATECH and by DARPA BG91-285, Advanced X-ray Lithography Program

PUPILMAP

RMS WFE: 0.275: 13 nm

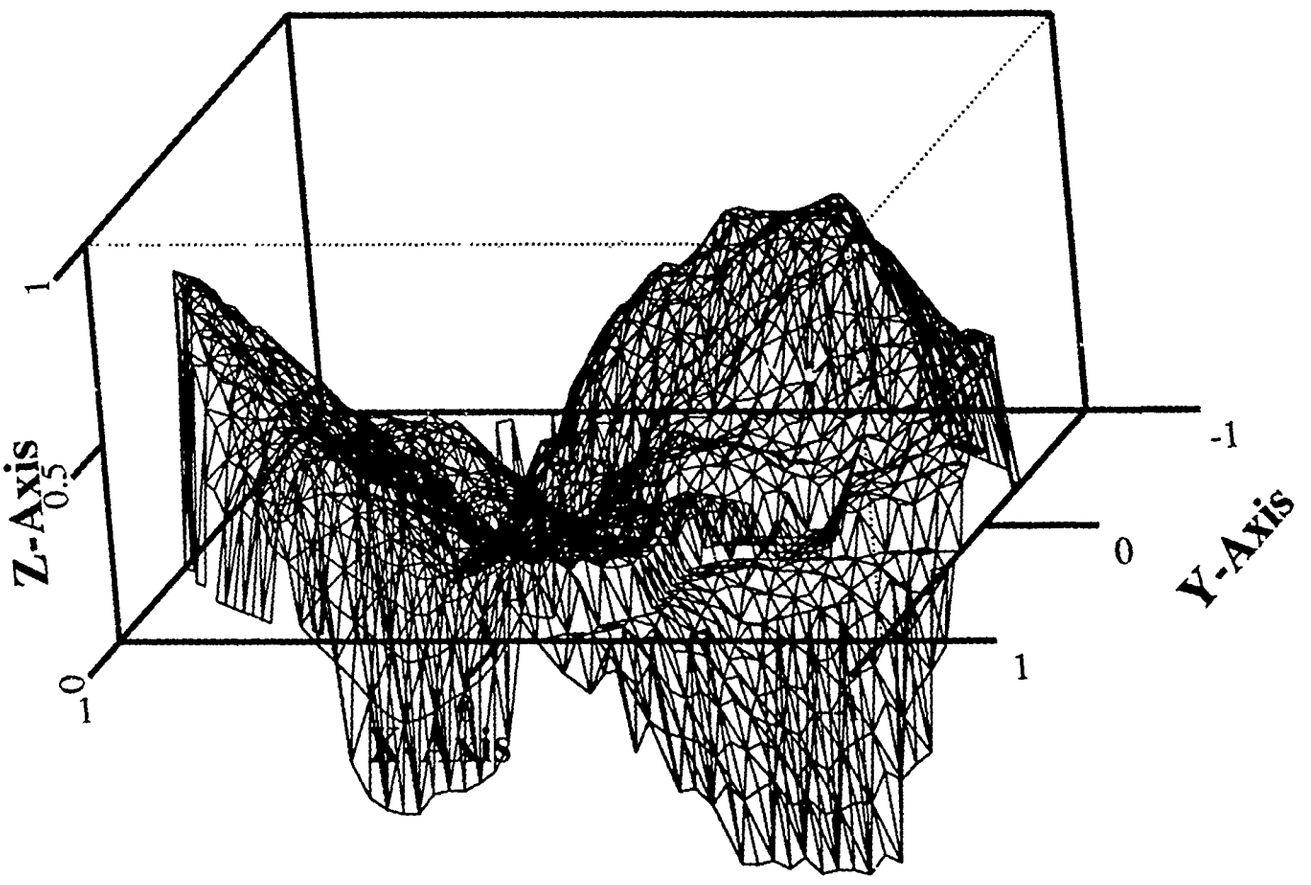

FIGURE 1.

"Computational Analysis of Debris Formation in SXPL Laser-Plasma Sources"

Timothy G. Trucano, Dennis E. Grady, Richard E. Olson, and Archie Farnsworth

Sandia National Laboratories, P. O. Box 5800, Albuquerque, NM 87185

(505)844-8812

E-Mail Address: tgtruca@cs.sandia.gov

Laser generated extreme ultraviolet sources applicable to soft x-ray projection lithography (SXPL) are undermined by target debris formation. This debris, in the form of vapor and condensed ejecta, can coat and damage the optical systems that direct and focus the emitted radiation for the lithographic application [1]. The purpose of this paper is to present ongoing work to develop a computational methodology for understanding and predicting the debris formation process in these laser sources.

Our approach consists of three elements. First, the Lagrangian hydrodynamics code LASNEX [2] is applied to simulate the interaction of a KrF laser with intensities on the order of 10^{11} W/cm^2, pulse energies of approximately 1.0 J, and pulse durations of approximately 30 ns, with high Z targets such as gold. LASNEX is used extensively in inertial confinement fusion applications where laser energies and intensities are far greater than in the current application. The application of LASNEX to studying laser-target interactions of interest for SXPL purposes has been previously documented ([3], [4]). The LASNEX hydrodynamics calculations proceed until the laser pulse terminates, typically around 36.0 ns. A schematic of the evolution of the laser coupling and resulting target hydrodynamics is found in Figure 1 below.

The LASNEX calculation predicts the thermodynamic state of the target at the moment of pulse termination. In addition, target ablation due to soft x-ray generation by the laser produced plasma is also simulated. As the second element of our approach, the resulting calculated state, which consists of undisturbed target material, "cratered target" material, and laser formed plasma in contact with the solid density target material (see Figure 1) is then mapped into the 2- and 3-D

Eulerian hydrodynamics code CTH [5]. This code incorporates the complete solid response of the target, including both strength and fracture characteristics. CTH is then used to directly predict the response of the target in the post-laser pulse environment to times that can be as long as microseconds. Material breakup on these time scales can be directly simulated in CTH. However, available data indicate that the condensed phase debris evolves on time scales which are much longer than microseconds, perhaps on the order of milliseconds, even though target vaporous ejecta evolves almost immediately after the initiation of the laser pulse. Target ejecta and breakup phenomena that occur on such time scales cannot be easily simulated in CTH.

Therefore, the third element of our computational methodology is to apply ideas from final-state theories of dynamic fragmentation [6] to extrapolate the CTH computed state of the target to a time regime in which condensed ejecta will be created. In this step, kinematic and thermodynamics predictions about the nature of the debris can be made: its mass, size distribution, velocity distribution, and temperature (whether it is melted or not, for example). These predictions can then be correlated with experimental data.

The predictions are made in such a way that information from the CTH calculations is used to provide time and spatially resolved input for the dynamic fragmentation theories. This process does not allow for a fully coupled debris prediction, in which the fragmentation theory influences the CTH calculations as they evolve in time. It has been our experience that such a fully coupled approach is not required to achieve reasonable understanding of the mechanisms and results of debris formation in dynamic events. For example, the debris observed in laser-target interactions of the type under discussion is similar to that created in impact crater events. There, the primary mechanism for ejecta formation is the conversion of impactor kinetic energy into target internal and kinetic energy. In the case of the present laser-target interactions, the primary mechanism is coupling of the generated soft x-rays emanating from the laser interaction region into the cold target, which produces target internal and kinetic energy. The detailed hydrodynamic simulations can then be carried out to a time in which extrapolation using the fragmentation theories makes sense, and for which various sensitivity issues can be studied.

As a practical matter, this work involves studying the influence of a variety of computational parameters upon the debris predictions. These factors include:

- Dependence of the computational debris results upon the numerical meshing in both CTH and LASNEX.
- Sensitivity of the computational debris results to the time of transition from LASNEX to CTH, and to specific details of the link algorithms.
- Sensitivity of the computational debris results to physical parameters that are critical in the dynamic fragmentation theories. For example, fracture data for

metals in the transition thermodynamic region between fully solid and fully melted is important, and very difficult to acquire.
- Dependence of trends and scaling issues in the computational results as a function of laser pulse and target material variations.

We will present preliminary results of our computational methodology for laser pulse variations in gold targets. We will compare our predictions with experimental data, in particular, recent measurements of the volume (or mass) of removed material due to single laser pulses [7]. In general, we find that we can predict general aspects of the debris production - mass of ejecta and mean speed of the condensed component of ejecta, for example - fairly accurately, whereas more detailed information, such as computational particle number versus particle velocity histograms, are quite sensitive to the numerical details.

1. G. D. Kubiak, et al., "Extreme Ultraviolet Resist and Mirror Characterization: Studies with a plasma source," J. Vacuum Sci. Tech. **B8**, 1643 (1990).

2. G. Zimmerman and W. Kruer, "Numerical Simulation of Laser-Initiated Fusion," Comm. Plasma Phys. **2**, 85 (1975).

3. P. D. Rockett, J. A. Hunter, and R. E. Olson, "XUV Conversion Efficiency in a Low Intensity KrF Laser-Plasma for Projection Lithography," OSA Proc. on Soft X-Ray Projection Lithography, **Volume 12**, Monterey, CA, April 10-12, 1991.

4. R. E. Olson, W. C. Sweatt, and P. D. Rockett, these proceedings.

5. J. M. McGlaun, S. L. Thompson, and M. G. Elrick, "CTH: A Three-Dimensional Shock-Wave Physics Code," Int. J. Impact Engng. **10**, 351, (1990).

6. D. E. Grady and M. E. Kipp, "Fragmentation of Solids Under Dynamic Loading," in Structural Failure, John Wiley & Sons (1989).

7. Glenn Kubiak, Private Communication.

This work was supported in part by the U. S. Department of Energy under contract DE-AC04-76DP00789.

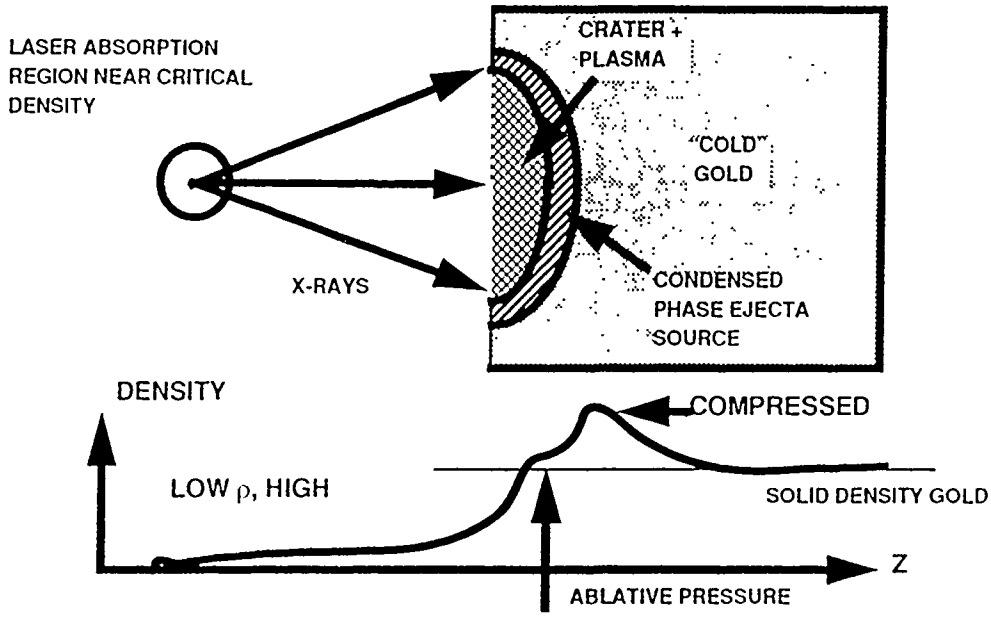

Figure 1. Schematic of the laser absorption region, re-emitted x-rays, and target hydrodynamic crater formation during the laser pulse duration.

Velocity Characterization of Target Debris from a Laser Produced Plasma Utilizing a "Time-of-Flight" Technique

H. A. Bender, A. M. Eligon, A. Hanzo, and W. T. Silfvast

Center for Research In Electro-Optics and Lasers
University of Central Florida
12424 Research Parkway
Orlando, Florida 32826
(407) 658-6800

The generation of significant amounts of target debris from laser produced plasmas is well known and has been characterized in terms of quantity, particle sizes, rate of deposition on surfaces, and other parameters for conditions relevant to soft x-ray projection lithography (SXPL).[1] This debris will be detrimental to the condenser and/or illumination optics in an SXPL system. Of the three categories of debris, high velocity ions, neutral atoms, and particulates (or clusters), it is the latter that is quite difficult to control and potentially the most damaging. It has been shown that atomic and ionic flux, as well as very small particulate (<0.3 μm) emission can be minimized by He background gas while the effect on larger clusters (>0.5 μm) requires He pressures that are significantly higher than that allowed for SXPL.[2,3] The damage due to collisional impact by many large clusters on a multilayer coated optic would be difficult if not impossible to repair. It is the purpose of this paper to report on the velocity distribution, along with size and mass distribution measurements of particulate emission, in order to understand the mass ejection process in more detail. In turn, this may provide answers as to potential interdiction techniques to stop debris from reaching expensive optical components.

Most of the larger ejected material comes from explosive removal of the target material through plasma electron collisions with the solid material and subsequent thermal transport and vaporization. The method we utilized to determine the velocity of these clusters is a "time-of-flight" technique whereby the propagation of the particles is interrupted by a high-speed, small aperture mechanical shutter. The layout of the experiment is diagrammed in Figure 1 showing the placement of the shutter relative to the Si collecting plate used to capture the particles. A

fixed delay from the initial laser pulse was used to actuate the shutter thus allowing only particles with a certain velocity to reach the collecting plate. To generate the debris we used an input laser pulse of 500 mJ at 1.06 μm and 18 ns duration, conditions consistent with the laser driver in a SXPL system. The laser was fired at 2 pps and a new target area was provided for each pulse via a rotating disc target. The shutter was synchronized to the laser pulse via a master trigger with a variable shutter delay. This allowed for relatively accurate velocity calculations.

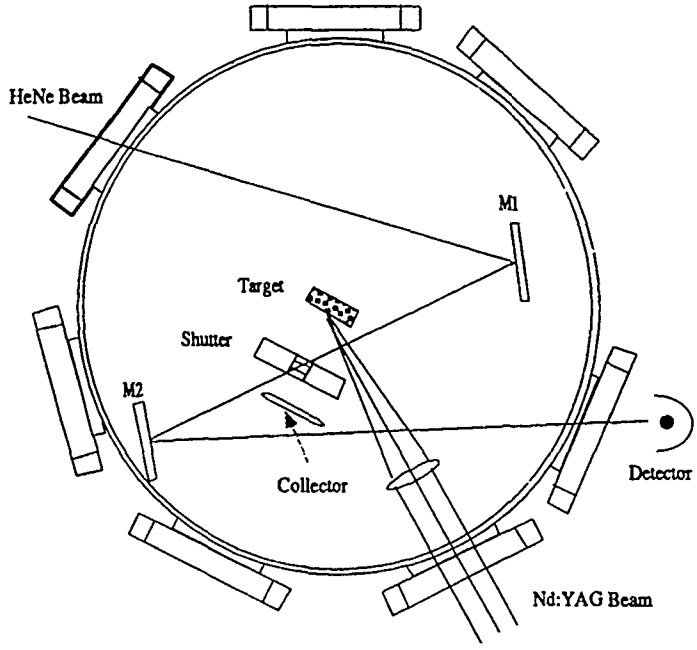

Fig. 1
Diagram of the experimental arrangement used in the velocity measurements

Measurements performed on both Sn and Au targets indicate a predominance of debris less than 1 μm in diameter. In addition approximately 72% of the Sn particles emitted and 64% of the Au particles emitted had velocities greater than 9000 cm/s. Figures 2 and 3 indicate density per shot (or total # clusters/shot/cm^2) for both Sn and Au versus velocity (for all sizes) and versus size (for all velocities), respectively. Figure 2 indicates that both Sn and Au follow a similar trend in their respective velocity distributions although Au has a much lower relative density/shot compared to Sn. This might suggest that the velocity distribution for a given target is material independent.

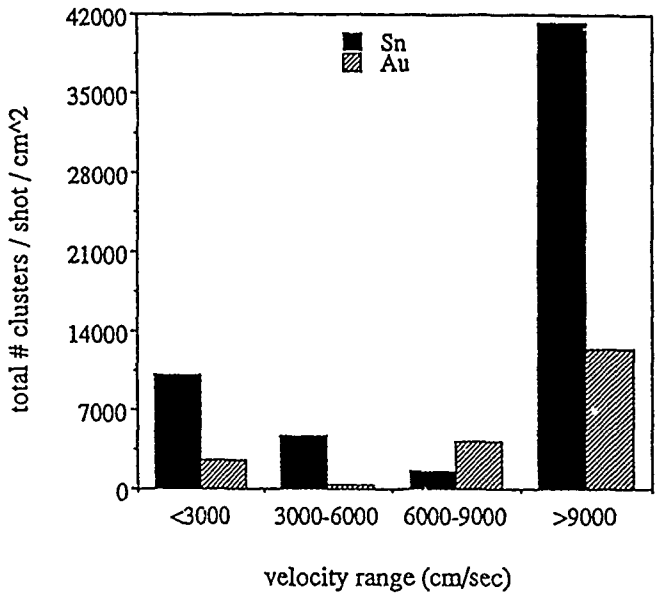

Fig. 2

Velocity distribution for Sn and Au targets

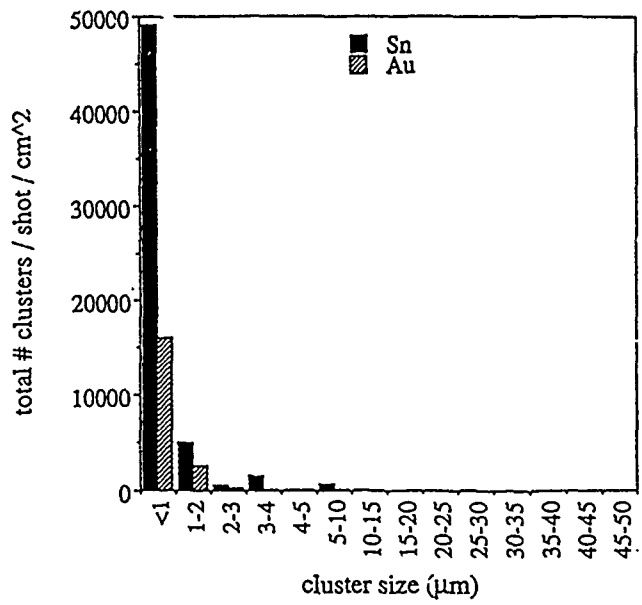

Fig. 3

Size distribution for Sn and Au targets

Additional data collected will be discussed for low pressure He background gas. Calculations of total mass ejected as a function of velocity and size will also be presented.

References

1. W. T. Silfvast, M. C. Richardson, H. Bender, A. Hanzo, V. Yanovsky, F. Jin, and J. Thorpe, "Laser-produced plasmas for soft x-ray projection lithography," J. Vac. Sci. Tech. B **10(6)**, Nov/Dec 1992, pp. 3126-3133.

2. M. Ginter and T. J. McIlrath, Appl. Opt. **27**, 5 (1988), pp. 885-889.

3. E. Louis, F. Bijkerk, G. E. van Dorssen and I. C. E. Turcu, Proc. 21st European Conf. on Laser Interaction with Matter, Warsaw 1991, p. 261.

Constraints on Pulse Power and Duration for Soft X-ray Lithography Systems

J. A. Liddle, AT&T Bell Laboratories, 600 Mountain Avenue, Murray Hill, NJ 07974, (908) 582 5405

INTRODUCTION

In any of the high-throughput lithography systems designed to operate at 0.25μm design rules and below, SXPL, X-ray 1:1, projection ion-beam or projection e-beam, there will be a significant amount of power flowing through the system. The effect of thermal loading must be included in the system design, for example, in the provision of heat sinks or the use of certain materials to reduce the effects of thermal expansion. In most cases distortions due to steady state heating can be compensated for or reduced to an acceptable level. However, in the case of a pulsed source, there are fundamental limits to the possible range of pulse power and duration that can be employed.

This paper describes a model for determining where the limits of operation lie, and then presents results obtained from the model for a range of system configurations.

MODEL

The first step is to establish the power, P (mW), required to expose wafers at a given rate, A ($cm^{-2}s^{-1}$), using resist of a given sensitivity, S ($mJcm^{-2}$), i.e. P = AxS. The power at any point in the system can be determined from the reflectivities of the various optical elements. This process can, of course, be continued to determine the necessary source power. In this paper, however, we are interested in what happens to all the parts of the system that experience the pulse power, as opposed to the steady state heating effects, that is the mirror surfaces and the resist.

The peak temperature reached is determined by the pulse energy deposited into a volume defined as the quadrature sum of the absorption depth and the heat diffusion distance. In a homogeneous medium this latter is simply $\sqrt{\kappa t}$, where κ is the thermal diffusivity and t is the pulse duration. Clearly there will be a limit on the maximum pulse energy, imposed by the necessity to avoid over-heating the resist. Problems caused by resist heating have been discussed for direct write e-beam systems.[1] Heating is also

important in terms of meeting overlay requirements. If the pattern on the mask expands during illumination, significant pattern placement errors may occur.[2]

The constraints on pulse power, duration and repetition rate will define a region within which the source must operate.

EXAMPLE

The figure below demonstrates the effect of changing resist sensitivity and pulse repetition rate on the degree of resist heating. In this example the illuminated area is 1mmx20mm and the pulse duration is 10ns.

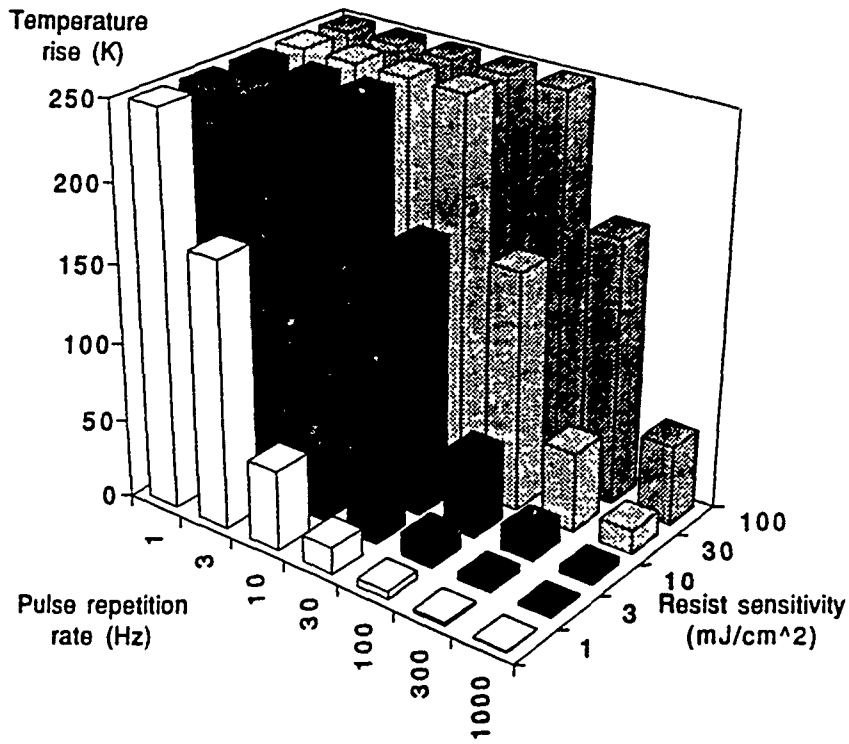

In this case, as the pulse repetition rate increases above 1kHz any effects associated with pulse heating will become negligible. The same type of calculation can be carried out for heating of the multilayers on the mask. This figure illustrates how the operating conditions of the source are constrained by the resist sensitivity.

REFERENCES

[1]K. Saito and T. Sakai, *J. Vac. Sci. Technol.* **B 9** p3464 (1991).

[2]I. Shareef, J.R. Maldonado and D. Katcoff, *J. Vac. Sci. Technol.* **B 7** p1575 (1989).

Computational Simulations of a Soft X-Ray Projection Lithography Laser Plasma Source

R. E. Olson, W. C. Sweatt, and P. D. Rockett
Sandia National Laboratories, Albuquerque, NM 87185
(505) 845-7527

A Sandia National Laboratories / AT&T Bell Laboratories team is developing a soft x-ray projection lithography tool that uses a compact laser plasma as a source of 14 nm x-rays. Optimization of the 14 nm x-ray source brightness is a key issue in this research. This paper describes our understanding of the source as it has been obtained through the use of computer simulations utilizing the LASNEX radiation-hydrodynamics code.

A Sandia National Laboratories research team has experimentally examined the efficiency with which focused ultraviolet (UV) laser light is converted into a 4.5% band about 13.9 nm[1]. Experiments were performed with a 1.2 J KrF laser at 32 ns fwhm, and a 1.5 J XeCl laser at 5 and 47 ns fwhm. LASNEX computer simulations have been used, together with the TDG postprocessing code, to predict the outputs of an array of absolutely calibrated, broadband, filtered x-ray diodes and filtered, time-integrated x-ray pinhole cameras. The experimentally-benchmarked LASNEX simulations have then been used to gain an understanding of key design issues relating to the time-dependent 14 nm conversion efficiency, source size and source shape for a soft x-ray projection lithography laser plasma source.

LASNEX is a two-dimensional Lagrangian radiation hydrodynamics code used extensively in the inertial confinement fusion program at Lawrence Livermore, Los Alamos, and Sandia National Laboratories. TDG is a LASNEX postprocessor that is routinely used to predict the response of diagnostics such as XRD's and x-ray pinhole cameras. As input for the LASNEX simulations, we used an experimentally determined laser power time history and a Gaussian spatial intensity profile with a normal incidence to a disk geometry target (i.e., the two-dimensional LASNEX calculation assumes the target to be rotationally symmetric about the axis of the laser beam). An equal ratio zoning scheme (finer zones near the target surface and laser spot center) was used in the target material. Radiation transport was performed via multigroup diffusion with a relatively course photon binning over a 0.1 to 5000 eV range and a fine group structure within the 80-100 eV range of interest in this problem. A non-LTE average atom approximation (the XSN code) was used in-line with LASNEX to compute zone-by-zone electron densities, level populations, and multi-group opacities. The time-dependent LASNEX output was combined with experimentally-determined filtered XRD response functions and experimental x-ray detector geometry (i.e., distance from the target, aperture size, angle from the laser axis) as input to the TDG postprocessor. The TDG output includes predictions of the amps vs. time output signal for each of the filtered XRD channels (Al, Be, parylene N, and parylene D filters were simulated), and

intensity contour predictions for Be and Al filtered, time-integrated x-ray pinhole cameras.

LASNEX/TDG predictions for the filtered XRD's predict a "shuttering" of the 14 nm output (i.e., the 14 nm output is cutoff while the laser pulse is still rising) for long (30-45 ns) laser pulses and an XRD turn-on delay of 5 to 10 ns for all channels. These features are in agreement with the experimental observations. The predicted overall efficiency of long pulse conversion into 87-91 eV x-rays is 0.75% -- within 20% of the experimental measurements. Upon examining the LASNEX output, we find that the shuttering is a fairly complicated effect that appears to be primarily due to the development of a "plume" of relatively cool plasma that becomes opaque to the 87-91 eV x-rays. Output of the softer x-rays, on the other hand, exceeds the fwhm of the laser pulse since they are related primarily to the ~20-70 eV x-rays of the cool plume.

This situation suggested that a decrease in laser pulse length might result in an increase in conversion efficiency into the 87-91 eV band. Presumably, with the shorter pulse length (at a given intensity) the cool plume plasma would not have enough time to obscure the hot source during the time of the laser pulse. The LASNEX/TDG calculations supported this conjecture and led to experiments involving a shorter pulse (5 ns) excimer laser in which higher conversion efficiencies have been observed.

One might also suspect a relationship between laser intensity and conversion efficiency. Our LASNEX calculations also tend to support this speculation. LASNEX-predicted efficiency for a 20 ns laser pulse length is predicted to increase from 1.6% to 1.8% if the 1.2 J laser spot size is decreased from 220 μm to 110μm. A further increase to 1.9% efficiency is predicted for a 80 μm diameter, 1.2 J laser spot.

While the conversion efficiency is important, the "brightness", size, and shape of the 14 nm source are also key design issues. Good brightness implies that the the ratio of the 14 nm flux per unit solid angle to the apparent source size as it is seen from the collection angle should be optimized. Per the previous discussion, one might expect that the size and shape of the 14 nm emitting region might be significantly different than the size and shape of the overall x-ray source. This speculation has been supported via LASNEX/TDG simulations in which predicted images of Al and Be filtered, time-integrated x-ray pinhole cameras have been compared to experimental data.

Since our excimer lasers are absorbed at relatively high densities (critical density of ~ 10^{22} cm^{-3}), one might infer that 14 nm source size, source shape, and brightness might be different than those experienced by a longer wavelength laser absorbed much further from solid density. This would suggest a larger source, and perhaps a lower brightness for the longer wavelength laser. On the other hand, each drives a shock wave into the bulk material, releasing fragments. One might expect a higher hydrodynamic efficiency with the much shorter excimer wavelength than with a YAG or equivalent laser. In order to study the process of fragmentation and debris generation, we are developing a

coupling of our Lasnex calculations to an Eulerian hydrocode that includes treatments of spall, fracture, melting, vaporization, and material breakup phenomena[2].

References:

1. P. D. Rockett, et al., these proceedings.
2. T. G. Trucano, et al., these proceedings.

Cryogenic targets for Laser Plasma X-Ray Lithography Sources

Martin Richardson, Kai Gabel, Feng Jin, & William T. Silfvast
CREOL
University of Central Florida,
Orlando, FL 32826
tel. # (407) 658 6819
fax # (407) 658 6880

It is now generally recognized that the source of preference for soft x-ray projection lithography is a high repetition-rate (1200 Hz) laser plasma source[1]. The design of this source is usually envisaged as comprising a compact high repetition-rate laser, preferably a solid-state laser, diode-pumped, and a renewable target system capable of operating for prolonged periods of time. For a production-line facility, this would imply uninterrupted shot cycles of $> 3 \times 10^6$ shots. In addition, current cost scenarios of the complete irradiation system suggest that the unit shot cost must be in the vicinity of $\$10^{-6}$ per shot[2]. These stringent requirements press the boundaries of current technologies. Moreover, recent studies of the particulate matter ablated from solid and tape targets under laser irradiation conditions similar to those deemed optimum for 13 nm soft x-ray generation, suggest that these types of targets will be unsuitable[3]. The levels of neutral clusters of particulate matter and of high velocity ions are many orders of magnitude above those that can be tolerated in an environment requiring the long-term preservation of expensive, high-reflecting multilayer collecting optics. It is thus our viewpoint that considerable progress must be made in the design of efficient soft x-ray-emitting laser plasmas for them to satisfy the needs of projection lithography.

In this paper we introduce a new concept for a high repetition-rate soft x-ray laser plasma source for projection lithography, that of the mass-limited cryogenic target. We commence with the premise that the optimum target for minimum debris production is one whose mass is limited to that of the minimum number of ions required for efficient x-ray generation. This precondition implies required target masses as small as ~50 ngm per shot for typical laser and x-ray conversion factors. If this target were configured as a disc target, for instance, having a diameter of ~100 μm it would have a thickness of <500

nm, equivalent to the plasma ablation depth. To configure this small mass as an isolated solid target and locate it precisely in the focal region of the laser beam under the required cost and operating conditions is technologically difficult.

The concept of using a mass-limited cryogenic gas target[4] as the laser-plasma target for a high repetition rate x-ray source for a production line soft x-ray lithography system will circumvent the principal problems associated with current configurations.

A target mass limited to the mass of the number of radiating ions will eliminate the generation of high-velocity particulate projectiles in the plasma. This will remove the primary threat to expensive state-of-the-art high reflectivity x-ray mirrors used to focus the soft x-ray emission onto the reflective mask. It is expected that the plasma ions that are generated, (~ 10^{16} ions) can be impeded in their ballistic trajectories from the plasma by collision with a background gas, or deflected to benign locations with the aid of electric or magnetic fields.

It is expected that a limited mass cryogenic target system could function continuously at a cost commensurate with the required unit shots costs. This offers distinct advantages over target assembly approaches that use solid targets or tape-drive targets, which would require periodic system deactivation for target replacement. Moreover it has been shown that these target system approaches will have great difficulty meeting the single shot costs required[3]. On the other hand, continuous automatic target fuel replenishment can be configured with cryogenic targets, permitting unimpeded x-ray source operation on the production line. With the use of inexpensive gases, it is expected that this concept will also be able to provide targets at a unit cost attractive for soft x-ray projection lithography.

We will discuss the implications of using cryogenic gas targets. Hydrodynamic and atomic physics codes are used to predict the x-ray emission from these targets. We will describe a number of different cryogenic target configurations capable of providing a continuous stream of limited mass targets to a high repetition-rate laser plasma system, and make preliminary estimates of the unit target costs.

This work is supported by DARPA through contracts with LLNL and Sandia National Laboratories and by the State of Florida.

1 W. T. Silfvast, M. Richardson, H. A. Bender, A. Hanzo, V. P. Yanovsky, F. Jin & J. Thorpe. J. Vac Sci. & Technol. B 10,1, (1992)
2 N. M. Ceglio & A. M. Hawryluk, J. X-ray Sci. & Tech. 3, 194 (1992)
3 M. Richardson, W. T. Silfvast H. A. Bender, A. Hanzo, V. P. Yanovsky, F. Jin & J. Thorpe. Appl. Opt. (to be published)
4 M. Richardson, W. T. Silfvast H. A. Bender, A. Hanzo, Feng Jin & V. P. Yanovsky Proc SPIE, 1848, (1993) to be published

Calibration and Metrology of X-Ray Optics at the Center for X-ray Optics

E. M. Gullikson, and J. H. Underwood
Center for X-Ray Optics
Materials Sciences Division
Lawrence Berkeley Laboratory
Berkeley, CA 94720

In the last 20 years x-ray optics has become an important branch of optics which is having more and more impact in a variety of scientific and technological areas. These activities require accurate and reliable calibration and standards facilities to enable scientists and engineers to measure the performance of optical elements and predict the performance of a system.

This paper summarizes the activities of the Center for X-Ray Optics in the areas of standards and metrology. Current experimental work is being done utilizing both conventional electron impact x-ray line sources and a more recently developed reflectometer based on a laser-produced plasma XUV source [1]. In addition to these facilities, a bending magnet beamline is planned for construction at the Advanced Light Source. The beamline will have a two branch lines. The low energy branch line will have a varied line spaced grating monochromator. A prototype of this monochromator is being constructed and will be installed at BESSY. The high energy branchline will use a two crystal monochromator.

Examples of recent work which illustrate the importance of absolute measurement in the XUV are being presented at this conference in separate papers. They include a study of the stability of Mo/Si multilayer mirrors. A degradation in the normal incidence refelctivity was found which turned out to be due to the oxidation of the Mo top layer. It was found that multilayers terminated with a Si layer instead of Mo were stable. It is unlikely that this problem would have been observed by measurements other than direct "at-wavelength" reflectance. Also presented at this conference is on ongoing project with AT&T where a set of Schwartzschild optics was coated for 6.8 nm [2]. Extremely tight tolerances for the multilayer d-spacing required an iterative process of deposition masking and d-spacing measurement.

A compilation of the atomic scattering factors has recently been completed [3] which is based on available experimental data in the literature and recent theoretical calculations. The optical constants were obtained from the absorption coefficient using the Kramers-Kronig relations. The advantage of compiling the atomic scattering factors is that the optical constants of any composite material may then be obtained with the assumption that response is atomic-like, ie. that due to a collection of non-interacting atoms. This assumption is reasonably good away from absorption edges in both the soft and hard x-ray regions.

There is a continuing need for improved measurements of the optical constants of materials in the XUV. This need is driven by the current activity in x-ray lithography as well as a variety of studies using synchrotron radiation. Particularly, in the spectral range 25 to 300 eV, which is the region of interest for projection x-ray lithography, the optical constants are poorly known because of the difficulties involved in their measurement. We plan to contribute to these needed measurements using both current facilities and the future ALS beamlines.

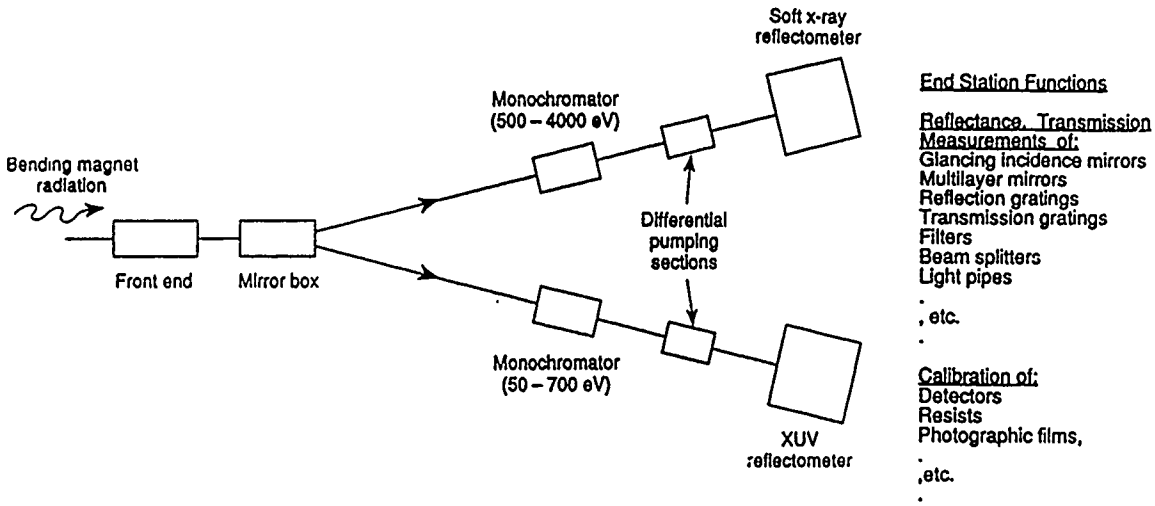

Figure 1: Schematic of the soft x-ray and EUV metrology beamline planned for the Advanced Light Source. A low energy branchline will utilize a varied line space grating monochromator and is expected to have a spectral resolution of 10^3 to 10^4 and a spatial resolution of less than $100\mu m$. The high energy branchline will have a double crystal monochromator.

Acknowledgments

This work was supported by the Defense Advanced Research Projects Agency and the Office of Basic Energy Sciences of the U. S. Department of Energy.

References

[1] E. M. Gullikson, J. H. Underwood, P. Batson, and V. Nikitin. J. X-Ray Sci. and Techn. (*in press*).

[2] J. B. Kortright, E. M. Gullikson, and P. E. Denham, (*this conference*).

[3] B. L. Henke, E. M. Gullikson, and J. C. Davis, Atomic Data and Nuclear Data Tables, (*to appear in July 1993*).

Sources 1

WA 8:30am–12:00m
Bonsai II & III

Donald C. Hofer, *Presider*
IBM Almaden Research Center

Enhanced performance of KrF laser-induced x-ray sources and multilayer mirrors for soft x-ray projection lithography

F. Bijkerk[a], E. Louis[a], L. Shmaenok[a], H.-J. Voorma[a], M.J. van der Wiel[a], R. Schlatmann[b], J. Verhoeven[b], E.W.J.M. van der Drift[c], J. Romijn[c], B.A.C. Rousseeuw[c], F. Voß[d], R. Désor[d], and B. Nikolaus[d]

[a]FOM-Institute for Plasma Physics Rijnhuizen, Edisonbaan 14, 3439 MN Nieuwegein, The Netherlands, tel +31 3402 31224, fax +31 3402 31204
[b]FOM-Institute AMOLF, Kruislaan 405, 1098 SJ Amsterdam, The Netherlands,
[c]Delft Institute for Microelectronics and Submicron technology DIMES, Feldmannweg 17, 2628 CT Delft, The Netherlands,
[d]Lambda Physik GmbH, Hans Böcklerstraße 12, D-3400 Göttingen, Germany

1. Introduction

The rapid development of high average power excimer lasers pushes the potential of a laser plasma x-ray source for SXPL. Now that the problem of debris production is solved at least at the prototype level [1] the source might be a candidate for operation in an industrial environment. The development of high reflectivity multilayer coatings for soft x-rays at normal incidence makes it possible to produce a demagnifying x-ray optical system. Together with an x-ray reflection mask all ingredients to develop a SXPL system are present. A cooperation of research institutes, semiconductor industry, resist and laser manufacturers has been set up to develop the process technology required.

2. Laser-induced x-ray source

The laser system characterized in this paper is a state-of-the-art high power, compact system (LPX 350i cc) designed for generating plasma-soft x-ray radiation. The laser consists of two identical high power laser heads that can be configured as power oscillator-power amplifier (popa) or as an injection seeded system. In the first case the full output energy of the oscillator is amplified in a single pass through the amplifier, resulting in a maximum pulse energy of 1.5 J. In the second case apertures in the oscillator define a low divergent beam that is seeded into the amplifier, resulting in a maximum of 0.95 J of output energy. The corresponding maximum powers amount to resp. 67 and 42 W (at 50 Hz). In a parallel effort compact excimer systems with powers up to 500 W are being developed, having comparable pulse properties as the 50 Hz laser tested here for its suitability to generate x-rays [2].

The beam divergence was measured to be 0.07×0.13 mrad in injection seeded mode and 0.15×0.12 mrad in popa mode. The laser energy is focused in a source chamber under moderate vacuum conditions or in ambient buffer gas. The plasmas are created on a metalized plastic tape moving through the laser focus or on rotating cylindrical metal disks. The tape target system is designed to enable routine operation during long x-ray exposure sessions.

The power density in the ~35 μm focus amounted 3×10^{12} W/cm^2 on a Ta target. Spectrally selective radiometry of the plasma emission was performed using calibrated *p-i-n* diodes,

spherical multilayer mirrors and submicron filters. We measured a narrowband conversion efficiency in the soft x-ray range of $\eta_{248\rightarrow 13.5} \geq 0.7$ % in a 2 % bandwidth at 13.5 nm. Although this efficiency is higher than reported for lower irradiance conditions [3] further optimization remains to be done.

We investigated two methods to overcome the production of target debris from the plasma [1,4]. One is the use of a buffer gas (e.g. low-pressure He) in the source chamber. This reduces the debris with a factor of 100 or more, depending on the distance to the laser target. The second solution is the use of a thin tape-target instead of bulk material. Thin film steel targets reduce the debris production with more than two orders of magnitude. A thin polymer tape coated with 1-2 μm target material is even more effective to minimize debris production without considerable loss in x-ray yield [2,3]. Application of the two methods together reduces the amount of debris drastically. The residual debris can only reach the illuminator which is a non critical surface and cannot damage the reflection mask.

The remaining debris will cause a small reduction in reflectivity of the illuminator. Extrapolation of our measurements shows that this reduction is less than 10% within the main service interval for the laser (10^9shots). The investigated methods extend the service interval to at least an equal period as required for other machine parts.

3. Multilayer coatings

All mirror substrates of our modified Schwarzschild optical system are spherical and are multilayer coated at the facility at FOM [5]. The coatings are produced by e-beam evaporation and the layer growth is monitored in situ by measuring the reflectivity of soft x-rays, e.g. C, B or N *K*-radiation. Several methods to improve the quality of the multilayers have been developed: one is to etch the deposited layer by ion bombardment after deposition, resulting in an improvement by a factor of ~2 in reflectivity [6]. Another method is to use ion bombardment during deposition. Using these techniques a reflectivity close to the theoretical value is expected, since the roughness of all interfaces throughout the layer stack is kept at the constant value of the substrate and does not increase towards the top layers [7]. A third method is to optimize the temperature of the substrate during deposition. Depending on the materials and the layer thickness used we measured a substantial improvement in the reflected signal during deposition. The optimal deposition temperature for MoSi amounted to 215 °C. [8,9].

The throughput of the four mirror design will be 13 % at 2 % bandwidth if we assume the MoSi multilayer coatings to have a peak reflectivity of 60 % for λ=13.5 nm. A large illuminator collects 15-18 % of the x-rays emitted preferentially along the target normal. Using the data on conversion efficiency we calculate that the laser power of 67 W results in 50 mW/cm^2 on the resist. This means that one exposure can be made in 400 ms using a resist with a sensitivity of 18 mJ/cm^2 [10].

4. Conclusions

We have demonstrated that a laser plasma generated with a compact and powerful semi-commercial KrF excimer laser system is a high-brightness source of soft x-ray radiation. We measured a conversion efficiency of 0.7 % for 13.5 nm radiation in 2 % bandwidth. This conversion efficiency and the use of a large illuminator will result in a brightness that is sufficient for a soft x-ray projection lithography system. The production of debris can be

reduced effectively.

Control of the temperature of the mirror substrate during deposition and ion-bombardment of the layer interfaces both enhance the reflectivity of the multilayer. These techniques should improve the multilayer reflectivities to close to the theoretical limit (60-70 %) resulting in a throughput of 13-24 % for a four-mirror projection system.

5. Acknowledgments

This work is part of the programme of FOM (the Foundation for Fundamental Research on Matter) and STW (the Netherlands Technology Foundation). The work is made possible by financial support from NWO (the Netherlands Organization for Scientific Research) and the Netherlands Government in the framework of EUREKA.

6. References

1 E. Louis, F. Bijkerk, G.E. van Dorssen and I.C.E. Turcu, Proc. 21st European Conf. on Laser Interaction with Matter, Warsaw 1991, p. 261

2 B. Nikolaus, D. Basting, Proc. Int. Symp. on Gas Flow and Chemical Lasers, Crete (1992)

3 P.D. Rockett, J.A. Hunter, R.P. Rensek, R.E. Olson, G.D. Kubiak and K.W. Berger, Osa Proc. on Soft X-ray Projection Lithography 12, Monterey, CA, 1991

4 F. Bijkerk, E. Louis, M.J. van der Wiel, I.C.E. Turcu, G.J. Tallents and D. Batani, J. X-ray Sci. and Technol. 3,133-151 (1992)

5 H.J. Voorma, F. Bijkerk, Proc. Microcircuit Engineering 17 (1992) 145-148

6 E.J. Puik, M.J. van der Wiel, H. Zeijlemaker and J. Verhoeven, Appl. Surf. Sc. 47 (1991) 251-260

7 R. Schlatmann, J. Verhoeven, andM.J. van der Wiel, Conf. Proc. Physics of multilayer structures, Jackson Hole (1992)

8 A. Kloidt, K. Nolting. U Kleineberg, B. Schmiedeskamp, U. Heinzmann, P. Müller and M. Kühne, Appl. Phys. Lett. 58 23 (1991) 2601-2603

9 E. Louis, H.J. Voorma, to be published

10 G.D. Kubiak, E.M. Kneedler, K.W. Berger, R.H. Stulen, J.E. Bjorkholm, W.M. Mansfield and H. Windischmann, Osa Proc. on Soft X-ray Projection Lithography 12, Monterey, CA, (1991)

Laser Plasma Source Characterization for Soft X-ray Projection Lithography

William Silfvast, M.C. Richardson, H. Bender, A.M. Eigon,
A. Hanzo, E. Miesak, F. Jin
University of Central Florida, CREOL

A review of the status of laser plasma soft x-ray sources will be made. This will include discussions of radiation properties as well as particulate emission and interdiction techniques.

Laser Plasma Source Targets for Soft X-ray Projection Lithography: Production and Mitigation of Debris*

Glenn D. Kubiak, Kurt W. Berger, and Steven J. Haney
Sandia National Laboratories/California
Livermore, CA 94550-0969
(510) 294-3375

The high cost and complexity of commercial illumination systems envisioned for soft x-ray projection lithography (SXPL) will require that their minimum replacement period is likely to be 6-12 months. For a laser plasma soft x-ray source, this corresponds to approximately 10^9 laser pulses. Given that a deposited film just 100 Å thick of a typical target element (Au, W, Ta, etc.) will reduce the reflectance of a multilayer mirror by an order of magnitude, it is clear that the contamination rate of condenser elements from plasma source debris must approach zero. In the present Sandia laser plasma source SXPL illumination systems, reflectance values of multilayer-coated plasma-facing optical elements are reduced by ~50% within 10^6 laser pulses. Clearly, large improvements in target debris production and/or mitigation are needed.

We have undertaken studies of the debris production from various laser plasma source target materials and geometries, as well as methods to suppress its deposition onto nearby optical elements. We will describe the effects of target ejecta on the performance and morphology of plasma facing, multilayer-coated optics, both before and after chemical removal of debris deposits. Earlier soft x-ray conversion efficiency measurements identified the target elements most efficient in the production of radiation near 14 nm[1,2]: Sn, W, Au, Ta, In, and Pb. Using 0.8 Joule, 248 nm laser radiation focused on foil samples of these, and other, targets to an intensity of ~2×10^{11} W/cm^2, we have determined the volume of material ejected per laser pulse, **V**. The results are examined as a function of the energy density required to melt each target material, **E**, defined as

$$\mathbf{E} = [(T_m - T_0)C_p + \Delta H_f]\rho$$

where T_m is the target melting temperature, T_0 is the initial target temperature, C_p is its specific heat, ΔH_f is its latent heat of fusion, and ρ is its density. We find that the results are reasonably well parameterized by the expression $\mathbf{V} \propto \mathbf{E}^{-1}$.

Debris production and mitigation from plastic-backed mass-limited target tapes and 25-100 μm thick solid target foils have also been investigated. Tape targets were fabricated by plating ~.5 μm of metal over a 0.1 μm-thick Cu plating base evaporated onto a 25 μm-thick mylar backing. Tape transport through the laser focus is performed using a high-speed transport device described previously[3]. Debris deposition measurements have been made under a number of debris mitigation conditions using such tape targets. Specifically, the results of experiments using flowing He, pulsed jets of various

gases, and magnetic deflection to reduce the deposition rate of target ejecta onto nearby silicon deposition substrates will be discussed.

*Work supported by the U. S. Department of Energy under co.ıtract DE-AC04-76DP00789 and by DARPA.

References

1. P. D. Rockett, J. A. Hunter, R. Kensek, R. E. Olson, G. D. Kubiak, and K. W. Berger, OSA Proc. Soft X-Ray Projection Lithography **12**, 76 (1991).
2. R. L. Kauffman and D. W. Phillion, OSA Proc. Soft X-Ray Projection Lithography **12**, 68 (1991).
3. S. J. Haney, K. W. Berger, G. D. Kubiak, P. D. Rockett, and J. Hunter, Appl. Optics, submitted.

The Investigation of Discharge-laser-driven Plasmas as Sources for Soft X-ray Projection Lithography*

Paul D. Rockett, John A. Hunter, Richard E. Olson, and William C. Sweatt
Sandia National Laboratories, Albuquerque, New Mexico 87185 (505/845-7466)

Glenn D. Kubiak, Kurt W. Berger, and Randal L. Schmitt
Sandia National Laboratories, Livermore, California 94551

Harry Shields and Michael Powers
Jamar Technology Co. Inc., 3956 Sorrento Valley Blvd., San Diego, CA 92121

David L. Windt
AT&T Bell Laboratories, Murray Hill, New Jersey

I. Introduction

Following two years of work to understand the conversion of excimer laser light into soft x-rays, we have moved onto implementing code predictions to improve conversion, and to studying the optical characteristics of these sources.

Laser-plasma sources of soft x-rays offer small footprint, reliable light bulbs for use in producing 0.1 μm design rules in IC processing. The key is to achieve high x-ray yield with a small source that produces no debris. Yield has been improving by use of appropriate targets with laser parameters conducive to producing a limited plasma expansion. Debris, however, continues to be a severe problem, threatening the multilayer-coated surface of the condenser optics close to the target. This area is being studied and will be reported on in another talk in this conference. We expect to use our excimer laser-plasma source this year to expose resist with high resolution over a mm scale area using a 10X Schwarzschild imaging system.

Our lithographic x-ray imaging systems have been tuned to operate at various wavelengths from 13.5 nm to 13.9 nm with a 4.5% bandwidth. Thus all measurements of conversion efficiency or source size are accomplished in this spectral region.

Experiments were performed using the KrF Laser Plasma Source at Sandia/California providing 1 J in 32 ns at 248 nm at a repetition rate of up to 100 Hz. Intensities varied from 1.4-2.8 x 10^{11} W/cm^2 and targets consisted of solid Au, Sn, Cu, and Cu-on-mylar. Additional experiments were conducted at Jamar Technology Inc., where they provided a compact XeCl laser at 308 nm. The laser pulse at Jamar was shortened to yield a 4.5 ns time history with approximately 0.4 J/pulse,

providing intensities of 2-6 x 10^{11}W/cm^2 on target. Laser focal spot size was maintained at 125 μm diameter with the LPS and 90 x 135 μm with the XeCl laser.

Our target chamber typically operated in the low 10^{-5} Torr range and included a target drum of 3" diameter which contained either gold in a .012" plating on stainless steel or thick sheet targets of other materials. Diagnostics included a six channel filtered x-ray diode array, a multilayer x-ray diode centered at 14.2 nm with a 10% bandwidth, a soft x-ray pinhole camera filtered with 1 mm Be, a filtered photographic plate capable of recording the angular distribution of the emitted x-rays, and detectors for laser energy and pulseshape monitoring.

II. Source Size

Knowledge of source size is mandatory in order to estimate the amount of light that can be collected in a given optical relay system. Present designs of condensers and imaging optics recommend a source size that is less than 150 μm along the plane formed by the laser and lithographic optic axis. In order to measure the extent of our laser-plasma sources we designed an x-ray pinhole camera, filtered by 1 μm Be and using Kodak SA-1 plates for recording A 50 μm diameter pinhole was used, providing limited resolution, but staying well above the limits for diffraction, which begin to affect image quality at 34 μm at our 13.9 nm wavelength. Pinhole-to-source distance was approximately 3.8 cm with a magnification of 14.8:1.

The beryllium filter and the overcoated film provided a detected spectrum peaking at about 100 eV (12.4 nm) with a breadth of roughly +8 eV, -20 eV. This placed the image in the relevant spectral region and assured its validity for use in predicting optical collecting efficiency of the multilayer coated condenser. Pinhole images were recorded, digitized, and compared to LASNEX TDG simulations of the radiating source size and gave very similar results.

The data from several experiments are shown in Figure 1. The lowest intensity data were recorded using a 100 cm focal length lens and a 32 ns pulse; the middle intensity used a 50 cm lens and a 32 ns pulse; and the highest intensity used a 40 cm lens and a 4.5 ns pulse. 100 eV sources appear to be larger than the laser focal spot for long pulses, and comparable to the laser spot size for short pulses. Since we are measuring the source size in the direction of the plasma expansion, this is

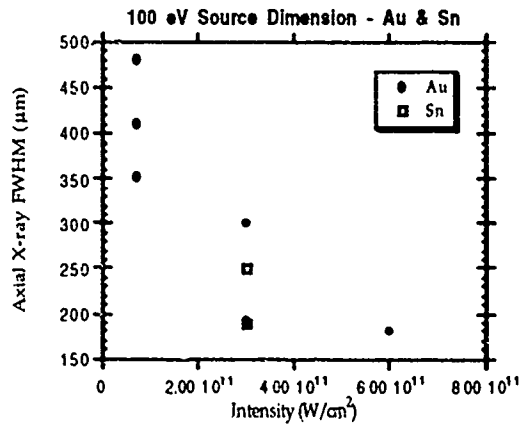

simply an indication of the time permitted for such an expansion to take place. Also note that we

have not yet achieved the small focal spot that is desired for optimum x-ray collection, but we clearly have the tools to achieve such a spot.

As an aside, one does not simply want to decrease the laser focal spot to achieve a small x-ray source size. Decreasing the laser spot size may increase the laser intensity on target, resulting in a larger production of debris. The 150 μm dimension is already a compromise between conversion efficiency, debris, and collection efficiency.

III. Conversion Efficiency

Past work with LASNEX simulations of our laser plasma source have indicated that short pulses (< 20 ns) will provide a higher fractional conversion of laser light into 13.9 nm light. In addition we had observed that the x-ray temporal history with 32 ns laser pulses was much shorter than the laser pulse, as if the plasma were "shuttering" the radiation emitted from the absorption region. Similar observations had not been made with 0.53 mm light at shorter pulselengths at Lawrence Livermore National Laboratories.[1]

We have now studied the effect of changing the pulselength, while keeping laser wavelength and intensity roughly constant at Jamar Technology Inc. The Jamar XeCl laser was used to amplify a chopped out 4.5 ns pulse. Energy and pulseshape were monitored regularly. The data showed roughly a factor of two increase in conversion efficiency over similar intensities at 32 ns. Targets of Au, Sn, Cu, and Cu-on-mylar all showed significant increases in yield.

Figure 2 suggests the reason for the observed increases in x-ray conversion efficiency. These are the spectra as recorded on our six channel broadband x-ray diode array. The high energy cutoffs for each channel are Al - 70 eV, Be - 108 eV, Parylene N - 282 eV with the multilayer XRD peaked at 14.2 nm. Note that the Jamar spectrum is far hotter than the 32 ns LPS spectrum, as indicated by the fact that the Be channel far exceeds the Al channel with the short pulse input. The multilayer XRD is comparably higher for shorter pulses. Pinhole photographs showed a pill box-shaped radiator with its thin side facing the laser. The short pulse permits little expansion, permitting the detectors to more directly observe the hot absorption region. Less plasma obscures your view, and no shuttering takes place.

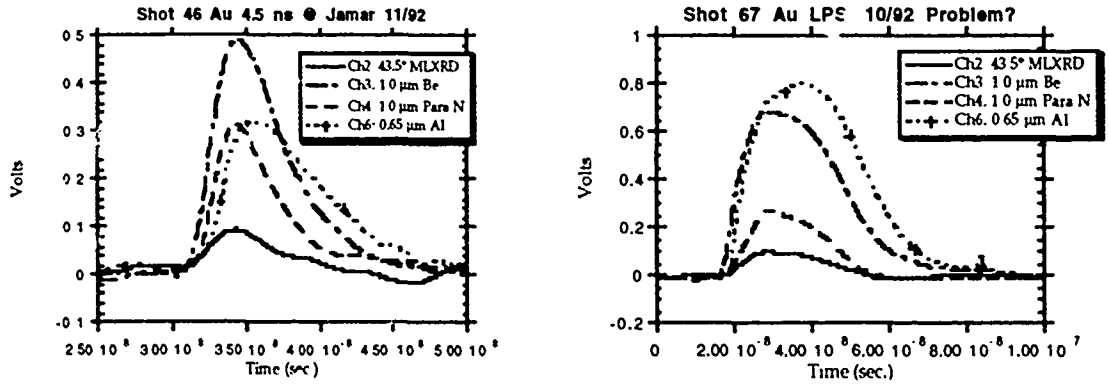

IV. Angular X-ray Distribution

The collection efficiency of the soft x-ray projection imaging optics is directly affected by the angular distribution of the emitted radiation in the relevant band. Early work by several authors had indicated that low energy radiation from low intensity laser plasmas was emitted with little azimuthal variation, measured values varying from $\cos^{0.3}\theta - \cos\theta$.[2–4]

We have implemented a photographic scheme to measure the Angular X-ray Emission of our discharge-laser-produced plasma sources. A photographic SA-1 plate was placed between the angles of 35^{o}-85^{o}, filtered by 1 μm Be to record single shot distributions. Data will be presented, identifying the angular variations of our emitted x-rays, based upon calibrated "at wavelength" D-Log E plots of this film

V. Conclusion

Efficient production of soft x-rays will mandate utilizing short laser pulses; the optimum pulselength will likely be wavelength dependent. High laser-plasma source brightness can readily be achieved by a combination of reducing the laser focal spot size and minimizing the laser pulselength to limit plasma expansion. Angular distributions can now be measured for each plasma source. Debris mitigation must be achieved and may be dependent upon the final configuration of laser spot size, pulselength, intensity, wavelength, and target design.

REFERENCES

1. P. Rockett, J. Hunter, R. Kensek, R. Olson, G. Kubiak, and K. Berger, "XUV Conversion Efficiency in a Low-Intensity KrF Laser Plasma for Projection Lithography," OSA Proc. on Soft X-ray Projection Lithography, **Vol. 12**, Monterey, CA, April 10-12 1991.

2. R. Kodama, K. Okada, N. Ikeda, M. Mineo, K. A. Tanaka, T. Mochizuki, and C. Yamanaka, J. Appl. Phys. **59**, 3050 (1986).

3. R. Popil, P. D. Gupta, R. Fedosejevs, and A. A. Offenberger, "Measurement of KrF-laser-plasma x-ray radiation from targets with various atomic numbers," Phys. Rev. A **35**, 3874 (1987).

4. M. Chaker, H. Pépin, V. Bareau, B. Lafontaine, I. Toubhans, R. Fabbro, and B. Faral, "Laser plasma x-ray sources for microlithography," J. Appl. Phys. **63**, 892 (1988).

*This work was supported by the U. S. Department of Energy under contract DE-AC04-76DP00789.

Spectral Characterization of Plasma Soft X-ray Sources for Lithographic Applications

Charles Cerjan
Lawrence Livermore National Laboratory
P. O. Box ~)8, L-438
Livermo. . , CA 94550
Ph: (510) 423-8032 / FAX: (510) 422-8761
email: cerjan@llnl.gov

The optimization of soft x-ray production from a laser-produced plasma source is an important issue for several current lithography schemes including proximity printing and point projection. Recent experiments at Lawrence Livermore National Laboratory by R. Spitzer and T. Orzechowski indicate that the conversion efficiency required by realistic system designs can be achieved using moderate laser intensities for a few select materials. Additionally, spectral data were collected for the two most promising materials, Sn and Au, as a function of laser wavelength and intensity in the region spanning 62 Å to 248Å (50 eV to 200 eV). Computer simulations of these experiments delineate the overall plasma characteristics of temperature and density. These quantities in turn predict the detailed spectral output in the region of interest, placing stringent demands on the accuracy of the simulation. The synthetic spectra produced are very sensitive to the quality of the atomic rate processes and to the number of ionization stages included. Results will be presented for Sn and compared to the experimental results. Previously unreported line indentifications for Sn will be assigned on the basis of accurate multi-configurational Dirac-Fock calculations yielding a more complete characterization of plasmas in this intermediate electron temperature regime than has been attempted before. This characterization provides more insight into the sensitivity of the desired spectral output to the choice of material. More general conclusions can be drawn about the extent to which computational simulations can limit parameter space studies in the search for optimal materials in laser-produced plasma x-ray sources.

Solid State Laser Driver for Projection X-ray Lithography

Lloyd A. Hackel
C. Brent Dane, Mark R. Hermann, Luis E. Zapata
Lawrence Livermore National Laboratory
Livermore, CA 94550

The design of a diode pumped solid state laser for use as an x-ray driver is described. The laser will deliver 400 mJ per pulse in a 5ns to 8ns pulselength at a 1000 Hz pulse repetition rate. The laser architecture is a master oscillator/power amplifier. A microchannel cooling technique developed at LLNL is used to allow the diodes to operate at the high repetition rate. The oscillator amplifier concept has been demonstrated in a Nd:glass system. Progress to date and experimental results will be presented.

Soft X-Ray Generation by a Table-Top High-Repetitive Glass Laser

H. Aritome, K. Haramura
Reserch Center for Extreme Materials and Faculty of Engineering Science, Osaka University, Toyonaka, Osaka 560, Japan, TEL:(06)844-1151

H. Sekiguchi, H. Hara, and T. Mochizuki
HOYA Corporation, Optronics Division, 3-3-1 Musashino, Akishima, Tokyo 196, Japan, TEL:(0425)46-2731

Soft x-rays generated from a laser produced plasma are of interest as a source for an x-ray microscope and also for x-ray lithography. In this paper, the x-ray generation from a recently developed, table-top, high repetitive, high energy moving glass slab laser[1] is demonstrated. The laser system can be operated at 5 Hz with laser pulse energy of 6 J. The size of the system is expected to be 3.4 m x 1.2 m x 1.3 m except for the power supply and the cooling unit.

The x-ray generation is measured using carbon as a target material. The laser pulse (width: 4 ns) can be focused on the target surface within less than 50 um in diameter. The x-ray emission spectrum is taken by the backside CCD camera[2], whose quantum efficiency is calibrated by using synchrotron radiation and a gas proportinal counter, using a transmission grating monochromator.

The line emissions from carbon such as H-like line (wavelnegth: 3.37 nm) or He-like line (4.03 nm) are resolved, therefore, the abosolute intensity of each line can be measured by using the calibrated data of the quantum efficiency of the CCD.

The x-ray intensity of H-like carbon line (wav length: 3.37 nm) increased almost linearly with laser energy between 0.2 - 6 J. The intensity was 8 x 10^{13} photons/sr at 6 J. It would be possible to generate 10 J/pulse at 10 Hz by improving a few optical components. This laser system would be applicable to an x-ray microscope and also x-ray lithography research.

1)H. Sekiguchi, H. Kawakami, T. Eguchi, J.R. Unternahrer, S. Amano, T. Mochizuki, CLEO'92 (Anaheim, CA), paper CTUE3.
2)H. Aritome, S. Nakayama, G. Zeng, H. Daido, M. Nakatsuka, S. Nakai, M. Sakurai, and K. Yamashita, Proc. SPIE, Vol.1741 (1992) 276.

A Compact Synchrotron and Condenser for Soft-X-Ray Projection Lithography

D. L. White
AT&T Bell Laboratories, 600 Mountain Ave. Murray Hill, NJ 07974
(908) 582-6129

A. A. MacDowell
AT&T Bell Laboratories, 510E Brookhaven Lab., Upton, NY 11973

J. B. Murphy
National Synchrotron Light Source, Brookhaven National Laboratory
Upton, NY 11973

O. R. Wood, II
AT&T Bell Laboratories, Crawfords Corner Road, Holmdel, NJ 07733

A compact 600 MeV synchrotron has been designed specifically for soft-x-ray projection lithography (SXPL). The storage ring has been optimized to produce copious amounts of radiation in the 13 nm wavelength region at a minimal price, e.g., using conventional warm electromagnets and a high current but low brightness electron beam. Since synchrotron design is a mature field, it should be possible to build such a ring without further research.[1]

The condenser optics are based on existing mirror technology and are able to collect more than 500 mrads of radiation and process it in divergence, uniformity and direction to match the requirements of an SXPL camera.[2] A typical condenser consists of at least two mirrors, a long multifaceted array of plane mirrors that captures radiation from the synchrotron and creates a fan converging on the pupil of the imaging system, and a final turning mirror that has a rippled or multifaceted surface to add a controlled amount of incoherence to the beam.

Since radiation from a synchrotron has a high degree of coherence, it is possible to capture all the radiation, with the losses coming only from the finite reflectivity of the mirrors. One mirror is coated with Mo/Si multilayers providing high normal incidence reflectance at 13 nm and the remainder are used at grazing incidence, thus losses due to the mirrors should be no more than 50%. Other condenser designs, using Lopez-Delgado and Szwarc[3] mirrors as collectors may also be practical and will be discussed.

A condenser should be able to capture several watts of radiation in the pass band of the camera (approximately 2% at 13 nm) and deliver over a watt to the mask. This is enough power to expose resist coated wafers at a rate of several square centimeters per second and is higher than the minimum required for economically viable production line SXPL.

While synchrotrons are more expensive than laser-produced plasma sources, they are very reliable and one storage ring could be used to power four to six SXPL printers. Figure 1 shows

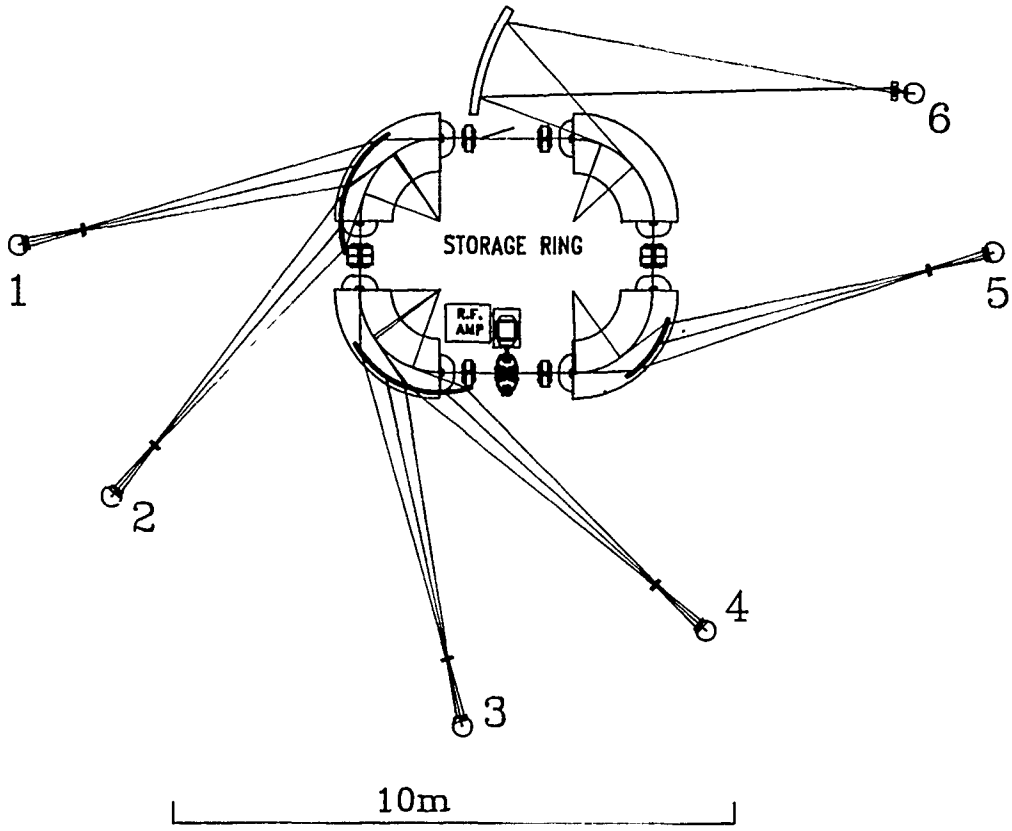

Figure 1. Schematic plan view of a 600 MeV storage ring and 6 lithography cameras (numbered). The cameras are illuminated with light using two different condenser designs. The electron injection system is not shown as it is on another level so as not to interfere with the collection beamlines.

a plan view of such a compact storage ring supplying flux to 6 soft-x-ray projection cameras. Beamlines 1 - 5 utilize condensers based on a faceted mirror design and beamline 6 utilizes a condenser based on a scatter plate design. The electron injection system for the storage ring is not shown in the figure since in a silicon foundry it would be located on another level so as not to interfere with the beamlines. If two such rings were used at the same facility, a single linear accelerator could be used to fill both synchrotrons, greatly reducing the cost.

In conclusion, a first pass design study has been carried out for condenser systems for SXPL cameras that use a small 600 MeV synchrotron storage ring as a soft-x-ray source. If the laser-produced plasma source debris problem[4] is not solved, synchrotrons, which are very clean, would be the logical alternative for a reliable soft-x-ray source.

1. J. B. Murphy, Proc. SPIE, **1263**, 116 (1990).

2. T. E. Jewell, K. P. Thompson, J. M. Rodgers, SPIE Proc. **1527**, 163 (1991).

3. R. Lopez-Delgado and H. Szwarc, Opt. Comm. **19**, 286 (1976).

4. M. L. Ginter and T. J. McIlrath, Appl. Opt. **27**, 885 (1988). M. C. Hettrick and J. H. Underwood, Appl. Opt. **25**, 4228 (1986).

Multilayer 2

WB 1:30pm–2:30pm
Bonsai II & III

David L. Windt, *Presider*
AT&T Bell Laboratories

"Residual Stresses in Mo/Si Multilayers and their Response to Thermal Annealing"

J. Koike, M. E. Kassner, F. J. Weber
Oregon State University
Corvallis, Oregon

D. G. Stearns, R. S. Rosen
Lawrence Livermore National Laboratory
Livermore, California

S. P. Vernon
Vernon Applied Physics
Torrance, California

The thermal stability of sputter-deposited Mo/Si multilayers was investigated by annealing studies at relatively low temperatures for various times. Two distinct stages of thermally-activated Mo/Si interlayer growth were found: a relatively rapid initial "surge" of approximately one monolayer, followed by a (slower) secondary "steady-state" growth that is diffusion controlled. The interdiffusion coefficients for the interlayer formed during deposition of Mo on Si are substantially higher than those of the interlayer formed during deposition of Si on Mo. It was also observed that significant residual tensile elastic strains develop within the Mo layer (normal to the multilayer) as a result of annealing. Explanations for these observed behaviors are presented.

EFFECTS OF MICROSTRUCTURE AND INTERFACIAL ROUGHNESS ON NORMAL INCIDENCE REFLECTIVITY OF RU/C AND RU/B_4C MULTILAYERS AT 7 NM WAVELENGTH

Tai D. Nguyen,[1,2] Ronald Gronsky,[2,3] and Jeffrey B. Kortright[1]

[1]Center for X-Ray Optics, Lawrence Berkeley Laboratory, Berkeley, CA 94720,
Tel. (510) 486-4051 FAX (510) 486-4550
[2]Department of Materials Science and Mineral Engineering, and Applied Science
and Technology Graduate Group, University of California, Berkeley, CA 94720,
[3]National Center for Electron Microscopy, Lawrence Berkeley Laboratory, Berkeley, CA 94720.

Recent developments of x-ray multilayers have focused on understanding and controlling the roughness at the interfaces to achieve high reflectance at wavelengths below 10 nm. The structure at the interfaces in generaldepends on the microstructures inside the layers, and on the interactions between the layer materials in multilayers. Studies of the microstructure-interfacial roughness relationship, and their effects on the reflectance performance are hence important in design of the multilayers.

Ru/C and Ru/B_4C were studied because both are candidates for normal incidence reflecting mirrors at wavelengths below 10 nm. The experimental procedure for this experiment has been described in detail elsewhere.[1] The multilayers were deposited by magnetron sputtering at floating temperature. Each sample contains 70 bi-layer periods. Annealing was performed at 600°C for 1 hour in vacuum of 10^{-6} torr. Normal incidence reflectance (θ=85°) at wavelength near the boron edge was measured using a laser-plasma source reflectometer.[2] Characterization of the microstructure and of the interfacial roughness was performed using High-Resolution Transmission Electron Microscopy (HRTEM), and x-ray specular and diffuse scattering (at SSRL). The specular reflectance measurement uses the symmetric θ-2θ geometry, while the offset scans measure diffuse intensity in direction nearly parallel to the specular direction in reciprocal space (ref. 3). In this experiment, the offset was set at 0.3 degree. The TEM samples were studied in a JEOL JEM 200CX operating at 200 kV.

Comparison of the normal incidence reflectance shows that the Ru/B_4C multilayer has superior performance than the Ru/C multilayer. The reflectance of the Ru/B_4C is 10%, while that of the Ru/C multilayer is 8%. The bandwidth is approximately 0.1 nm for both multilayers. Dramatic changes were observed in the performance of the multilayers after annealing. The reflectivity of the Ru/B_4C multilayer decreases by 30%, while that of the Ru/C multilayer decreases by more than 60% upon annealing. The bandwidth of the annealed Ru/B_4C multilayer remains approximately the same as that of the as-prepared sample, while the bandwidth of the Ru/C shows a slight increase (~ 15%) upon annealing. The Ru/C measurements also show a shift of the peak toward shorter wavelength after annealing, which indicates that the period has expanded (by 14%) upon annealing, as observed earlier in many metal/carbon multilayers.[4-7] The Ru/B_4C multilayer however shows only a slight shift or increase in the period (roughly 1%).

Changes in the reflectance of the multilayers upon annealing result from the changes in the microstructure and the interfacial structure in the multilayers. Criteria for high reflectance include smooth and uniform layers, and sharp and defined interfaces. Limiting factors affecting the interfaces include structural roughness, and intermixing between the layer materials. Roughness at the interfaces reduces the specular component, and produces a diffuse component in the x-ray scattering.[3,8-10] In general, multilayers with smooth and modulated structure show strong higher-order Bragg peaks. Samples with a higher degree of roughness exhibit lower Bragg intensities and higher smooth background in the diffuse scattering measurements. Two limiting types of roughness present in the multilayer structures are correlated and uncorrelated. Correlated roughness originates from either the substrate or a defect in the structure, and grows conformally from one layer to the next, while uncorrelated roughness is intrinsic to the individual layers. Vertically correlated components of roughness result in diffuse scattering with Bragg peaks like in specular scans. Uncorrelated components of roughness contribute a more featureless and smooth component to the diffuse intensity. The structure at the interfaces however depends on the microstructures inside the layers. The microstructure undergoes changes upon moderate annealing, or under intense x-radiation.[4-5] Interdiffusion and compound formation, or phase separation between the layers, in the structures have been observed by cross-sectional HRTEM.[11] Changes in the layer microstructure from thermal annealing thus result in different structure and roughness at the interfaces.

Cross-sectional HRTEM of as-prepared Ru/B_4C and Ru/C multilayers shows little differences in the uniformity and structure of the layers and interfaces. Comparison of the x-ray measurements however indicates a higher quality in the Ru/B_4C than in the Ru/C multilayer. The Ru/B_4C multilayer shows stronger higher order peaks than the Ru/C multilayer. The diffuse component of the as-prepared Ru/B_4C is relatively weaker than that of the Ru/C multilayer, which indicates smoother interfaces in the Ru/B_4C than in the Ru/C multilayer. The two materials systems show the same amorphous microstructure in the as-prepared multilayers, but different responses upon annealing. Annealing of the Ru/B_4C multilayers results in the formation of a boride phase RuB_2 in the Ru-rich layers, while grain-growth of Ru is observed in the Ru/C multilayer. Cross-sectional HRTEM image of the annealed Ru/B_4C multilayer shows well-defined and smooth layers, and reveals lattice images of a nano-crystalline structure in the Ru-rich layers. Both as-prepared and annealed Ru/B_4C multilayers exhibit as high as 8 orders of Bragg peaks above the smooth background, which indicates the presence of uniform layers and smooth interfaces. Measurements from the specular and diffuse components of the annealed Ru/B_4C multilayer show almost identical scattering profile as that of the as-prepared sample. The first order Bragg peak in the specular scattering decreases by a small amount (70% to 60%), while that of the diffuse component shows only a slight increase after annealing. Transformation of the Ru phase into the RuB_2 phase in the Ru-rich layers, which changes the scattering characteristics of the layers, upon annealing hence probably has a more dominant effect on the reduction in the reflectance after annealing than the slight changes in the interfacial roughness in this multilayer.

The Ru/C multilayer shows different behaviors on annealing from the Ru/B_4C. Annealing of the Ru/C multilayer results in dramatic changes in the diffuse scattering. The highest order Bragg peaks in both specular and diffuse scattering disappears after annealing, which suggests enhanced roughness and interdiffusion between the layers. The first order specular Bragg peak also shows a significant decrease after annealing. A strong enhanced

smooth diffuse background is observed in the annealed sample, which indicates that the roughness of annealed sample is much higher than that of the as-prepared sample. The increase in the smooth background indicates that this annealing-induced roughness is largely uncorrelated. The increase in the roughness in the Ru/C multilayer upon annealing, as suggested by the diffuse scattering measurement, is consistent with the observation of the multilayer in cross-section using HRTEM. Electron micrograph of the annealed Ru/C multilayers shows that the Ru layers in the Ru/C multilayers have agglomerated. The multilayer structure is still apparent, but the interfaces are no longer smooth and flat. The size of the Ru grains ranges from approximately 2 to 12 nm in the plane of the layers, and extends to as long as 4 nm in the perpendicular direction. This agglomeration occurs randomly in the layers, which results in the increase in the uncorrelated roughness that was measured in the diffuse scattering. This agglomeration and crystallization of the Ru layers in annealed Ru/C multilayers, which has also been observed in shorter period multilayers earlier,[6,12-13] is a result of the reduction of surface or interfacial energy from the amorphous non-equilibrium state of the as-prepared sample.

The results showed that the morphology, or roughness at the interfaces depends on the interactions of the layer materials in the multilayers. The difference in the evolution of the interfacial structure on annealing can be explained by the interactions of their layer materials. In the Ru/C system, clusters of like-atoms are preferred over those of unlike-atoms, since like-atoms have lower interatomic forces than unlike-atoms, which results in the separation and agglomeration of the Ru layers and in lower reflectances. In the Ru/B_4C system, however, compound formation is preferred, which stabilizes the layered structure of the multilayer. The microstructures in the layers, and interactions between the layer materials in the multilayers hence have a important effect on the interfacial structure, and the performance of x-ray multilayers.

This work was supported by the Director, Office of Energy Research, Office of Basic Sciences, Materials Sciences Division, of the U.S. Department of Energy under Contract No. DE-AC03-76SF00098 and by the Air Force Office of Scientific Research, of the U.S. Department of Defense under Contract No. F49620-87-K-0001. X-ray measurements were performed at SSRL, which is operated by the Chemical Sciences Division of the U.S. Department of Energy. The work on x-ray lithography is supported by the Defense Advanced Research Projects Agency, U.S. Department of Defense.

REFERENCE

1. T.D. Nguyen, R. Gronsky, and J.B. Kortright, presented at MRS Fall 1992 Meeting (San Francisco, CA) and to be published in the proceedings.
2. E.M. Gullikson, J.H. Underwood, P.C. Batson, and V. Nikitin, in Physics of X-Ray Multilayer Structures (OSA, Washington, D.C., 1992), 142.
3. J.B. Kortright. J. Appl. Phys. 70, 7, 3620 (1991).
4. T.D. Nguyen, R. Gronsky, and J.B. Kortright, MRS Proc. 139 (1989) 357.
5. T.D. Nguyen, R. Gronsky, and J.B. Kortright, MRS Proc. 187 (1990) 95.
6. X. Jiang, D. Xian, and Z. Wu, Appl. Phys. Lett. 57, 2549 (1990).
7. C.A. Lucas, T.D. Nguyen, and J.B. Kortright, Appl. Phys. Lett. 59, 17, 2100 (1991).
8. D.E. Savage, J. Kleiner, N. Schimke, Y.H. Phang, T. Jankowski, J. Jacobs, R. Kariotis, and M.G. Lagally, J. Appl. Phys. 69, 1411 (1991).

9. D.G. Stearns, J. Appl. Phys. **71**, 4286 (1992).
10. Y.H. Phang, R. Kariotis, D.E. Savage, and M.G. Lagally, J. Appl. Phys. **72**, 10, 4627 (1992).
11. T.D. Nguyen, R. Gronsky, and J.B. Kortright, in Physics of X-Ray Multilayer Structures (OSA Washington, D.C., 1992) 150.
12. T.D. Nguyen, R. Gronsky, and J.B. Kortright, Proc. 5th Asia-Pacific Elec. Microsc. Conf. (1992).
13. T.D. Nguyen, R. Gronsky, and J.B. Kortright, Elec. Microsc. Soc. Amer. Proc. (1992).

Tarnishing and Restoration of Mo/Si Multilayer X-ray Mirrors

J. H. Underwood, E. M. Gullikson and Khanh Nguyen

Center for X-ray Optics, 2-400, Lawrence Berkeley Laboratory, Berkeley, California, 94720. Telephone: (510) 486-4958

Introduction. Multilayer x-ray mirrors of molybdenum and silicon operating at normal incidence at wavelengths just longward of the Si $L_{II,III}$ absorption edges, are a key component in the development of soft x-ray projection lithography. In this application high reflectivity is essential. Because the achievement and maintenance of high reflectivity surfaces is vital to the success of soft x-ray projection lithography, it is important to know if Mo/Si multilayers show "aging" effects, e.g. decreasing reflectivity with time. Since, in a series of measurements of such mirrors at x-ray wavelengths, we had found evidence of such decay, a series of systematic experiments was carried out.

Aging Tests. All Mo/Si multilayer mirrors used for these studies were deposited on Si wafers and/or superpolished optical flats by magnetron sputtering with argon plasma. One set was prepared to reflect 14.8 nm radiation at normal incidence, and had 50 bi-layers, with Mo on top, d = 7.62 nm, and $\Gamma \sim 0.4$. The reflectivity of two of these multilayers on silicon wafers was immediately measured using a laser plasma reflectometer. Following these measurements one sample was immediately transferred to an argon atmosphere for storage and the other was stored in laboratory air for the duration of the tests. The reflectivity of both samples was measured at intervals from one to ten days.

The results are shown in figure 1. Immediately after deposition the samples had a reflectivity at 5 degrees incidence of 61.5, a typical value for a "good" Mo/Si multilayer having 50 layer pairs. Over the course of time, the reflectivity of the 92-184b, stored in air, decayed exponentially to an asymptotic value of about 52% with a half life of about 38 days, while the argon-stored mirror, which was only intermittently exposed to air to

transfer it from the storage container to the reflectometer vacuum chamber and back again, decayed much more slowly and linearly, losing about 2% of its reflectivity in 100 days.

Another set of samples was prepared,with Si on top. These samples had 50 bi-layers, with d = 7 nm and $\Gamma \sim 0.4$, and reached peak reflectivity at 13.2 nm. Again, one sample was stored in argon and the other allowed to "age" naturally in air, and the reflectivities of both were measured at intervals. The results are shown in figure 2. There is no evidence that either sample decayed in reflectivity with time.

ESCA Analysis. To determine the chemistry of the surface layers Mo/Si mirrors was were examined using ESCA. One sample was composed of 20 bi-layers (Mo on top), each 8.68 nm thick with $\Gamma \sim 0.4$,and a peak reflectivity at 16.5 nm. It had been deposited on a silicon wafer 537 days before the ESCA measurements were made and had since been stored in laboratory air. In to obtain maximum sensitivity to the chemistry of the outermost surface layers, the sample was examined with a photoelectron take-off angle of 75 degrees to the normal. An electron energy scan of revealed a strong Mo *3d* peak with the $3d_{5/2}$ component at a binding energy of 232.65 eV, corresponding to molybdenum trioxide. MoO_3. No trace of peak at lower binding energy, in particular the elemental molybdenum peak at 232 65, or the MoO_2 peak at 229.3 eV could be detected. However, a strong oxygen *1s* peak at 531.8 eV and a carbon *1s* peak at 284.9 eV were observed. Integration of the peaks showed a surface atomic composition of approximately 38% carbon, 48% oxygen and 14% molydenum. These observations are consistent with an outermost surface completely oxidized to MoO_3 and contaminated with carbonaceous material. This conclusion was reinforced by ESCA depth profiling sputtering with argon ions.

Following the sputtering of this sample, its reflectivity was measured in the region where the surface layer had been sputtered away, and also on an unsputtered control area. It was found that the sputtered area had higher reflectivity, 41.5% versus 32.5% on the

areas that had not been ion etched. Thus removal of the oxide restored the reflectivity of the structure This observation encouraged attempts to remove the oxide layer using wet processes such as baths of cold or boiling deionized water, 25 - 30% ammonium hydroxide solution, hydrogen peroxide and other chemicals. All were more or less effective at increasing the reflectivity. These restoration methods have also been used with success on a tarnished Schwarzschild objective used for photoemission microscopy.

Conclusions It is evident that oxidation of the surface of Mo/Si x-ray reflecting multilayers, when the molybdenum is deposited last, is a potential problem in applications, such as soft x-ray reflection lithography, where the highest possible reflectivity is required. The decrease in reflectivity from 63% to 52%, as illustrated in Figure 1, would decrease the throughput of a 5-element projection system by a factor of more than 2.5, and of a 7-element system by a factor of almost 3.5, an intolerable degradation. The reflectivity degradation becomes much more severe at longer wavelengths. However, a number of solutions are available, the simplest of which is to make the silicon the top layer. Silicon is self-passivating, the native oxide SiO_2 layer growing to no more than 1 or 2 nm. Alternatively, the molybdenum can be protected from oxidation by storage of the optical elements in an inert atmosphere or vacuum, or as a last resort an oxidized surface can be restored by sputter etching, washing, or chemical treatments. After such treatment the exposed surface is $MoSi_2$, which is chemically inert and should resist oxidation.

It should be noted that other multilayer materials have the potential for degradation by oxidation, in particular those containing tungsten, which is chemically similar to molybdenum.

Acknowledgements. This work was supported by the Director, Office of Energy research, Office of Basic Energy Sciences, Materials Science U.S. Department of Energy, under contract number DE-AC03-76SF00098.

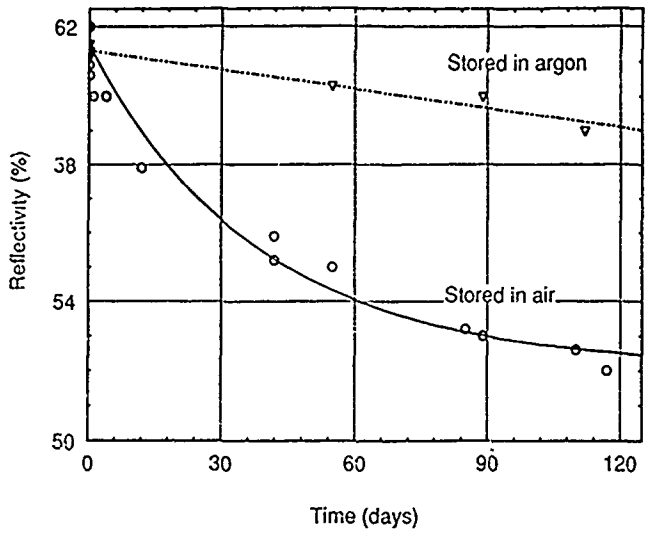

Figure 1. Decrease in peak reflectivity (at 14.7 nm) with time of Mo/Si multilayer mirror 92-184, Mo on top. Circles: stored in laboratory air. Squares: stored in an argon atmosphere. The solid curve is an exponential fit of the form $R = a + (61.5 - a)exp(-t/\tau)$ to the air-stored data with $a = 51\%$ and $\tau = 38$ days.

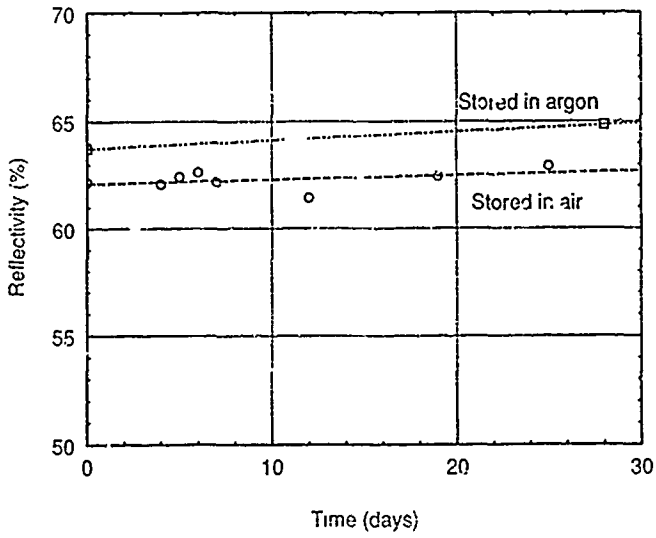

Figure 2. Peak reflectivity (at 13.2 nm) *vs.* time for Mo/Si multilayer mirror 92-237C, Si on top. Circles: stored in laboratory air. Squares. stored in argon. The higher reflectivity of the sample stored in argon is due to the fact that it was deposited on a superpolished fused silica optical flat, whereas the air-stored sample was deposited on a silicon wafer.

Alternate Strategies

WC 3:00pm–3:40pm
Bonsai II & III

John Frank, *Presider*
SEMATECH

Soft-x-ray projection lithography using two arrays of phase zone plates

Scott D. Hector and Henry I. Smith

Dept. of Elec. Eng. and Comp. Sci., Massachusetts Institute of Technology,
Mail Stop 39-427, 77 Massachusetts Avenue, Cambridge, MA 02139
Tel: (617) 253-6865, FAX: (617) 253-8509

I. Introduction

At feature sizes below 70nm, the mask-to-sample gap in proximity x-ray lithography must be less than 5μm, which, although this is not a problem in research, it may be undesirable in manufacturing. Thus, for sub-70nm features, one is persuaded to consider the feasibility of x-ray projection systems.

Current designs of x-ray projection lithography systems are based on multilayer reflective optics. However, such systems cannot operate in the wavelength bands that are optimal for lithography (i.e. 0.8-1.6nm or 4-6nm). Fresnel zone plates, on the other hand, do operate effectively as imaging elements at these wavelengths, and have demonstrated resolution about equal to the minimum zone width of ~30nm[1]. In principle, it should be feasible to achieve a resolution with zone-plate-based lithography about equal to the finest features that can be fabricated using scanning-electron-beam lithography (SEBL).

Previously, Burge et al. proposed using zone plates to replicate x-ray masks in a demagnifying configuration [2]. For imaging patterns several centimeters in diameter, a single-zone-plate system is impractical because the field-of-view of such zone plates is only a few tens of microns. This shortcoming can be overcome by using large area arrays of zone-plate lenses at unity magnification. Because each zone-plate lens of an array inverts an image, a second, matching array of zone plates is required, as illustrated in Figure 1. Appropriate apodization, and apertures in the first focal plane, screen out much of the undesired background radiation (e.g. zero, -1, and higher diffracted orders). Feldman has proposed an alternative scheme that also employs two arrays of zone plates. The first zone-plate array produces an array of diffraction-limited spots on the mask; the second refocuses them to spots on the substrate [3]. This scheme should have an improved image-to-background intensity ratio, but requires a large area plane-wave illuminator.

The fact that unity magnification is required is not viewed as a serious shortcoming because e-beam lithography systems capable of large-area, zero-distortion patterning are under development and will be available in a few years [4]. Dividing the total area of a zone-plate array by the number of zone-plate lenses gives the "unit cell" area. The area in the image plane that is associated with a single lens of the array, and is free of aberrations , is only a fraction (0.1 to 0.4) of the unit cell area. We call this fraction the "filling factor." Thus, the pair of zone-plate arrays must be scanned in both the X and Y directions in order to fill in a large-area image.

It is well known that the fraction of the incident power in the first-order focus of a zone plate lens (i.e the efficiency) is 10% for an amplitude zone plate and 40% for a pure phase zone plate. At wavelengths between 0.8 and 6.0nm, x-ray absorbers are also phase shifters, and thus a properly designed zone plate should have an efficiency between 10% and 40%. Efficiencies of x-ray phase zone plates as high as 33% have been measured [5]. Assuming an efficiency of 25% the overall efficiency of two zone plates in series is 6.25%. Multiplying this by a filling factor of 0.25 yields an overall efficiency of 3.9×10^{-3}. When combined with undulator radiation (or radiation from a comparably narrow-band source), and assuming an array covering one to several square centimeters, the resulting pixel transfer rate is ~10^9 pixels/second [6].

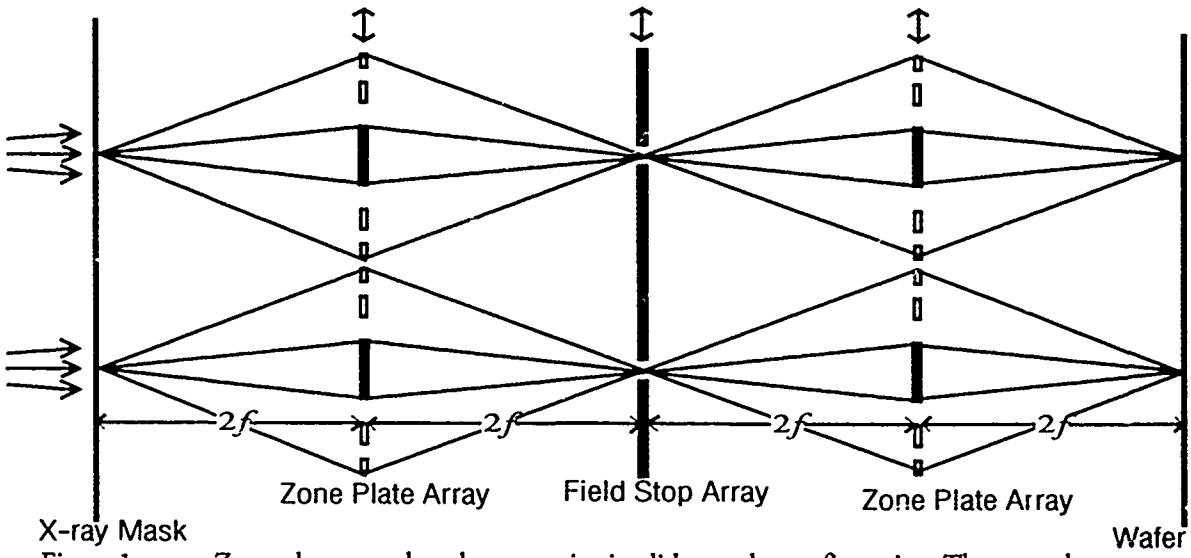

Figure 1 Zone-plate-array-based x-ray projection lithography configuration. The zone plate arrays and field stops are synchronously scanned. Note that the central zones are opaque.

Zone plate arrays can be supported on membranes such as those developed for proximity x-ray lithography (Si, SiC, or SiNx for $\lambda < 4.5$ nm, diamond for $\lambda = 4.5$-6.0 nm). It is well known that membrane distortion can be well below 0.5 nm (and probably below 0.1 nm for the symmetric array of zone plates) by controlling the stress of the absorber [7]. The 1:1 mask will also be supported on a membrane as in proximity XRL. Zone-plate-array-based x-ray projection lithography can be carried out in He gas at atmospheric pressure and hence efficient cooling of the system elements should be feasible. Zone plate arrays have a distinct advantage over multilayer reflective projection schemes in that pattern distortion can be eliminated, and the area of the mask and image can be many centimeters in diameter.

II. System Design

The system consists of an x-ray mask illuminated by plane parallel x-rays. Two parallel, planar arrays of zone plates image the x-ray mask pattern onto a wafer. The zone plate arrays are designed to achieve 30 nm resolution while maximizing the aberration-free field-of-view (FOV). In order to achieve unity magnification imaging of the x-ray mask, the zone plate arrays are arranged in an $8f$ configuration (f is the zone plate focal length) as shown in Figure 1. Each zone plate is apodized to remove the zero-order beam. The zone plate arrays are separated by an array of field stops placed in the focal plane of the first array. The arrays of zone plates and stops are scanned together to fill in the entire image.

This imaging configuration with object distance, p, and imaging distance, q, where $p=q=2f$, is free of spherical aberration if the zone radii are given by [8]:

$$r_n = \sqrt{n\lambda f + \frac{n^2\lambda^2}{16}} \tag{1}$$

where n is the zone index, r_n is the zone radius with index n, and λ is the design wavelength. With a sufficient number of zones (N>100), the diffraction-limited resolution, δ, of a zone plate is [9]:

$$\delta = \frac{1.22}{m}\left(r_{N+1} - r_N\right) \tag{2}$$

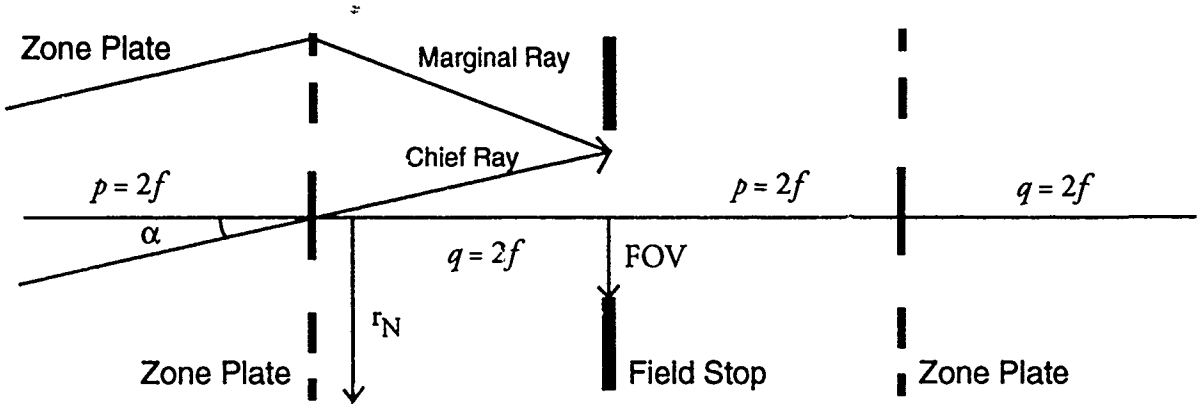

Figure 2 Illustration of ray tracing used to determine the FOV.

where m is the order of the focus (here m=1) and N is the number of zones. Substituting Eq. (1) into Eq. (2) yields:

$$\delta = \frac{1.22}{m}\left(\sqrt{(N+1)\lambda f + \frac{(N+1)^2\lambda^2}{16}} - \sqrt{N\lambda f + \frac{N^2\lambda^2}{16}}\right) \tag{3}$$

The value of N can be found from a consideration of the aberrations of two zone plates in series.

The resolution of a zone plate is limited by chromatic aberration. It can be shown that the maximum zone index that keeps the optical path difference (OPD) due to the changing focal length with wavelength within $\lambda/4$ is $N \approx \lambda/\Delta\lambda$ where $\Delta\lambda$ is the full-width- at-half -maximum (FWHM) source bandwidth [10]. Using undulator radiation combined with a monochromator, the fractional bandwidth can be $\Delta\lambda/\lambda$=1/700 [6,11]. In the design of the zone plate arrays, we therefore assign N=500. Using this value of N, the focal length, f, is determined by iteratively solving Eq. (3) with desired resolution, δ. For a wavelength of λ = 1.32 nm and δ = 30 nm, f = 920 μm. This focal length corresponds to a 0.013 NA, 24.6 μm-radius zone plate with minimum zone width of 25 nm.

The diffraction-limited field-of-view (FOV) of an imaging system is limited by off-axis aberrations: coma, astigmatism, field curvature, and distortion. The OPD between the marginal ray and the chief ray (shown in Figure 2) for an oblique angle of incidence, α, on the first array can be shown to be [10]:

$$OPD = \left(r_N{}^3\frac{\alpha}{2}\right)\left(\frac{1}{q^2} - \frac{1}{p^2}\right)\cos\phi - \left(\frac{r_N{}^2\alpha^2}{2f}\right)\cos^2\phi - \frac{r_N{}^2\alpha^2}{4f} \tag{4}$$

where ϕ is the azimuthal angle. The first term corresponds to coma, the second term corresponds to astigmatism, and the third term corresponds to field curvature. Notice that no distortion or spherical aberration exists. Coma is not present when the object and image distances are equal (p=q). The acceptable FOV has been determined using ray tracing to be $FOV \approx 15$ μm, where the FOV is determined by the largest field angle, α, over which the image is diffraction limited according to Marechal's criterion (i. e. the Strehl ratio is larger than 0.8) [12]. The "filling factor", $\gamma = V(FOV/r_N)^2$, is reduced by vignetting where V is the fraction of the x-ray flux diffracted into the first-order focus that reaches the image plane. Calculating V=0.72, the filling factor is γ=0.27.

The efficiency of the zone plates depends on the index of refraction of the zone plate material at the wavelength of the illumination. In the soft x-ray region, the index can be expressed as $n = 1 - a - ib$ (for most materials, $a, b << 1$)

[13]. Thus, materials in this region act as slightly lossy dielectrics. Kirz has shown the efficiency of lossy, phase-shifting zone plates to be [8]:

$$\eta = \frac{1}{m^2\pi^2}\left[1 + e^{-2kbt} - 2e^{-kbt}\cos(kat)\right] \tag{5}$$

where t is the thickness of the zone plate, and k is the free space wave number. Materials with a large ratio a/b have the highest efficiency when used for phase zone plates. To partially eliminate undiffracted light, light diffracted into higher-order and virtual foci, and aberrated wavefront regions, an array of field stops is placed in the focal plane of the first zone plate array. The radius of this field stop is equal to the FOV.

III. Fabrication

Anderson and Kern have shown that distortion-free zone plates can be fabricated by scanning-electron-beam lithography (SEBL) with minimum zone widths (and hence resolution) of 30 nm [1,14]. Because of the long times incurred in the SEBL writing process, we propose to fabricate zone plate arrays of $10^4/cm^2$ by step and repeat proximity XRL. Once an array, or a portion of one, is fabricated it can be replicated by proximity XRL.

IV. Conclusion

We have shown that x-ray projection lithography is feasible using zone plate arrays, and may be the method of choice if proximity x-ray lithography fails to meet manufacturing needs below 70 nm feature sizes.

V. References

1 C. David, J. Thieme, P. Guttman, G. Schneider, D. Rudolph, and G. Schmahl, "Electron-beam generated x-ray optics for high resolution microscopy studies," *Optik* **91**, 95-99 (1992).

2 R. Burge, M. Browne, and P.Charalambous, "An x-ray projection method using zone plates for mask preparation with sub-micron sizes," *Microelectronic Engineering* **8**, 227-32 (1987).

3 M. Feldman, "Projection x-ray lithography using arrays of zone plates," Proceedings of the Electrochemical Society in patterning Science and Technology Number 2, eds. W. Greene, G. Hefferon, and L. White, Proceedings volume 92-6, 136-146 (1991).

4 H.I. Smith, S.D. Hector, M.L. Schattenburg, and E.H. Anderson, "A new approach to high fidelity e-beam and ion-beam lithography based on an in situ global-fiducial grid," *JVST B* **9**, 2992-5 (1991).

5 B. Lai, B. Yun, D. Legnini, Y. Xiao, J. Chrzas, P. Viccaro, V. White, S. Bajikar, D. Denton, F. Cerrina, E. Di Fabrizio, M. Gentili, L. Grella, and M. Baciocchi, "Hard x-ray phase zone plate fabricated by lithographic techniques," *Applied Physics Letters* **61**, 1877-1879 (1992).

6 C. Jacobsen, M. Howells, J. Kirz, S. Rothman, "X-ray holographic microscopy using photoresists," *JOSA A* **7**, 1847-61 (1990).

7 Y.C. Ku, Lee-Peng Ng, R. Carpenter, K. Lu, H.I. Smith, L.E. Haas, and I. Plotnick, "In-situ stress monitoring and deposition of zero stress W for x-ray masks," *JVST B* **9**, 3297-3300 (1991).

8 J. Kirz, "Phase zone plates for x rays and the extreme uv," *JOSA* **64**, 301-309 (1974).

9 D. Stigliani, R. Mittra, and R. Semonin, "Resolving power of a zone plate," *JOSA* **57**, 610-613 (1967).

10 M. Young, "Zone plates and their aberrations," *JOSA* **62**, 972-6 (1972).

11 N. Ceglio, "Invited review: Revolution in x-ray optics," *Journal of X-ray Science and Technology* **1**, 7-78 (1989).

12 M. Born and E. Wolf, Principles of Optics, 6th edition, p. 469 (Pergamon Press, Oxford, 1980).

13 B. Henke, E. Gullikson, J. Davis, M. Fryer, and A. Oren, "Low energy x-ray interaction coefficients: photoabsorption, scattering and reflection," *Atomic Data and Nuclear Data Tables* **27**, No. 1 (1982).

14 E. Anderson and D. Kern, "Nanofabrication of zone plates for x-ray microscopy," X-Ray Microscopy III, eds. A. Michette, G. Morrison, and C. Buckley, (Springer-Verlag, Berlin, 1992).

THE USE OF ZONE PLATE ARRAYS IN PROJECTION X-RAY LITHOGRAPHY

M. Feldman
Electrical & Computer Engineering Department
Louisiana State University
Baton Rouge, LA 70803-5901
(504) 388-5489

Projection X-ray lithography has demonstrated the ability to print very fine features, (1,2) but the technical requirements of useful versions of the proposed systems are beyond the present state of the art. However, X-ray projection lithography using zone plates as the imaging elements is well within the state of art (3,4).We discuss two systems: a simple 1:1 imaging system utilizing existing X-ray masks, and a more mechanically complex reduction system.

The resolution, R, of a zone plate is given by $R = \frac{\lambda}{2NA}$ where λ is the wavelength of the exposing light and NA is the numerical aperture. For zone plates used at a large reduction ratio, R is also the approximate width of the narrowest, outer ring. Using zone plates patterned by e-beam lithography resolution well below 0.1 micron is routinely obtained, and X-ray microscopes based on zone plates are a well established technology (5,6,7).

To obtain the high flux needed for lithographic applications the zone plate must function over a band of wavelengths, $d\lambda$. This introduces chromatic aberration since the focal length, f, of a zone plate is proportional to $1/\lambda$. To keep df less than the depth of focus, f must be less than $\frac{\lambda}{d\lambda}\frac{2R^2}{\lambda}$. For example, with a 1% bandwidth X ray beam centered at 10A and R=0.1 micron, we have $f \leq 2mm$, NA $\approx$ .005 which implies a maximum zone plate diameter of 20 microns. It is impractical to image a large field with such a small zone plate. However, many zone plates can be combined into an array to produce a useful imaging system. For efficient utilization of the X-ray beam, the array should fully cover the projected area of the X-ray beam. Complete patterning of the wafer surface is obtained by scanning, just as in proximity printing.

The image formed by a lens or zone plate is inverted. The inverted images formed by adjacent zone plates in a two dimensional array bring together images of portions of the mask which were previously well separated (Fig. 1). This complicates replication of the mask by scanning unless one of two strategies is followed 1) A second array of zone plates is used to invert the image again, so that a noninverted final image is formed, (4), 2) The field of each zone plate is restricted to a single point on axis. This may be done by a corresponding array of zone plate condensing lenses. This approach has the advantages that mask and wafer can be mechanically locked together and scanned,and that the incident X-ray flux is fully utilized.

Each condensing zone plate and its corresponding imaging zone plate form a simple imaging system (Fig. 2). At a wavelength of 10A the zone plate arrays would use a thick absorber on a substrate. They are in fact nearly the equivalent of X-ray masks for

p oximity printing. However, because the imaging zone plates are used at 1:1, they must have a minimum feature size which is half that of the features to be printed.

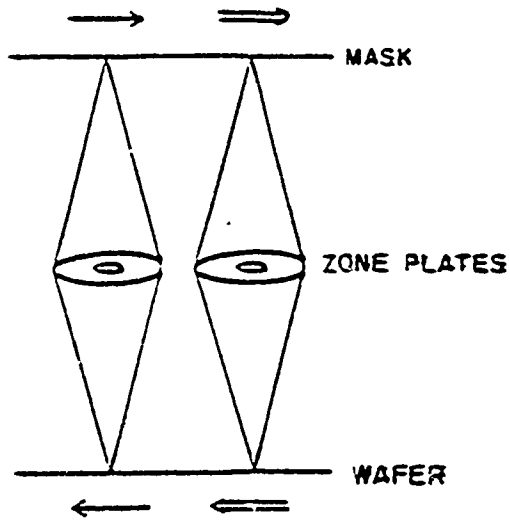

Fig. 1. Inverted images formed by adjacent zone plates.

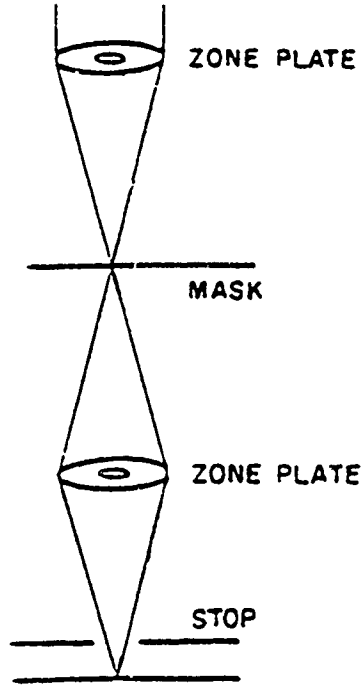

Fig. 2. Single point image.

During exposure each imaging zone plate scans a line on the mask onto the wafer. An array of 100 columns of zone plates, with adjacent columns offset by 0.1 micron from each other, (Fig. 3), uniformly covers the wafer with 100 scan lines in every 10 microns. While this is satisfactory, it requires critical control of the angle between the zone plate arrays and the direction of scanning. For example, the loss of entire scan lines could be caused by an error of only 0.1 mrad. A more satisfactory layout of the arrays is shown in Figure 4. In this arrangement an error of 0.1 mrad modulates the average spacing between scan lines, resulting in an intensity variation of 1%, but with no gaps in the coverage.

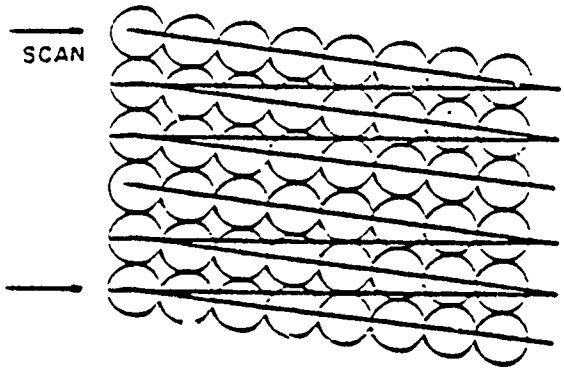

Fig. 3. Zone plate placement for conventional scan.

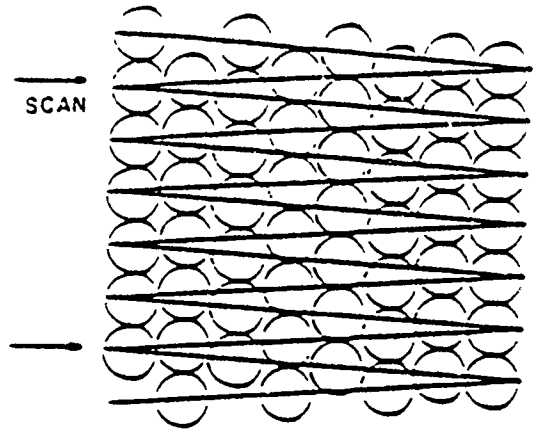

Fig. 4. Modified placement for more robust scan.

The narrow bandwidth (~ 1%) required for zone plate imaging may be obtained by filtering the spectrum of a conventional bending magnet X-ray lithography beam line. However, much higher throughput would be achieved by utilizing the high brightness and narrow bandwidth of undulator beams.

Arrays of condensing and imaging zone plates may be used to form simple reduction imaging systems similar to those used for 1:1 printing. For a 4:1 reduction ratio the spot size on the mask is 4 times as large as that on the wafer. The zone plates may be arrayed in either of the configurations shown for 1:1 imaging (Figure 3 and 4). However, adjacent columns are offset four times as much. Consequently, only every 4th line is printed on the wafer, even though these lines are adjacent to each other on the mask. Subsequently, the same area of the wafer is rescanned three more times to fill in the missing scan lines (Fig. 5).

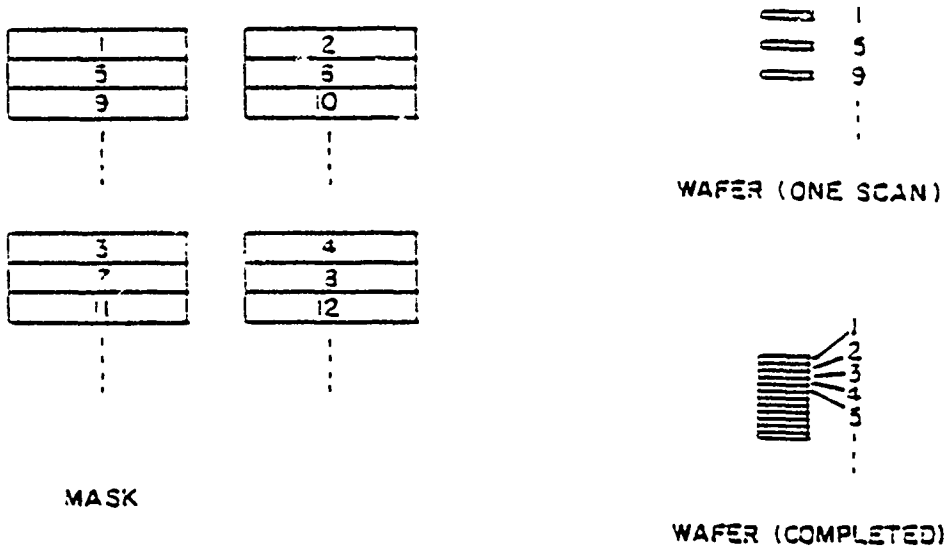

Fig. 5. Mask and wafer layouts for reduction imaging. The first scan images areas 1, 5, 9,..., the second scan 2, 6, 10,..., and so on. The wafer is completed after 4 scans.

Reduction imaging may also be performed with a single column of zone plates, each of which images a separated strip on the mask. Both mask and wafer are scanned (in opposite directions) so that each zone plate images a strip on the mask into a strip on the wafer whose width and length are smaller by the reduction ratio. The inversion produced by the zone plates is compensated by inverting each strip on the mask, so that the strip imaged on the wafer is correctly oriented. Dividing the mask pattern into separated strips not only solves the inversion problem, but relaxes the mechanical tolerances and the collimation required of the X-ray beam. However, more scans are needed to fill in the blank area on the wafer between patterned strips.

In summary, to print a field on a wafer with the 1:1 projection system, the mask and wafer are simultaneously scanned, while the X-ray beam and the zone plate arrays remain fixed. The scan is identical to that used in conventional X-ray proximity printing on a storage ring beam line. Reduction imaging requires multiple scans, with accurate tracking of the mask and wafer positions.

All of the zone plate imaging systems considered here have an extremely flat field and large depth of focus. The condensing and imaging zone plate arrays are essentially X-ray masks with relatively small fields, and can be made by conventional processing. If they are distortion free, or at least matched to each other, then the imaging with a collimated X-ray beam is also distortion free. In addition, the on-axis imaging systems are telecentric.

The techniques described here are capable of diffraction limited projection X-ray lithography with resolutions well below 0.1 micron. The mechanical requirements to maintain registration over the full scan are severe, especially in the case of reduction imaging. However, they present no fundamental limitations, and in fact are similar to those of existing optical scanning systems. The system is based on existing X-ray mask technology, and all of the elements used have been demonstrated separately. The combination into a practical exposure tool appears to be well within the present state of the art in lithography.

REFERENCES

1. T.E. Jewell, et al, *PIE E-Beam, X-Ray, and I-Beam Tech*, 1263, 90 (1990).

2. N.M. Ceglio, A.M. Hawryluk, D.G. Stearns, D.P. Gaines, R.S. Rosen, and S.P. Vernon, *J. Vac. Sci. Tech.*, B8, 1325 (1990).

3. M. Feldman, Projection "X-ray lithography using arrays of zone plates," *Proc. Electrochem.Soc.PatterningScienceTech.*, no. 2, vol. 92-6, pp. 136-146 (1992).

4. S.D. Hector and H.I. Smith, *These Proceedings*, (1993).

5. D. Attwood, "Soft X-ray lithography at Berkeley's Advanced Light Source," p.25, *Proceedings of the Workshop,* Berkeley, CA, (1991).

6. Y. Vladimirsky, D.P. Kern, W. Meyer-Ilse, B. Greinke, P. Guttmann, S.A. Rishton, and D. Attwood, *Microelec Engr.*, 9, 87, (1989).

7. H. Rarback, et al, *Rev. Sci. Instrum.*, 59, 52 (1988).

TECHNICAL PROGRAM COMMITTEE

Andrew M. Hawryluk, *Chair*
Lawrence Livermore National Laboratory

Richard H. Stulen, *Chair*
Sandia National Laboratories

David T. Attwood
Lawrence Berkeley Laboratory

Jeffrey Bokor
University of California, Berkeley

John H. Bruning
GCA/Tropel

Natale M. Ceglio
Lawrence Livermore National Laboratory

John Frank
SEMATECH

Donald C. Hofer
IBM Almaden Research Center

Hiroo Kinoshita
NTT LSI Laboratories, Japan

Marc Levenson
IBM Almaden Research Center

David A. Markle
Ultratechstepper

William T. Silfvast
University of Central Florida (CREOL)

David L. Windt
AT&T Bell Laboratories

Frits Zernike
SVG Lithography Systems, Inc.